Catalysts **2015**, *5*, 145-269; doi:10.3390/catal5010145

OPEN ACCESS

catalysts

ISSN 2073-4344

www.mdpi.com/journal/catalysts

Review

Heterogeneous Catalyst Deactivation and Regeneration: A Review

Morris D. Argyle and Calvin H. Bartholomew *

Chemical Engineering Department, Brigham Young University, Provo, UT 84602, USA;
E-Mail: mdargyle@byu.edu

* Author to whom correspondence should be addressed; E-Mail: calb@byu.edu;
Tel: +1-801-422-4162, Fax: +1-801-422-0151.

Academic Editor: Keith Hohn

Received: 30 December 2013 / Accepted: 12 September 2014 / Published: 26 February 2015

Abstract: Deactivation of heterogeneous catalysts is a ubiquitous problem that causes loss of catalytic rate with time. This review on deactivation and regeneration of heterogeneous catalysts classifies deactivation by type (chemical, thermal, and mechanical) and by mechanism (poisoning, fouling, thermal degradation, vapor formation, vapor-solid and solid-solid reactions, and attrition/crushing). The key features and considerations for each of these deactivation types is reviewed in detail with reference to the latest literature reports in these areas. Two case studies on the deactivation mechanisms of catalysts used for cobalt Fischer-Tropsch and selective catalytic reduction are considered to provide additional depth in the topics of sintering, coking, poisoning, and fouling. Regeneration considerations and options are also briefly discussed for each deactivation mechanism.

Keywords: heterogeneous catalysis; deactivation; regeneration

1. Introduction

Catalyst deactivation, the loss over time of catalytic activity and/or selectivity, is a problem of great and continuing concern in the practice of industrial catalytic processes. Costs to industry for catalyst replacement and process shutdown total billions of dollars per year. Time scales for catalyst deactivation vary considerably; for example, in the case of cracking catalysts, catalyst mortality may be on the order of seconds, while in ammonia synthesis the iron catalyst may last for 5–10 years. However, it is inevitable that all catalysts will decay.

Typically, the loss of activity in a well-controlled process occurs slowly. However, process upsets or poorly designed hardware can bring about catastrophic failure. For example, in steam reforming of methane or naphtha, great care must be taken to avoid reactor operation at excessively high temperatures or at steam-to-hydrocarbon ratios below a critical value. Indeed, these conditions can cause formation of large quantities of carbon filaments that plug catalyst pores and voids, pulverize catalyst pellets, and bring about process shutdown, all within a few hours.

While catalyst deactivation is inevitable for most processes, some of its immediate, drastic consequences may be avoided, postponed, or even reversed. Thus, deactivation issues (*i.e.*, extent, rate, and reactivation) greatly impact research, development, design, and operation of commercial processes. Accordingly, there is considerable motivation to understand and treat catalyst decay. Over the past three decades, the science of catalyst deactivation has been steadily developing, while literature addressing this topic has expanded considerably to include books [1–4], comprehensive reviews [5–8], proceedings of international symposia [9–14], topical journal issues (e.g., [15]), and more than 20,000 U.S. patents for the period of 1976–2013. (In a U.S. patent search conducted in November 2013 for the keywords catalyst and deactivation, catalyst and life, and catalyst and regeneration, 14,712, 62,945, and 22,520 patents were found respectively.) This area of research provides a critical understanding that is the foundation for modeling deactivation processes, designing stable catalysts, and optimizing processes to prevent or slow catalyst deactivation.

The purpose of this article is to provide the reader with a comprehensive overview of the scientific and practical aspects of catalyst deactivation with a focus on mechanisms of catalyst decay, prevention of deactivation, and regeneration of catalysts. Case studies of deactivation and regeneration of Co Fischer-Tropsch catalysts and of commercial catalysts for selective catalytic reduction of nitrogen oxides in stationary sources have been included.

2. Mechanisms of Deactivation

There are many paths for heterogeneous catalyst decay. For example, a catalyst solid may be poisoned by any one of a dozen contaminants present in the feed. Its surface, pores, and voids may be fouled by carbon or coke produced by cracking/condensation reactions of hydrocarbon reactants, intermediates, and/or products. In the treatment of a power plant flue gas, the catalyst can be dusted or eroded by and/or plugged with fly ash. Catalytic converters used to reduce emissions from gasoline or diesel engines may be poisoned or fouled by fuel or lubricant additives and/or engine corrosion products. If the catalytic reaction is conducted at high temperatures, thermal degradation may occur in the form of active phase crystallite growth, collapse of the carrier (support) pore structure, and/or solid-state reactions of the active phase with the carrier or promoters. In addition, the presence of oxygen or chlorine in the feed gas can lead to formation of volatile oxides or chlorides of the active phase, followed by gas-phase transport from the reactor. Similarly, changes in the oxidation state of the active catalytic phase can be induced by the presence of reactive gases in the feed.

Thus, the mechanisms of solid catalyst deactivation are many; nevertheless, they can be grouped into six intrinsic mechanisms of catalyst decay: (1) poisoning, (2) fouling, (3) thermal degradation, (4) vapor compound formation and/or leaching accompanied by transport from the catalyst surface or particle, (5) vapor–solid and/or solid–solid reactions, and (6) attrition/crushing. As mechanisms 1, 4,

and 5 are chemical in nature while 2 and 6 are mechanical, the causes of deactivation are basically threefold: chemical, mechanical, and thermal. Each of the six basic mechanisms is defined briefly in Table 1 and treated in some detail in the subsections that follow, with an emphasis on the first three. Mechanisms 4 and 5 are treated together, since 4 is a subset of 5.

Table 1. Mechanisms of catalyst deactivation.

Mechanism	Type	Brief definition/description
Poisoning	Chemical	Strong chemisorption of species on catalytic sites which block sites for catalytic reaction
Fouling	Mechanical	Physical deposition of species from fluid phase onto the catalytic surface and in catalyst pores
Thermal degradation and sintering	Thermal Thermal/chemical	Thermally induced loss of catalytic surface area, support area, and active phase-support reactions
Vapor formation	Chemical	Reaction of gas with catalyst phase to produce volatile compound
Vapor–solid and solid–solid reactions	Chemical	Reaction of vapor, support, or promoter with catalytic phase to produce inactive phase
Attrition/crushing	Mechanical	Loss of catalytic material due to abrasion; loss of internal surface area due to mechanical-induced crushing of the catalyst particle

2.1. Poisoning

Poisoning [3,16–22] is the strong chemisorption of reactants, products, or impurities on sites otherwise available for catalysis. Thus, poisoning has operational meaning; that is, whether a species acts as a poison depends upon its adsorption strength relative to the other species competing for catalytic sites. For example, oxygen can be a reactant in partial oxidation of ethylene to ethylene oxide on a silver catalyst and a poison in hydrogenation of ethylene on nickel. In addition to physically blocking of adsorption sites, adsorbed poisons may induce changes in the electronic or geometric structure of the surface [17,21]. Finally, poisoning may be reversible or irreversible. An example of reversible poisoning is the deactivation of acid sites in fluid catalytic cracking catalysts by nitrogen compounds in the feed. Although the effects can be severe, they are temporary and are generally eliminated within a few hours to days after the nitrogen source is removed from the feed. Similar effects have been observed for nitrogen compound (e.g., ammonia and cyanide) addition to the syngas of cobalt Fischer-Tropsch catalysts, although these surface species require weeks to months before the lost activity is regained [23]. However, most poisons are irreversibly chemisorbed to the catalytic surface sites, as is the case for sulfur on most metals, as discussed in detail below. Regardless of whether the poisoning is reversible or irreversible, the deactivation effects while the poison is adsorbed on the surface are the same.

Many poisons occur naturally in feed streams that are treated in catalytic processes. For example, crude oil contains sulfur and metals, such as vanadium and nickel, that act as catalyst poisons for many petroleum refinery processes, especially those that use precious metal catalysts, like catalytic reforming, and those that treat heavier hydrocarbon fractions in which the sulfur concentrates and metals are almost exclusively found, such as fluid catalytic cracking and residuum hydroprocessing.

Coal contains numerous potential poisons, again including sulfur and others like arsenic, phosphorous, and selenium, often concentrated in the ash, that can poison selective catalytic reduction catalysts as discussed later in Section 4.3.3.1. As a final example, some poisons may be added purposefully, either to moderate the activity and/or to alter the selectivity of fresh catalysts, as discussed as the end of this section, or to improve the performance of a product that is later reprocessed catalytically. An example of this latter case is lubricating oils that contain additives like zinc and phosphorous to improve their lubricating properties and stability, which become poisons when the lubricants are reprocessed in a hydrotreater or a fluid catalytic cracking unit.

Mechanisms by which a poison may affect catalytic activity are multifold, as illustrated by a conceptual two-dimensional model of sulfur poisoning of ethylene hydrogenation on a metal surface shown in Figure 1. To begin with, a strongly adsorbed atom of sulfur physically blocks at least one three- or fourfold adsorption/reaction site (projecting into three dimensions) and three or four topside sites on the metal surface. Second, by virtue of its strong chemical bond, it electronically modifies its nearest neighbor metal atoms and possibly its next-nearest neighbor atoms, thereby modifying their abilities to adsorb and/or dissociate reactant molecules (in this case H_2 and ethylene molecules), although these effects do not extend beyond about 5 atomic units [21]. A third effect may be the restructuring of the surface by the strongly adsorbed poison, possibly causing dramatic changes in catalytic properties, especially for reactions sensitive to surface structure. In addition, the adsorbed poison blocks access of adsorbed reactants to each other (a fourth effect) and finally prevents or slows the surface diffusion of adsorbed reactants (effect number five).

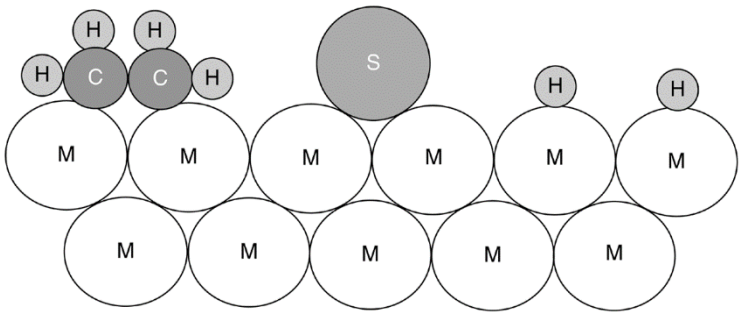

Figure 1. Conceptual model of poisoning by sulfur atoms of a metal surface during ethylene hydrogenation. Reproduced from [8]. Copyright 2006, Wiley-Interscience.

Catalyst poisons can be classified according to their chemical makeup, selectivity for active sites, and the types of reactions poisoned. Table 2 lists four groups of catalyst poisons classified according to chemical origin and their type of interaction with metals. It should be emphasized that interactions of Group VA–VIIA elements with catalytic metal phases depend on the oxidation state of the former, e.g., how many electron pairs are available for bonding and the degree of shielding of the sulfur ion by ligands [16]. Thus, the order of decreasing toxicity for poisoning of a given metal by different sulfur species is H_2S, SO_2, SO_4^{2-}, *i.e.*, in the order of increased shielding by oxygen. Toxicity also increases with increasing atomic or molecular size and electronegativity, but decreases if the poison can be gasified by O_2, H_2O, or H_2 present in the reactant stream [21]; for example, adsorbed carbon can be gasified by O_2 to CO or CO_2 or by H_2 to CH_4.

Table 2. Common poisons classified according to chemical structure.

Chemical type	Examples	Type of interaction with metals
Groups VA and VIA	N, P, As, Sb, O, S, Se, Te	Through *s* and *p* orbitals; shielded structures are less toxic
Group VIIA	F, Cl, Br, I	Through *s* and *p* orbitals; formation of volatile halides
Toxic heavy metals and ions	As, Pb, Hg, Bi, Sn, Cd, Cu, Fe	Occupy *d* orbitals; may form alloys
Molecules that adsorb with multiple bonds	CO, NO, HCN, benzene, acetylene, other unsaturated hydrocarbons	Chemisorption through multiple bonds and back bonding

Table 3 lists a number of common poisons for selected catalysts in important representative reactions. It is apparent that organic bases (e.g., amines) and ammonia are common poisons for acidic solids, such as silica–aluminas and zeolites in cracking and hydrocracking reactions, while sulfur- and arsenic-containing compounds are typical poisons for metals in hydrogenation, dehydrogenation, and steam reforming reactions. Metal compounds (e.g., of Ni, Pb, V, and Zn) are poisons in automotive emissions control, catalytic cracking, and hydrotreating. Acetylene is a poison for ethylene oxidation, while asphaltenes are poisons in hydrotreating of petroleum residuum.

Table 3. Poisons for selected catalysts in important representative reactions.

Catalyst	Reaction	Poisons
Silica–alumina, zeolites	Cracking	Organic bases, hydrocarbons, heavy metals
Nickel, platinum, palladium	Hydrogenation/dehydrogenation	Compounds of S, P, As, Zn, Hg, halides, Pb, NH_3, C_2H_2
Nickel	Steam reforming of methane, naphtha	H_2S, As
Iron, ruthenium	Ammonia synthesis	O_2, H_2O, CO, S, C_2H_2, H_2O
Cobalt, iron	Fischer–Tropsch synthesis	H_2S, COS, As, NH_3, metal carbonyls
Noble metals on zeolites	Hydrocracking	NH_3, S, Se, Te, P
Silver	Ethylene oxidation to ethylene oxide	C_2H_2
Vanadium oxide	Oxidation/selective catalytic reduction	As/Fe, K, Na from fly ash
Platinum, palladium	Oxidation of CO and hydrocarbons	Pb, P, Zn, SO_2, Fe
Cobalt and molybdenum sulfides	Hydrotreating of residuum	Asphaltenes, N compounds, Ni, V

Poisoning selectivity is illustrated in Figure 2, a plot of activity (the reaction rate normalized to initial rate) *versus* normalized poison concentration. “Selective” poisoning involves preferential adsorption of the poison on the most active sites at low concentrations. If sites of lesser activity are blocked initially, the poisoning is “antiselective”. If the activity loss is proportional to the

concentration of adsorbed poison, the poisoning is "nonselective." An example of selective poisoning is the deactivation of platinum by CO for the para-H_2 conversion (Figure 3a) [24] while Pb poisoning of CO oxidation on platinum is apparently antiselective (Figure 3b) [25], and arsenic poisoning of cyclopropane hydrogenation on Pt is nonselective (Figure 3c) [26]. For nonselective poisoning, the linear decrease in activity with poison concentration or susceptibility (σ) is defined by the slope of the activity *versus* poison concentration curve. Several other important terms associated with poisoning are defined in Table 4. Poison tolerance, the activity at saturation coverage of the poison, and resistance (the inverse of deactivation rate) are important concepts that are often encountered in discussions of poisoning including those below.

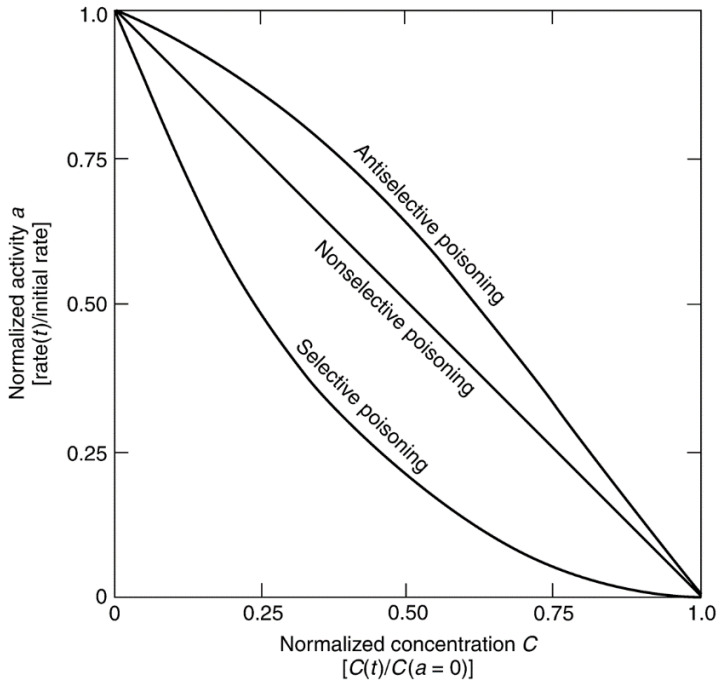

Figure 2. Three kinds of poisoning behavior in terms of normalized activity *versus* normalized poison concentration. Reproduced from [8]. Copyright 2006, Wiley-Interscience.

Table 4. Important Poisoning Parameters.

Parameter	Definition
Activity (a)	Reaction rate at time t relative to that at $t = 0$
Susceptibility (σ)	Negative slope of the activity *versus* poison concentration curve [$\sigma = (a - 1)/C(t)$]. Measure of a catalyst's sensitivity to a given poison
Toxicity	Susceptibility of a given catalyst for a poison relative to that for another poison
Resistance	Inverse of the deactivation rate. Property that determines how rapidly a catalyst deactivates
Tolerance ($a(C_{sat})$)	Activity of the catalyst at saturation coverage (some catalysts may have negligible activity at saturation coverage)

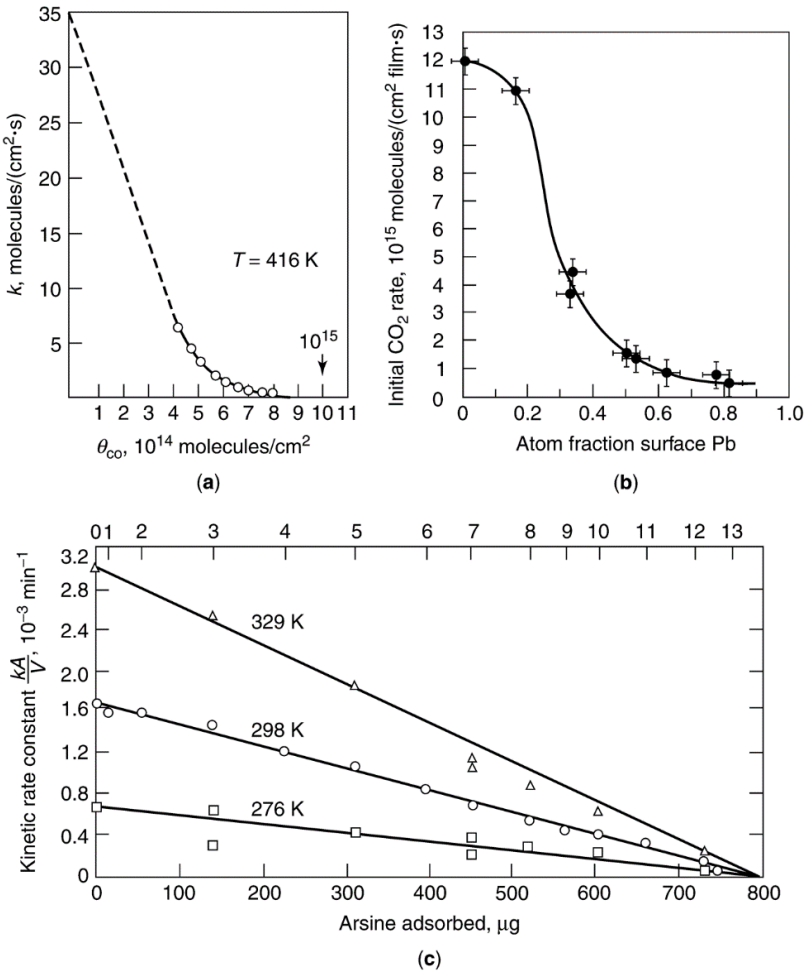

Figure 3. (**a**) CO poisoning of para-H_2 conversion over a Pt foil, reproduced from [24], copyright 1974, Wiley-VHC; (**b**) effect of lead coverage on the rate of CO oxidation of Pt film, reproduced from [25], copyright 1978, Elsevier; (**c**) rate constants of cyclopropane hydrogenolysis over a Pt film as a function of the amount of AsH_3 adsorbed, reproduced from [26], copyright 1970, Elsevier.

The activity *versus* poison concentration patterns illustrated in Figure 2 are based on the assumption of uniform poisoning of the catalyst surface and surface reaction rate controlling, *i.e.*, negligible pore-diffusional resistance. These assumptions, however, are rarely met in typical industrial processes because the severe reaction conditions of high temperature and high pressure bring about a high pore-diffusional resistance for either the main or poisoning reaction or both. In physical terms, this means that the reaction may occur preferentially in the outer shell of the catalysts particle, or that poison is preferentially adsorbed in the outer shell of the catalyst particle, or both. The nonuniformly distributed reaction and/or poison leads to nonlinear activity *versus* poison concentration curves that mimic the patterns in Figure 2 but do not represent truly selective or antiselective poisoning. For example, if the main reaction is limited to an outer shell in a pellet where poison is concentrated, the drop in activity with concentration will be precipitous. Pore diffusional effects in poisoning (nonuniform poison) are treated later in this review.

As sulfur poisoning is a difficult problem in many important catalytic processes (e.g., hydrogenation, methanation, Fischer–Tropsch synthesis, steam reforming, and fuel cell power production), it merits separate discussion as an example of catalyst poisoning phenomena. Studies of sulfur poisoning in hydrogenation and CO hydrogenation reactions have been thoroughly reviewed [8,21,27–31]. Much of the previous work focused on poisoning of nickel metal catalysts by H_2S, the primary sulfur poison in many important catalytic processes, and thus provides some useful case studies of poisoning.

Previous adsorption studies [28–30] indicate that H_2S adsorbs strongly and dissociatively on nickel metal surfaces. The high stability and low reversibility of adsorbed sulfur is illustrated by the data in Figure 4 [28], in which most of the previous equilibrium data for nickel are represented on a single plot of log (P_{H_2S}/P_{H_2}) *versus* reciprocal temperature. The solid line corresponds to the equilibrium data for formation of bulk Ni_3S_2. Based on the equation $\Delta G = RT \ln(P_{H_2S}/P_{H_2}) = \Delta H - T\Delta S$, the slope of this line is $\Delta H/R$, where $\Delta H = -75$ kJ/mol and the intercept is $-\Delta S/R$. Most of the adsorption data lie between the dashed lines corresponding to $\Delta H = -125$ and -165 kJ/mol for coverages ranging from 0.5 to 0.9, indicating that adsorbed sulfur is more stable than the bulk sulfide. Indeed, extrapolation of high temperature data to zero coverage using a Tempkin isotherm [29] yields an enthalpy of adsorption of −250 kJ/mol; in other words, at low sulfur coverages, surface nickel–sulfur bonds are a factor of 3 more stable than bulk nickel–sulfur bonds. It is apparent from Figure 4 that the absolute heat of adsorption increases with decreasing coverage and that the equilibrium partial pressure of H_2S increases with increasing temperature and increasing coverage. For instance, at 725 K (450 °C) and $\theta = 0.5$, the values of P_{H_2S}/P_{H_2} range from about 10^{-8} to 10^{-9}. In other words, half coverage occurs at 1–10 ppb H_2S, a concentration range at the lower limit of our present analytical capability. At the same temperature (450 °C), almost complete coverage ($\theta > 0.9$) occurs at values of P_{H_2S}/P_{H_2} of 10^{-7}–10^{-6} (0.1–1 ppm) or at H_2S concentrations encountered in many catalytic processes after the gas has been processed to remove sulfur compounds. These data are typical of sulfur adsorption on most catalytic metals. Thus, we can expect that H_2S (and other sulfur impurities) will adsorb essentially irreversibly to high coverage in most catalytic processes involving metal catalysts.

Two important keys to reaching a deeper understanding of poisoning phenomena include (1) determining surface structures of poisons adsorbed on metal surfaces and (2) understanding how surface structure and hence adsorption stoichiometry change with increasing coverage of the poison. Studies of structures of adsorbed sulfur on single crystal metals (especially Ni) [3,28,32–38] provide such information. They reveal, for example, that sulfur adsorbs on Ni(100) in an ordered p(2 × 2) overlayer, bonded to four Ni atoms at $S/Ni_s < 0.25$ and in a c(2 × 2) overlayer to two Ni atoms for $S/Ni_s = 0.25$–0.50 (see Figure 5; Ni_s denotes a surface atom of Ni); saturation coverage of sulfur on Ni(100) occurs at $S/Ni_s = 0.5$. Adsorption of sulfur on Ni(110), Ni(111), and higher index planes of Ni is more complicated; while the same p(2 × 2) structure is observed at low coverage, complex overlayers appear at higher coverages—for example, at $S/Ni_s > 0.3$ on Ni(111) a $(5\sqrt{3}\times 2)$S overlayer is formed [32–34]. In more open surface structures, such as Ni(110) and Ni(210), saturation coverage occurs at $S/Ni_s = 0.74$ and 1.09 respectively; indeed, there is a trend of increasing S/Ni_s with decreasing planar density and increasing surface roughness for Ni, while the saturation sulfur concentration remains constant at 44 ng/cm^2 Ni (see Table 5).

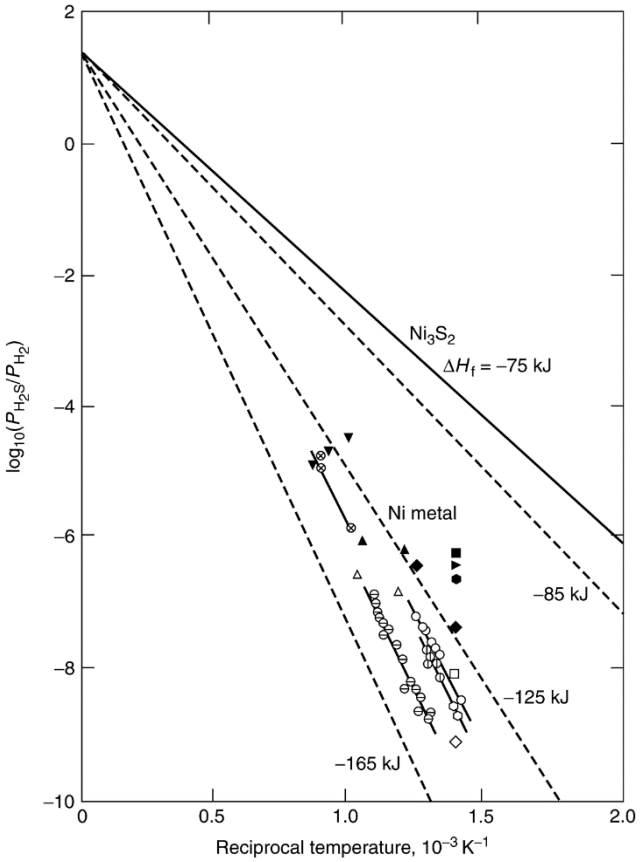

Figure 4. Equilibrium partial pressure of H_2S *versus* reciprocal temperature (values of ΔH_f based on 1 mole of H_2S); open symbols: θ = 0.5–0.6; closed symbols: θ = 0.8–0.9. Reproduced from [28]. Copyright 1982, Academic Press.

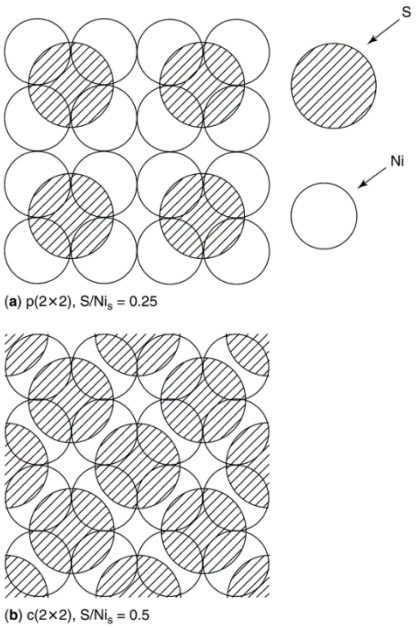

Figure 5. Schematic view of sulfur adsorbed on a Ni(100) surface at a (**a**) $S/Ni_s = 0.25$ in a p(2 × 2) structure and (**b**) $S/Ni_s = 0.50$ in a c(2 × 2) structure. Reproduced from [39]. Copyright 2001, Elsevier.

Table 5. Sulfur Adsorption Densities on Various Crystal Faces of Nickel [a].

Crystal face	Sulfur conc. at saturation, ng·S/cm^2	Number of S atoms/cm^2 ($\times 10^{15}$)	Number of Ni atoms/cm^2 ($\times 10^{15}$)	S atoms per surface Ni atom
(111)	47 ± 1	0.86	1.8	0.48
(100)	43 ± 1	0.80	1.6	0.50
(110)	44.5 ± 1	0.82	1.1	0.74
(210)	42 ± 1	0.78	0.72	1.09
Polycrystalline	44.5 ± 1	0.82	—	—

[a] Data from [35].

Reported saturation stoichiometries for sulfur adsorption on polycrystalline and supported Ni catalysts (S/Ni_s) vary from 0.25 to 1.3 [28]. The values of saturation coverage greater than $S/Ni_s = 0.5$ may be explained by (1) a higher fractional coverage of sites of lower coordination number, *i.e.*, atoms located on edges or corners of rough, high-index planes (Table 5); (2) enhanced adsorption capacity at higher gas phase concentrations of H_2S in line with the observed trend of increasing saturation coverage with increasing H_2S concentration in Figure 4; and/or (3) reconstruction of planar surfaces to rougher planes by adsorbed sulfur at moderately high coverages and adsorption temperatures.

The first effect would be favored, and in fact is observed, for supported metals of higher dispersion [28]. The second effect may explain the typically lower observed values of S/Ni_s for single crystal Ni, which are measured at extremely low pressures (high vacuum) relative to the higher values of S/Ni_s for polycrystalline and supported Ni, typically measured at orders of magnitude higher pressure; thus, in the case of the single crystal studies, the surface is not in equilibrium with gas phase H_2S/H_2.

The third effect, reconstruction of nickel surfaces by adsorbed sulfur, has been reported by a number of workers [28,32,33,36–38]; for example, McCarroll and co-workers [37,38] found that sulfur adsorbed at near saturation coverage on a Ni(111) face was initially in a hexagonal pattern, but upon heating above 700 K reoriented to a distorted c(2 × 2) (100) overlayer. Oudar [36] reported that sulfur adsorbed on a Ni(810) surface caused decomposition to (100) and (410) facets. During adsorption of H_2S at RT, Ruan *et al.* [33] observed surface restructuring of Ni(111) from a p(2 × 2) at low coverage to a missing-row $(5\sqrt{3}\times 2)S$ terrace structure (0.4 monolayer) sparsely covered with small, irregular islands composed of sulfur adsorbed on disordered nickel; upon annealing to 460 K for 5 min, the islands ordered to the $(5\sqrt{3}\times 2)S$ phase and their size increased, suggesting further diffusion of Ni atoms from the terraces. The reconstruction of Ni (111) involving ejection and migration of Ni atoms was attributed to compressive surface stresses induced by sulfur adsorption; the role of compressive surface stress due to sulfur coverages exceeding 0.3 was confirmed by Grossmann *et al.* [32]. From these and similar studies, it is concluded that at moderately high temperatures (300–600 K) and coverages greater than 0.3, restructuring by sulfur of different facets of Ni to rougher, more open, stable structures is probably a general phenomenon. Thus, reconstruction probably accounts at least in part for observed increases in saturation S coverage with decreasing Ni site density.

The nature of reconstruction of a surface by a poison may depend on its pretreatment. For example, in a scanning tunneling microscopy (STM) study of room temperature H_2S adsorption on Ni(110), Ruan and co-workers [40] found that the S/Ni structure at saturation varied with the initial state of the

surface, *i.e.*, whether clean or oxygen covered. Beginning with a clean Ni(110) surface, oxygen adsorbs dissociatively to form a (2 × 1)O overlayer at 1/2 monolayer coverage (Figure 6a); this is accompanied by a homogeneous nucleation of low-coordinated -Ni-O- rows along the [001] direction. As the oxygen-covered surface is exposed stepwise to 3 and then 8 Langmuirs (L) of H_2S, oxygen atoms are removed by reaction with hydrogen to water; the surface is first roughened, after which white islands and black troughs having a c(2 × 2) structure are formed as sulfur atoms replace oxygen atoms (Figure 6b). Upon exposure to 25 L of H_2S, the c(2 × 2) islands dissolve, while low-coordinated rows (periodicity of 1) form in the [001] direction, developing into ordered regions with a periodicity of 4 in the [1 $\bar{1}$ 0] direction (Figure 6c). After exposure to 50 L of H_2S (Figure 6d), a stable, well-ordered (4 × 1)S structure appears, a surface clearly reconstructed relative to the original Ni(110). Moreover, the reconstructed surface in Figure 6d is very different from that observed upon direct exposure of the Ni(110) to H_2S at room temperature, *i.e.*, a c(2 × 2)S overlying the original Ni(110) (similar to Figure 5b); in other words, it appears that no reconstruction occurs by direct exposure to H_2S at room temperature, rather only in the presence of O_2 (or air). This emphasizes the complexities inherent in predicting the structure and stability of a given poison adsorbed on a given catalyst during a specified reaction as a function of different pretreatments or process disruptions, e.g., exposure to air.

In the previous discussion of Figure 4, $-\Delta H_{ads}$ was observed to decrease with increasing sulfur coverage; data in Figure 7 [41] show that $-\Delta H_{ads}$ decreases with increasing gas-phase H_2S concentration and coverage. However, in contrast to the data in Figure 4, those in Figure 7 [41] show that at very high H_2S concentrations and high adsorption temperatures, $-\Delta H_{ads}$ falls well below the $-\Delta H_{formation}$ of bulk Ni_3S_2; at the same time, the S/Ni_s ratio approaches that of Ni_2S_3. This is a unique result, since all of the data obtained at lower temperatures and H_2S concentrations [28] show $-\Delta H_{ads}$ to be greater than $-\Delta H_{formation}$ of Ni_3S_2.

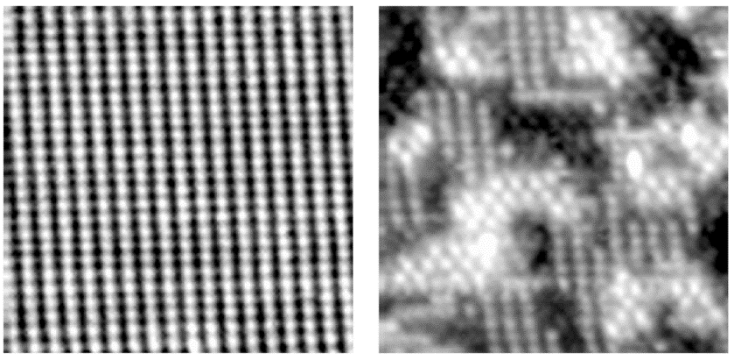

Figure 6. *Cont.*

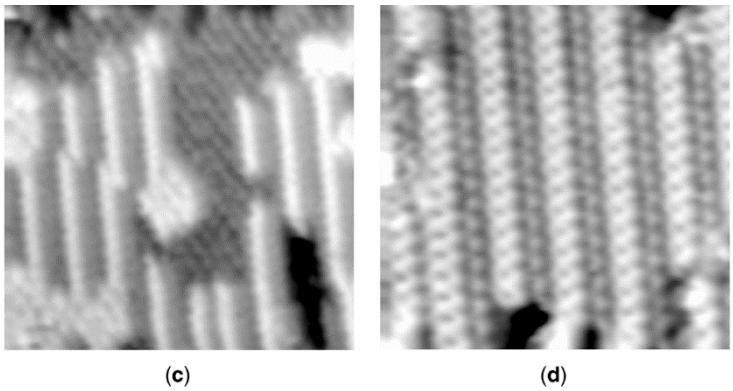

Figure 6. A series of *in situ* scanning tunneling microscope (STM) images recorded after exposure of Ni(110) to oxygen and then progressively higher exposures of H_2S: (**a**) (2 × 1)O overlayer; (**b**) white islands and black troughs with a c(2 × 2)S structure after exposure to 3 and 8 L of H_2S; (**c**) 25 L, islands transform to low-coordinated rows in the [001] direction; and (**d**) 50 L, stable, well-ordered (4 × 1)S. Reproduced from [40]. Copyright 1992, American Physical Society.

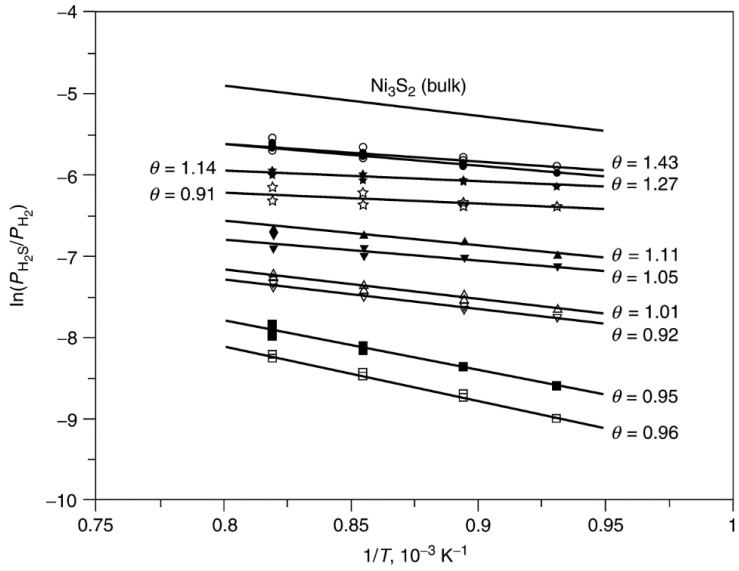

Figure 7. Sulfur chemisorption isosteres on a Ni/α-Al_2O_3 catalyst at high temperatures and high H_2S concentrations. Reproduced from [41]. Copyright 1999,Elsevier.

From the above discussion, the structure and stoichiometry of sulfur adsorbed on nickel evidently are complex functions of temperature, H_2S concentration, sulfur coverage, and pretreatment, phenomena that account at least in part for the complex nature of nickel poisoning by sulfur. Could one expect similar complexities in the poisoning of other metals? Probably, since poisoning of nickel is prototypical, *i.e.*, similar principles operate and similar poisoning behaviors are observed in other poison/metal systems, although none have been studied to the same depth as sulfur/nickel.

Since one of the necessary steps in a catalytic reaction is the adsorption of one or more reactants, investigation of the effects of adsorbed sulfur on the adsorption of other molecules, can provide useful insights into the poisoning process [21,28]. Previous investigations [28,42–48] indicate that both H_2 and CO adsorptions on nickel are poisoned by adsorbed sulfur. For example, thermal desorption

studies of CO from presulfided Ni(100) [44] reveal a weakening of the CO adsorption bond and a rapid, nonlinear decline in the most strongly bound β_2 state (bridged CO) with increasing sulfur coverage, corresponding to a poisoning of about 8–10 Ni atoms for bridged CO adsorption per adsorbed sulfur atom at low sulfur coverage (see Figure 8); moreover, the β_2 CO species is completely poisoned at about 0.2–0.4 mL of sulfur relative to a saturation coverage of 0.5 mL. Hydrogen adsorption is poisoned in a similar nonlinear fashion. On the other hand, the coverage of the β_1 state (linear CO) is constant with increasing sulfur coverage. The sharp nonlinear drop in CO and hydrogen adsorptions at low sulfur coverages has been interpreted in terms of a combination of short-range electronic and steric effects operating over a range of less than 5 atomic units [13]. The different effects of sulfur on β_1 and β_2 states of CO have important implications for sulfur poisoning in reactions involving CO; that is, sulfur poisoning can affect reaction selectivity as well as activity [28].

Because sulfur adsorbs so strongly on metals and prevents or modifies the further adsorption of reactant molecules, its presence on a catalyst surface usually effects substantial or complete loss of activity in many important reactions. This is illustrated by the data in Figure 9 showing the steady-state methanation activities of Ni, Co, Fe, and Ru relative to the fresh, unpoisoned surface activity as a function of gas phase H_2S concentration. These data indicate that Ni, Co, Fe, and Ru all suffer 3–4 orders of magnitude loss in activity at 15–100 ppb of H_2S, *i.e.*, their sulfur tolerances are extremely low. Moreover, the sharp drop in activity with increasing H_2S concentration suggests highly selective poisoning. Nevertheless, the rate of sulfur poisoning and hence sulfur resistance varies from catalyst to catalyst and is apparently a function of catalyst composition [28] and reaction conditions [49]. Indeed, it is possible to significantly improve sulfur resistance of Ni, Co, and Fe with catalyst additives such as Mo and B that selectively adsorb sulfur. Because the adsorption of sulfur compounds is generally rapid and irreversible, surface sulfur concentrations in catalyst particles and beds are nonuniform, e.g., H_2S adsorbs selectively at the entrance to a packed bed and on the outer surface of catalyst particles, making the experimental study and modeling of sulfur poisoning extremely difficult.

There are other complications in the study of sulfur poisoning. For example, the adsorption stoichiometry of sulfur in CO hydrogenation on Ni is apparently a function of the temperature, H_2/CO ratio, and water partial pressure [49]. Moreover, at high CO partial pressures sulfur may be removed from the surface as COS, which is not as strongly adsorbed as H_2S. At low temperature conditions, e.g., those representative of Fischer–Tropsch synthesis or liquid phase hydrogenations, the gas phase concentration of H_2S in poisoning studies must be kept very low, *i.e.*, below 0.1–5 ppm, to avoid formation of bulk metal sulfides—a phenomenon that seriously compromises the validity of the results. Thus, the importance of studying poisoning phenomena *in situ* under realistic reaction conditions, at low process-relevant poison concentrations, and over a process-representative range of temperature and concentration conditions is emphasized.

As mentioned earlier, there are a number of industrial processes in which one intentionally poisons the catalyst in order to improve its selectivity. For example, Pt-containing naphtha reforming catalysts are often pre-sulfided to minimize unwanted cracking reactions. On basic Pt/KL zeolite catalysts, these short term, low concentration exposures are beneficial to produce Pt ensemble sizes that promote aromatization, while longer term or higher concentration exposures poison the catalyst both by forming Pt-S bonds and producing large crystallites that block pores, as shown by transmission electron microscopy (TEM) and X-ray absorption fine structure spectroscopy (EXAFS), and favor only

dehydrogenation [50–53]. Other examples are sulfur added to Fischer-Tropsch catalysts that have been reported to have either beneficial or negligibly harmful effects, which are important considerations in setting the minimum gas clean-up requirements [27,30,54–56]. S and P are added to Ni catalysts to improve isomerization selectivity in the fats and oils hydrogenation industry, while S and Cu are added to Ni catalysts in steam reforming to minimize coking. In catalytic reforming, sulfided Re or Sn is added to Pt to enhance the dehydrogenation of paraffins to olefins while poisoning hydrogenolysis/coking reactions. V_2O_5 is added to Pt to suppress SO_2 oxidation to SO_3 in diesel emissions control catalysts.

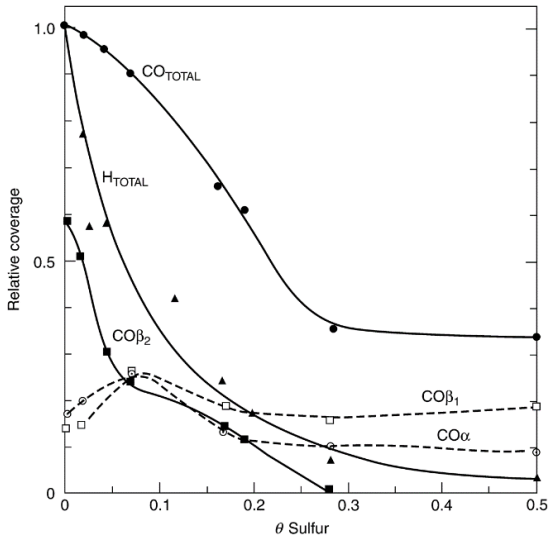

Figure 8. Area under thermal programmed desorption spectra for H_2 and the α, β_1, β_2, and total CO adsorption curves, as a function of sulfur precoverage. Reproduced from [44]. Copyright 1981, Elsevier.

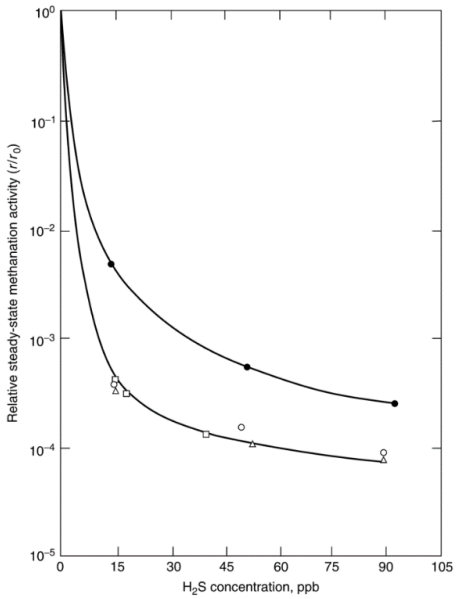

Figure 9. Relative steady-state methanation activity profiles for Ni (●), Co (Δ), Fe (○), and Ru (□) as a function of gas-phase H_2S concentration. Reaction conditions: 100 kPa, 400 °C, 1% CO/99% H_2 for Co, Fe, and Ru, 4% CO/96% H_2 for Ni. Reproduced from [28]. Copyright 1982, Academic Press.

2.2. Fouling, Coking, and Carbon Deposition

2.2.1. Fouling

Fouling is the physical (mechanical) deposition of species from the fluid phase onto the catalyst surface, which results in activity loss due to blockage of sites and/or pores. In its advanced stages, it may result in disintegration of catalyst particles and plugging of the reactor voids. Important examples include mechanical deposits of carbon and coke in porous catalysts, although carbon- and coke-forming processes also involve chemisorption of different kinds of carbons or condensed hydrocarbons that may act as catalyst poisons. The definitions of carbon and coke are somewhat arbitrary and by convention related to their origin. Carbon is typically a product of CO disproportionation while coke is produced by decomposition or condensation of hydrocarbons on catalyst surfaces and typically consists of polymerized heavy hydrocarbons. Nevertheless, coke forms may vary from high molecular weight hydrocarbons to primarily carbons such as graphite, depending upon the conditions under which the coke was formed and aged. A number of books and reviews treat the formation of carbons and coke on catalysts and the attendant deactivation of the catalysts [1,4,57–62].

The chemical structures of cokes or carbons formed in catalytic processes vary with reaction type, catalyst type, and reaction conditions. Menon [62] suggested that catalytic reactions accompanied by carbon or coke formation can be broadly classified as either coke-sensitive or coke-insensitive, analogous to Boudart's more general classification of structure-sensitive and structure-insensitive catalytic reactions. In coke-sensitive reactions, unreactive coke is deposited on active sites, leading to activity decline, while in coke-insensitive reactions, relatively reactive coke precursors formed on active sites are readily removed by hydrogen (or other gasifying agents). Examples of coke-sensitive reactions include catalytic cracking and hydrogenolysis; on the other hand, Fischer–Tropsch synthesis, catalytic reforming, and methanol synthesis are examples of coke-insensitive reactions. On the basis of this classification, Menon [62] reasoned that the structure and location of a coke are more important than its quantity in affecting catalytic activity.

Consistent with Menon's classification, it is also generally observed that not only structure and location of coke vary but also its mechanism of formation varies with catalyst type, e.g., whether it is a metal or metal oxide (or sulfide, sulfides being similar to oxides). Because of these significant differences in mechanism, formation of carbon and coke is discussed below separately for supported metals and for metal oxides and sulfides.

2.2.2. Carbon and Coke Formation on Supported Metal Catalysts

Possible effects of fouling by carbon (or coke) on the functioning of a supported metal catalyst are illustrated in Figure 10. Carbon may (1) chemisorb strongly as a monolayer or physically adsorb in multilayers and in either case block access of reactants to metal surface sites, (2) totally encapsulate a metal particle and thereby completely deactivate that particle, and (3) plug micro- and mesopores such that access of reactants is denied to many crystallites inside these pores. Finally, in extreme cases, strong carbon filaments may build up in pores to the extent that they stress and fracture the support material, ultimately causing the disintegration of catalyst pellets and plugging of reactor voids. For example, in steam methane reforming (SMR) catalysts, which are typically nickel supported on alumina

with alkaline earth oxides, the carbon can diffuse through and begin to grow filaments from the back side of the nickel particles (structural type 3 in Table 6) especially at high reaction temperatures and low steam to methane ratios, which push the nickel particles off the support surface. Thermal or mechanical shock can then cause the carbon filaments to fall off the support, thus permanently deactivating the catalyst [8,60]. However, the behavior is complex because for other reaction conditions and other metals, the filaments may grow from the top surface of the metal particles or the carbon may diffuse into the metal and form bulk carbides [8].

An example of recent interest for biomass reactions that points to the complex interaction between the active metal and the support during carbon deposition is the steam reforming of light alcohols and other oxygenates, in which deactivation occurs primarily through coking. For traditional SMR catalysts (e.g., $Ni/MgAl_2O_4$) the coke is believed to originate primarily from alkene formation [63,64]. However, for the case of Ni/La_2O_3 catalysts, carbon appears to form at the interface between the active metal and the support to block the active phase [65].

Mechanisms of carbon deposition and coke formation on metal catalysts from carbon monoxide and hydrocarbons, including methane during SMR for hydrogen production [4,57–61], are illustrated in Figures 11 and 12. Different kinds of carbon and coke that vary in morphology and reactivity are formed in these reactions (see Tables 6 and 7). For example, CO dissociates on metals to form C_α, an adsorbed atomic carbon; C_α can react to C_β, a polymeric carbon film. The more reactive, amorphous forms of carbon formed at low temperatures (e.g., C_α and C_β) are converted at high temperatures over a period of time to less reactive, graphitic forms [60]

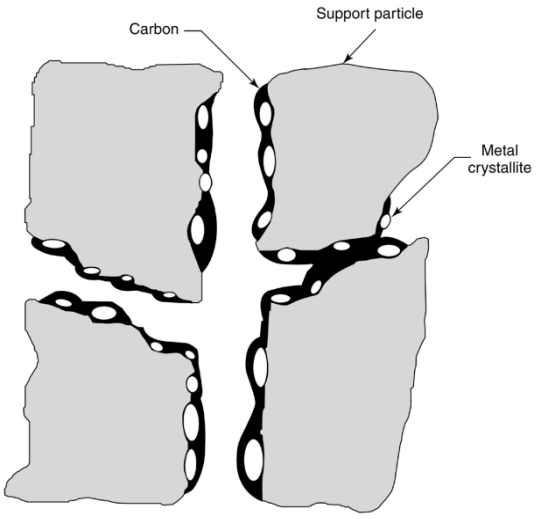

Figure 10. Conceptual model of fouling, crystallite encapsulation, and pore plugging of a supported metal catalyst owing to carbon deposition. Reproduced from [8]. Copyright 2006, Wiley-Interscience.

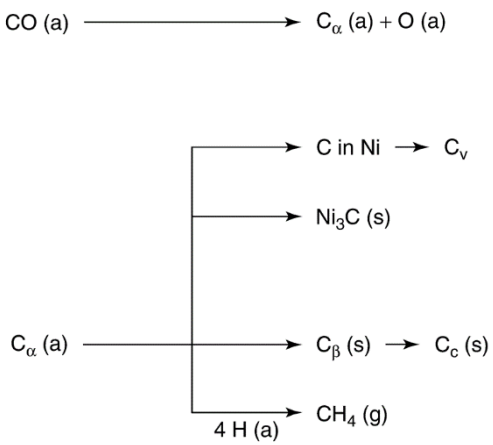

Figure 11. Formation, transformation, and gasification of carbon on nickel (a, g, s refer to adsorbed, gaseous, and solid states respectively). Reproduced from [60]. Copyright 1983, Elsevier.

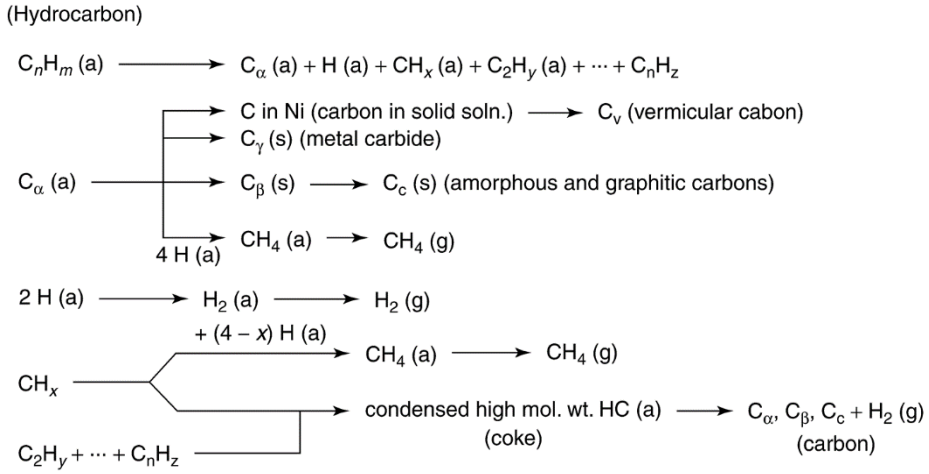

Figure 12. Formation and transformation of coke on metal surfaces (a, g, s refer to adsorbed, gaseous, and solid states respectively); gas phase reactions are not considered. Reproduced from [60]. Copyright 1983, Elsevier.

Table 6. Forms and Reactivities of Carbon Species Formed by Decomposition of CO on Nickel [a].

Structural type	Designation	Temp. formed, °C	Peak temp. for reaction with H_2, °C
1. Adsorbed, atomic (surface carbide)	C_α	200–400	200
2. Polymeric, amorphous films or filaments	C_β	250–500	400
3. Vermicular filaments, fibers, and/or whiskers	C_v	300–1000	400–600
4. Nickel carbide (bulk)	Cγ	150–250	275
5. Graphitic (crystalline) platelets or films	C_c	500–550	550–850

[a] Ref. [60].

Table 7. Carbon Species Formed in Steam Reforming of Hydrocarbons on Nickel Catalysts [a].

Attribute	Encapsulating film	Whisker-like	Pyrolytic carbon
Formation	Slow polymerization of C_nH_m radicals on Ni surface, into encapsulating film	Diffusion of C through Ni crystal, nucleation and whisker growth with Ni crystal at top	Thermal cracking of hydrocarbon; deposition of C precursors on catalyst
Effects	Progressive deactivation	No deactivation of Ni surface. Breakdown of catalyst and increasing ΔP	Encapsulation of catalyst particle; deactivation and increasing ΔP
Temp. range, °C	<500	>450	>600
Critical parameters	Low temperature, low H_2O/C_nH_m, low H_2/C_nH_m, aromatic feed	High temperature, low H_2O/C_nH_m, no enhanced H_2O adsorption, low activity, aromatic feed	High temperature, high void fraction, low H_2O/C_nH_m, high pressure, acidic catalyst

[a] Ref. [60].

It should also be emphasized that some forms of carbon result in loss of catalytic activity and some do not. For example, at low reaction temperatures (<300–375 °C) condensed polymer or β-carbon films and at high temperatures (>650 °C) graphitic carbon films encapsulate the metal surfaces of methanation and steam reforming catalysts [60]. Deactivation of steam reforming catalysts at high reaction temperatures (500–900 °C) may be caused by precipitation of atomic (carbidic) carbon dissolved in the Ni surface layers to a depth of more than 50–70 nm [62,66]. If it accumulates on the metal surface (at high or low temperatures), adsorbed atomic carbon can deactivate metal sites for adsorption and/or reaction. For example, Durer and co-workers [67] demonstrated that carbon atoms residing in the fourfold hollow sites of Rh(100) block the adsorption of hydrogen (and hence could block sites for hydrogenation). In the intermediate temperature range of 375–650 °C, carbon filaments (Figure 13) are formed by precipitation of dissolved carbon at the rear side of metal crystallites, causing the metal particles to grow away from the support [57]. Filament growth ceases when sufficient carbon accumulates on the free surface to cause encapsulation by a carbon layer; however, encapsulation of the metal particles does not occur if H_2/CO or H_2O/hydrocarbon ratios are sufficiently high. Thus, carbon filaments sometimes formed in CO hydrogenation or steam reforming of hydrocarbons would not necessarily cause a loss of intrinsic catalyst activity unless they are formed in sufficient quantities to cause plugging of the pores [60] or loss of metal occurs as the carbon fibers are removed during regeneration [68,69]. However, in practice, regions of carbon forming potential in steam reforming must be carefully avoided, since once initiated, the rates of filamentous carbon formation are sufficiently high to cause catastrophic pore plugging and catalyst failure within a few hours to days.

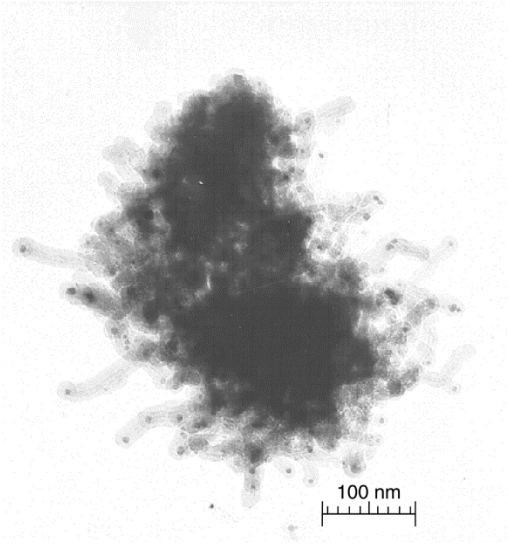

Figure 13. Electron micrograph of 14% Ni/Al_2O_3 having undergone extensive carbon deposition during CO disproportionation at 673 K, P_{CO} = 4.55 kPa (magnification of 200,000). Courtesy of the BYU Catalysis Laboratory.

The rate at which deactivation occurs for a given catalyst and reaction depends greatly on reaction conditions—especially temperature and reactant composition. A fundamental principle for coke-insensitive reactions on metals (e.g., methanation, Fischer–Tropsch synthesis, steam reforming, catalytic reforming, and methanol synthesis) is that deactivation rate depends greatly on the difference in rates of formation and gasification of carbon/coke precursors, *i.e.*, $r_d = r_f - r_g$. If the rate of gasification, r_g, is equal to or greater than that of formation, r_f, carbon/coke is not deposited. Rates of carbon/coke precursor formation and gasification both increase exponentially with temperature, although the difference between them varies a great deal with temperature because of differences in preexponential factors and activation energies. Thus, carbon/coke formation is avoided in regions of temperature in which precursor gasification rate exceeds deposition rate. This is illustrated in Figure 14, an Arrhenius plot for rates of formation and hydrogenation of alpha and beta carbons on nickel during CO methanation. Since at temperatures below 600 K ($1/T > 1.66 \times 10^{-3}$ K^{-1}) the rate of C_α gasification exceeds that of C_α formation, no carbon is deposited. However above 600 K, C_α accumulates on the surface since the rate of C_α formation exceeds that of C_α gasification. As C_α accumulates (at 600–700 K), it is converted to a C_β polymeric chain or film that deactivates the nickel catalyst; however, above 700 K ($1/T < 1.43 \times 10^{-3}$ K^{-1}), the rate of C_β hydrogenation exceeds that of formation and no deactivation occurs. Thus, the "safe" regions of methanation for avoiding deactivation by carbon are below 600 K and above 700 K; of course, these regions will vary somewhat with reactant concentrations and catalyst activity. A similar principle operates in steam reforming, *i.e.*, at a sufficiently low reaction temperature, the rate of hydrocarbon adsorption exceeds the rate of hydrocracking and a deactivating polymer film is formed [70]; accordingly, it is necessary to operate above this temperature to avoid deactivation.

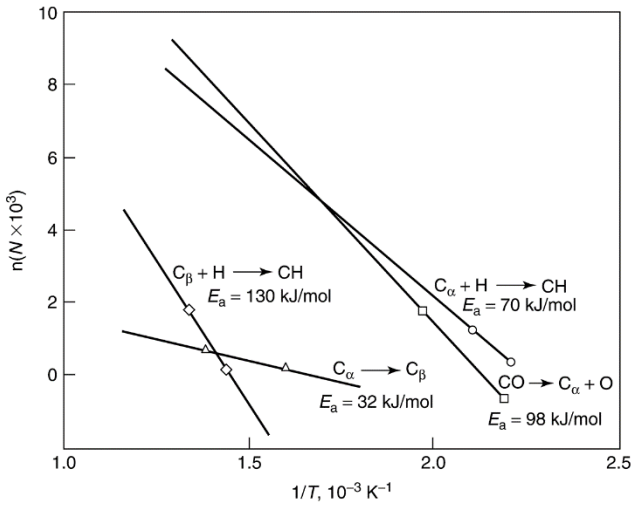

Figure 14. Rates of formation (log scale) and hydrogenation of C_α and C_β *versus* reciprocal temperature. Reproduced from [60]. Copyright 1983, Elsevier.

In steam reforming, filamentous carbon formation rate is a strong function of reactant hydrocarbon structure; for example, it decreases in the order acetylenes, olefins, paraffins, *i.e.*, in order of decreasing reactivity, although activation energies for nickel are in the same range (125–139 kJ) independent of hydrocarbon structure and about the same as those observed for formation of filamentous carbon from decomposition of CO [60]. This latter observation suggests that the reactions of CO and different hydrocarbons to filamentous carbon proceed by a common mechanism and rate-determining step—probably the diffusion of carbon through the metal crystallites [60].

The rate at which a carbon or coke is accumulated in a given reaction under given conditions can vary significantly with catalyst structure, including metal type, metal crystallite size, promoter, and catalyst support. For example, supported Co, Fe, and Ni are active above 350–400 °C for filamentous carbon formation from CO and hydrocarbons; the order of decreasing activity is reportedly Fe > Co > Ni [60]. Pt, Ru, and Rh catalysts, on the other hand, while equally or more active than Ni, Co, or Fe in steam reforming, produce little or no coke or carbon. This is attributed to reduced mobility and/or solubility of carbon in the noble metals, thus retarding the nucleation process. Thus, it is not surprising that addition of noble metals to base metals retards carbon formation; for example, addition of Pt in Ni lowers carbon deposition rate during methanation, while addition of Cu or Au to Ni substantially lowers carbon formation in steam reforming [60,71]. In contrast to the moderating effects of noble metal additives, addition of 0.5% Sn to cobalt substantially increases the rate of carbon filament formation from ethylene [72], an effect desirable in the commercial production of carbon filament fibers.

Since carbon formation and gasification rates are influenced differently by modifications in metal crystallite surface chemistry, which are in turn a function of catalyst structure, oxide additives or oxide supports may be used to moderate the rate of undesirable carbon or coke accumulation. For example, Bartholomew and Strasburg [73] found the specific rate (turnover frequency) of filamentous carbon deposition on nickel during methanation at 350 °C to decrease in the order Ni/TiO_2 > $NiAl_2O_3$ > Ni/SiO_2, while Vance and Bartholomew [74] observed C_α hydrogenation rates at 170 °C to decrease in this same order (the same as for methanation at 225 °C). This behavior was explained in terms of promotional or inhibiting effects due to decoration of metal crystallites by the support, for example

silica, inhibiting both CO dissociation and carbon hydrogenation. This hypothesis is consistent with observations [75,76] that silica evaporated on metal surfaces and supported metals inhibits formation of filamentous carbon. Similarly Bitter and co-workers [77] observed rates of carbon formation in CO_2/CH_4 reforming to decrease in the order $Pt/\gamma\text{-}Al_2O_3 \rightarrow Pt/TiO_2 > Pt/ZrO_2$; while 90% of the carbon deposited on the support, the authors linked deactivation to carbon accumulated on the metal owing to an imbalance between carbon formed by methane dissociation and oxidation by chemisorbed CO_2. The rate of formation of coke in steam reforming is delayed and occurs at lower rates in nickel catalysts promoted with alkali or supported on basic MgO [78].

Since formation of coke, graphite, or filamentous carbon involves the formation of C-C bonds on multiple atoms sites, one might expect that coke or carbon formation on metals is structure-sensitive, *i.e.*, sensitive to surface structure and metal crystallite size. Indeed, Bitter and co-workers [77] found that catalysts containing larger Pt crystallites deactivate more rapidly than those containing small crystallites. Moreover, a crystallite size effect, observed in steam reforming of methane on nickel [60,78], appears to operate in the same direction, *i.e.*, formation of filamentous carbon occurs at lower rates in catalysts containing smaller metal crystallites.

In summary, deactivation of supported metals by carbon or coke may occur chemically, owing to chemisorption or carbide formation, or physically and mechanically, owing to blocking of surface sites, metal crystallite encapsulation, plugging of pores, and destruction of catalyst pellets by carbon filaments. Blocking of catalytic sites by chemisorbed hydrocarbons, surface carbides, or relatively reactive films is generally reversible in hydrogen, steam, CO_2, or oxygen. Further details of the thermodynamics, kinetics, and mechanisms of carbon and coke formation in methanation and steam reforming reactions are available in reviews by Bartholomew [60] and Rostrup-Nielsen [70,78]. In recent reviews addressing deactivation of Co catalysts by carbon during Fischer-Tropsch synthesis [79,80], the same or similar carbon species, e.g., α, β, polymeric, and graphitic carbons, are observed on Co surfaces as on Ni; moreover, poisoning or fouling of the Co surfaces with β, polymeric, and graphitic carbon layers are found to be major causes of deactivation.

2.2.3. Coke Formation on Metal Oxide and Sulfide Catalysts

In reactions involving hydrocarbons, coke may be formed in the gas phase and on both noncatalytic and catalytic surfaces. Nevertheless, formation of coke on oxides and sulfides is principally a result of cracking reactions involving coke precursors (typically olefins or aromatics) catalyzed by acid sites [81,82]. Dehydrogenation and cyclization reactions of carbocation intermediates formed on acid sites lead to aromatics, which react further to higher molecular weight polynuclear aromatics that condense as coke (see Figure 15). Reactions 1–3 in Figure 15 illustrate the polymerization of olefins, reactions 4–8 illustrate cyclization from olefins, and reactions 9–14 illustrate chain reaction formation of polynuclear aromatics that condense as coke on the catalyst surface. Because of the high stability of the polynuclear carbocations (formed in reactions 10–13), they can continue to grow on the surface for a relatively long time before a termination reaction occurs through the back donation of a proton.

From this mechanistic scheme (Figure 15), it is clear that olefins, benzene and benzene derivatives, and polynuclear aromatics are precursors to coke formation. However, the order of reactivity for coke formation is clearly structure dependent, *i.e.*, decreases in the order polynuclear aromatics > aromatics

> olefins > branched alkanes > normal alkanes. For example, the weight percent coke formed on silica–alumina at 500 °C is 0.06, 3.8, 12.5, and 23% for benzene, naphthalene, fluoranthene, and anthracene respectively [83].

Coking reactions in processes involving heavy hydrocarbons are very complex; different kinds of coke may be formed and they may range in composition from CH to C and have a wide range of reactivities with oxygen and hydrogen, depending upon the time on stream and temperature to which they are exposed. For example, coke deposits occurring in hydrodesulfurization of residuum have been classified into three types [84]:

(1) Type I deposits are reversibly adsorbed normal aromatics deposited during the first part of the cycle at low temperature.
(2) Type II deposits are reversibly adsorbed asphaltenes deposited early in the coking process.
(3) Type III deposits result from condensation of aromatic concentrates into clusters and then crystals that constitute a "mesophase." This crystalline phase is formed after long reaction times at high temperature. This hardened coke causes severe deactivation of the catalyst [84].

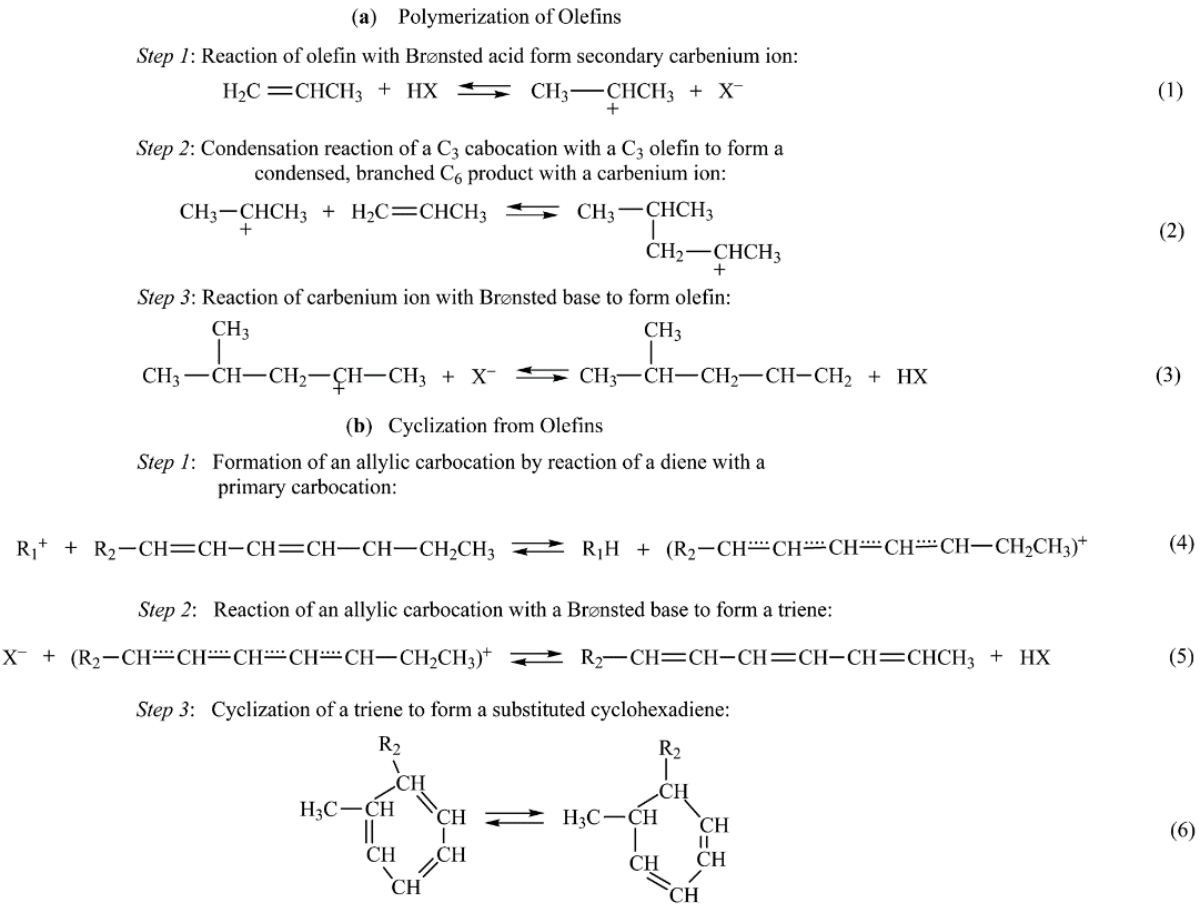

Figure 15. *Cont.*

Step 4: Formation of a tertiary carbocation:

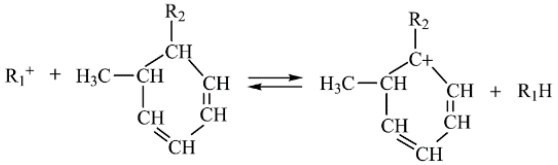

(7)

Step 5: Reaction of a tertiary carbocation with Brønsted base to form substituted benzene:

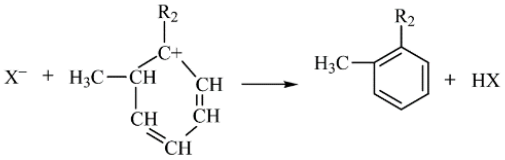

(8)

(**c**) Formation of Polynuclear Aromatics from Benzene

Step 1: Initiation (protonation of benzene):

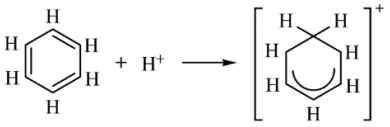

(9)

Step 2: Propagation (condensation reaction of carbocation with benzene, followed by H abstraction):

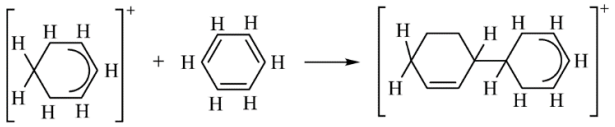

(10)

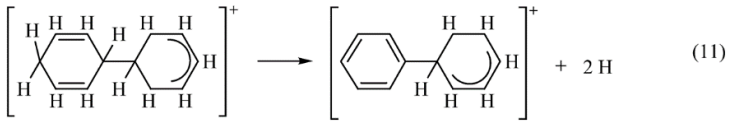

(11)

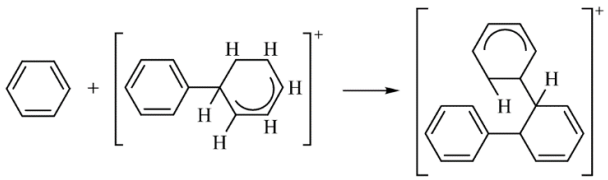

(12)

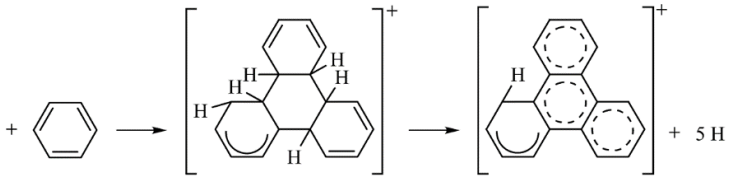

(13)

and so forth.

Step 3: Termination (reaction of carbocation with Brønsted base):

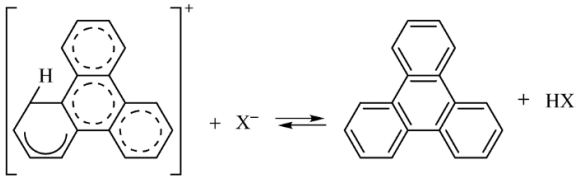

(14)

Figure 15. Coke-forming reactions of alkenes and aromatics on oxide and sulfide catalysts: (**a**) polymerization of alkenes, (**b**) cyclization from alkenes, and (**c**) formation of polynuclear aromatics from benzene. Reproduced from [8], Copyright 2006, Wiley-Interscience.

In addition to hydrocarbon structure and reaction conditions, extent and rate of coke formation are also a function of the acidity and pore structure of the catalyst. Generally, the rate and extent of coke formation increase with increasing acid strength and concentration. Coke yield decreases with decreasing pore size (for a fixed acid strength and concentration); this is especially true in zeolites where shape selectivity plays an important role in coke formation. For example, coke yield in fluid catalytic cracking is only 0.4% for ZSM-5 (pore diameters of 0.54 × 0.56 nm) compared to 2.2% for Y-faujasite (aperture diameter of 0.72 nm) [82]. However, in pores of molecular diameter, a relatively small quantity of coke can cause substantial loss of activity. It should be emphasized that coke yield can vary considerably into the interior pores of a catalyst particle or along a catalyst bed, depending upon the extent to which the main and deactivation reactions are affected by film mass transport and pore diffusional resistance.

The mechanisms by which coke deactivates oxide and sulfide catalysts are, as in the case of supported metals, both chemical and physical. However, some aspects of the chemistry are quite different. The principal chemical loss of activity in oxides and sulfides is due to the strong adsorption of coke molecules on acidic sites. However, as discussed earlier, strong acid sites also play an important role in the formation of coke precursors, which subsequently undergo condensation reactions to produce large polynuclear aromatic molecules that physically coat catalytic surfaces. Physical loss of activity also occurs as coke accumulates, ultimately partially or completely blocking catalyst pores as in supported metal catalysts. For example, in isomerization of *cis*-butene on SiO_2/Al_2O_3 [85] catalyst deactivation occurs by rapid, selective poisoning of strong acid sites; coke evolved early in the reaction is soluble in dichloromethane and pyridine and is slightly aromatic. Apparently, the blocking of active sites does not significantly affect porosity or catalyst surface area, as SiO_2/Al_2O_3 contains relatively large mesopores.

In the case of supported bifunctional metal/metal oxide catalysts, different kinds of coke are formed on the metal and the acidic oxide support, e.g., soft coke (high H/C ratio) on Pt or Pt–Re metals and hard coke (low H/C ratio) on the alumina support in catalytic reforming [86]. In this case, coke precursors may be formed on the metal via hydrogenolysis, following which they migrate to the support and undergo polymerization and cyclization reactions, after which the larger molecules are dehydrogenated on the metal and finally accumulate on the support, causing loss of isomerization activity. Mild sulfiding of these catalysts (especially Pt–Re/alumina) substantially reduces the rate of hydrogenolysis and the overall formation of coke on both metal and support; it especially reduces the hard coke, which is mainly responsible for deactivation.

Several recent studies [82,87–97] have focused on coke formation during hydrocarbon reactions in zeolites including (1) the detailed chemistry of coke precursors and coke molecules formed in zeolite pores and pore intersections (or supercages) and (2) the relative importance of adsorption on acid sites *versus* pore blockage. The principal conclusions from these studies can be summarized as follows: (1) the formation of coke and the manner in which it deactivates a zeolite catalyst are shape-selective processes, (2) deactivation is mainly due to the formation and retention of heavy aromatic clusters in pores and pore intersections, and (3) while both acid-site poisoning and pore blockage participate in the deactivation, the former dominates at low coking rates, low coke coverages (e.g., in Y-zeolite below 2 wt%), and high temperatures, while the latter process dominates at high reaction rates, high

coke coverages, and low temperatures. Thus, pore size and pore structure are probably more important than acid strength and density under typical commercial process conditions. Indeed, deactivation is typically more rapid in zeolites having small pores or apertures and/or a monodimensional structure [95]. Figure 16 illustrates four possible modes of deactivation of HZSM-5 by carbonaceous deposits with increasing severity of coking [95].

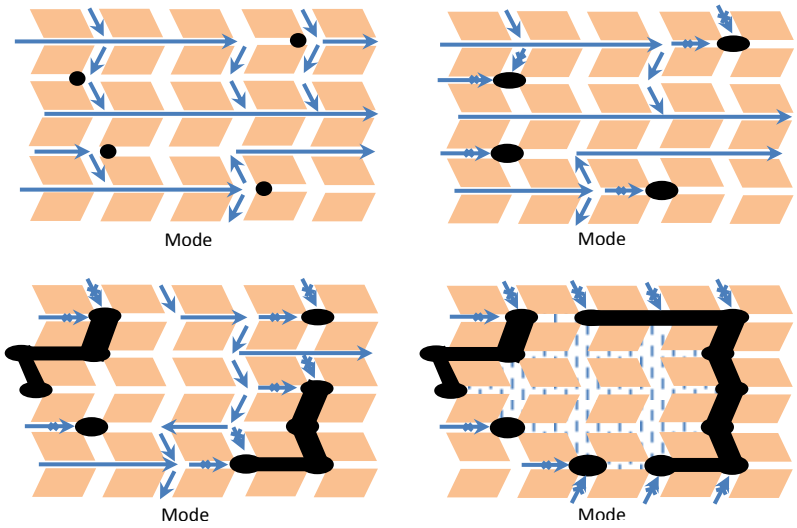

Figure 16. Schematic of the four possible modes of deactivation by carbonaceous deposits in HZSM-5: (1) reversible adsorption on acid sites, (2) irreversible adsorption on sites with partial blocking of pore intersections, (3) partial steric blocking of pores, and (4) extensive steric blocking of pores by exterior deposits. Adapted from [95].

These conclusions (in the previous paragraph) are borne out, for example, in the study by Cerqueira and co-workers [97] of USHY zeolite deactivation during methylcyclohexane transformation at 450 °C, showing the following:

(1) Coke is probably mainly formed by rapid transformation of toluenic C_7 carbenium ions with lesser contributions from reactions of cyclopentadiene, C_3–C_6 olefins, and aromatics.

(2) Soluble coke consists of polynuclear aromatic clusters containing three to seven five- and six-membered rings having a typical compositions of $C_{30}H_{40}$ to $C_{40}H_{44}$ and having dimensions of 0.9 × 1.1 nm to 1.1 × 1.5 nm, *i.e.*, sizes that would cause them to be trapped in the supercages of Y-zeolite.

(3) At short contact times, coking is relatively slow and deactivation is mainly due to acid-site poisoning, while at long contact times, coking is much faster because of the high concentrations of coke precursors; under these latter conditions coke is preferentially deposited at the outer pore openings of zeolite crystallites and deactivation is dominated by pore-mouth blockage.

That coke formed at large contact times not only blocks pores and/or pore intersections inside the zeolite, but also migrates to the outside of zeolite crystallites, where it blocks pore entrances, has been observed in several studies [91,93,94,97]. However, the amount, structure, and location of coke in ZSM-5 depends strongly on the coke precursor, e.g., coke formed from mesitylene is deposited on the external zeolite surface, whereas coking with isobutene leads to largely paraffinic deposits inside

pores; coke from toluene, on the other hand, is polyaromatic and is deposited both on external and internal zeolite surfaces [91].

2.3. Thermal Degradation and Sintering

2.3.1. Background

Thermally induced deactivation of catalysts results from (1) loss of catalytic surface area due to crystallite growth of the catalytic phase, (2) loss of support area due to support collapse and of catalytic surface area due to pore collapse on crystallites of the active phase, and/or (3) chemical transformations of catalytic phases to noncatalytic phases. The first two processes are typically referred to as "sintering". The third is discussed in the next section under solid–solid reactions. Sintering processes generally take place at high reaction temperatures (e.g., > 500 °C) and are generally accelerated by the presence of water vapor.

Most of the previous sintering and redispersion work has focused on supported metals. Experimental and theoretical studies of sintering and redispersion of supported metals published before 1997 have been reviewed fairly extensively [8,98–107]. Three principal mechanisms of metal crystallite growth have been advanced: (1) crystallite migration, (2) atomic migration, and (3) (at very high temperatures) vapor transport. The processes of crystallite and atomic migration are illustrated in Figure 17. Crystallite migration involves the migration of entire crystallites over the support surface, followed by collision and coalescence. Atomic migration involves detachment of metal atoms or molecular metal clusters from crystallites, migration of these atoms over the support surface, and ultimately, capture by larger crystallites. Redispersion, the reverse of crystallite growth in the presence of O_2 and/or Cl_2, may involve (1) formation of volatile metal oxide or metal chloride complexes that attach to the support and are subsequently decomposed to small crystallites upon reduction and/or (2) formation of oxide particles or films that break into small crystallites during subsequent reduction.

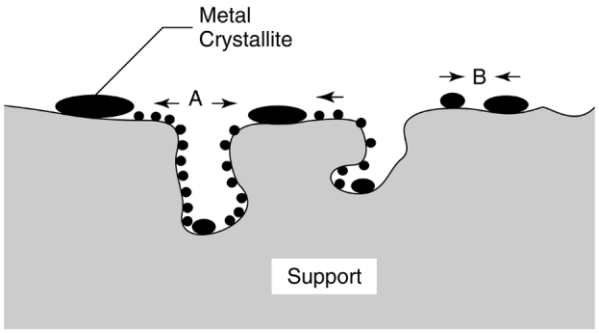

Figure 17. Two conceptual models for crystallite growth due to sintering by (**A**) atomic migration or (**B**) crystallite migration. Reproduced from [8], Copyright 2006, Wiley-Interscience.

There is controversy in the literature regarding which mechanism of sintering (or redispersion) operates at a given set of conditions. Logically, atomic migration would be favored at lower temperatures than crystallite migration, since the higher diffusivities of atoms or small cluster would facilitate their migration, whereas the thermal energy necessary to induce motion of larger crystallites would only be available at higher temperatures. Moreover, migration of small crystallites might be favorable early in the sintering process but unfavorable as crystallites become larger. However,

focusing on only one of the three sintering mechanisms (and two dispersion mechanisms) is a simplification that ignores the possibility that all mechanisms may occur simultaneously and may be coupled with each other through complex physicochemical processes, including the following: (1) dissociation and emission of metal atoms or metal-containing molecules from metal crystallites, (2) adsorption and trapping of metal atoms or metal-containing molecules on the support surface, (3) diffusion of metal atoms, metal-containing molecules and/or metal crystallites across support surfaces, (4) metal or metal oxide particle spreading, (5) support surface wetting by metal particles, (6) metal particle nucleation, (7) coalescence of, or bridging between, two metal particles, (8) capture of atoms or molecules by metal particles, (9) liquid formation, (10) metal volatilization through volatile compound formation, (11) splitting of crystallites in O_2 atmosphere owing to formation of oxides of a different specific volume, and (12) metal atom vaporization. Depending upon reaction or redispersion conditions, a few or all of these processes may be important; thus, the complexity of sintering/redispersion processes is emphasized.

In general, thermal sintering processes are kinetically slow (at moderate reaction temperatures) and irreversible or difficult to reverse. Thus, sintering is more easily prevented than cured.

2.3.2. Factors Affecting Metal Particle Growth and Redispersion in Supported Metals

Temperature, atmosphere, metal type, metal dispersion, promoters/impurities, and support surface area, texture, and porosity are the principal parameters affecting rates of sintering and redispersion (see Table 8) [8,103–107]. Sintering rates increase exponentially with temperature. Metals sinter relatively rapidly in oxygen and relatively slowly in hydrogen, although depending upon the support, metal redispersion can be facilitated by exposure at high temperature (e.g., 500–550 °C for Pt/Al_2O_3) to oxygen and chlorine, followed by reduction. Water vapor also increases the sintering rate of supported metals, likely through chemical-assisted sintering effects similar to those described in Section 2.4.3.

Table 8. Effects of Important Reaction and Catalyst Variables on Sintering Rates of Supported Metals Based on General Power-Law Expression (GPLE) Data [a].

Variable	Effect
Temperature	Sintering rates are exponentially dependent on T; E_{act} varies from 30 to 150 kJ/mol. E_{act} decreases with increasing metal loading; it increases in the following order with atmosphere: $NO < O_2 < H_2 < N_2$
Atmosphere	Sintering rates are much higher for noble metals in O_2 than in H_2 and higher for noble and base metals in H_2 relative to N_2. Sintering rate decreases for supported Pt in atmospheres in the following order: $NO > O_2 > H_2 > N_2$
Metal	Observed order of decreasing thermal stability in H_2 is $Ru > Ir \cong Rh > Pt$; thermal stability in O_2 is a function of (1) volatility of metal oxide and (2) strength of metal oxide–support interaction
Support	Metal–support interactions are weak (bond strengths of 5–15 kJ/mol); with a few exceptions, thermal stability for a given metal decreases with support in the following order: $Al_2O_3 > SiO_2 >$ carbon
Promoters	Some additives decrease atom mobility, e.g., C, O, CaO, BaO, CeO_2, GeO_2; others increase atom mobility, e.g., Pb, Bi, Cl, F, or S. Oxides of Ba, Ca, or Sr are "trapping agents" that decrease sintering rate
Pore size	Sintering rates are lower for porous *versus* nonporous supports; they decrease as crystallite diameters approach those of the pores

[a] Refs. [8,103–107]. For the definition of a GPLE, see Equation 2 later in this section.

Normalized dispersion (percentage of metal exposed at any time divided by the initial percentage exposed) *versus* time data in Figure 18 show that at temperatures of 650 °C or higher, rates of metal surface area loss (measured by hydrogen chemisorption) due to sintering of Ni/silica in hydrogen atmosphere are significant, causing 70% loss of the original metal surface area within 50 h at 750 °C. In reducing atmosphere, metal crystallite stability generally decreases with decreasing metal melting temperature, *i.e.*, in the order Ru > Ir > Rh > Pt > Pd > Ni > Cu > Ag, although this order may be affected by relatively stronger metal–support interactions, e.g., the observed order of decreasing stability of supported platinum in vacuum is Pt/Al_2O_3 > Pt/SiO_2 > Pt/C. In oxidizing atmospheres, metal crystallite stability depends on the volatility of metal oxides and the strength of the metal–oxide–support interaction. For noble metals, metal stability in air decreases in the order Rh > Pt > Ir > Ru; formation of volatile RuO_4 accounts for the relative instability of ruthenium.

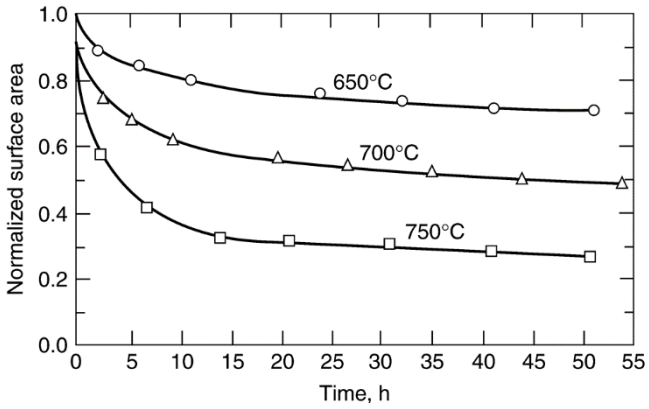

Figure 18. Normalized nickel surface area (based on H_2 adsorption) *versus* time data during sintering of 13.5% Ni/SiO_2 in H_2 at 650, 700, and 750 °C. Reproduced from [108]. Copyright 1983, Elsevier.

The effect of temperature on sintering of metals and oxides can be understood physically in terms of the driving forces for dissociation and diffusion of surface atoms, which are both proportional to the fractional approach to the absolute melting point temperature (T_{mp}). Thus, as temperature increases, the mean lattice vibration of surface atoms increases; when the Hüttig temperature ($0.3T_{mp}$) is reached, less strongly bound surface atoms at defect sites (e.g., edges and corner sites) dissociate and diffuse readily over the surface, while at the Tamman temperature ($0.5T_{mp}$), atoms in the bulk become mobile. Accordingly, sintering rates of a metal or metal oxide are significant above the Hüttig temperature and very high near the Tamman temperature; thus, the relative thermal stability of metals or metal oxides can be correlated in terms of the Hüttig or Tamman temperatures [109]. This can be illustrated from values of the melting and Tamman temperatures for noble and base metals and their compounds listed in Table 9. For example, sintering of copper catalysts for methanol synthesis is promoted by traces of chlorine in the feed, which react at about 225 °C (500 K) with the active metal/metal oxide surface to produce a highly mobile copper chloride phase having a Tamman temperature of only 79–174 °C (352–447 K) relative to 405–527 °C (678–800 K) for copper metal or metal oxides [110].

Table 9. Values of Melting and Tamman Temperatures (°C) for Common Catalytic Metals and Their Compounds [a].

Compound	T_{mp}, K	T_{Tamman}, K	$T_{Hüttig}$, K
Ag	1233	617	370
Au	1336	668	401
Co	1753	877	526
Cu	1356	678	407
CuO	1599	800	480
Cu_2O	1508	754	452
$CuCl_2$	893	447	268
Cu_2Cl_2	703	352	211
Fe	1808	904	542
Mo	2883	1442	865
MoO_3	1068	534	320
MoS_2	1458	729	437
Ni	1725	863	518
NiO	2228	1114	668
$NiCl_2$	1281	641	384
$Ni(CO)_4$	254	127	76
Rh	2258	1129	677
Rh_2O_3	1373	687	412
Ru	2723	1362	817
Pd	1828	914	548
PdO	1023	512	307
Pt	2028	1014	608
PtO	823	412	247
PtO_2	723	362	217
$PtCl_2$	854	427	256
$PtCl_4$	643	322	193
Zn	693	347	208
ZnO	2248	1124	674

[a] Adapted from Ref. [109].

Promoters or impurities affect sintering and redispersion by either increasing (e.g., chlorine and sulfur) or decreasing (e.g., oxygen, calcium, cesium) metal atom mobility on the support; in the latter case, this is due to their high resistance to dissociation and migration due to high melting points, as well as their hindering dissociation and surface diffusion of other atoms. Similarly, support surface defects or pores impede surface migration of metal particles—especially micropores and mesopores with pore diameters about the same size as the metal crystallites.

Historically, sintering rate data were fitted to a simple power-law expression (SPLE) of the form

$$-\frac{d(\frac{D}{D_0})}{dt} = k_s(\frac{D}{D_0})^n \quad (1)$$

where k_s is the sintering rate constant, D_0 the initial dispersion, and n is the sintering order, which for typical catalyst systems may vary from 3 to 15; unfortunately, the SPLE is, in general, not valid for

sintering processes because it assumes that surface area or dispersion ultimately reaches zero, given sufficient time, when in fact, for a given temperature and atmosphere, a nonzero or limiting dispersion is observed after long sintering times. Moreover, the use of the SPLE is further questionable because variations in sintering order are observed as a function of time and temperature for a given catalyst in a fixed atmosphere [105–107]; thus, data obtained for different samples and different reaction conditions cannot be quantitatively compared. Nevertheless, it has been shown by Fuentes [111,112] and Bartholomew [104–106] that the effects of temperature, atmosphere, metal, promoter, and support can be quantitatively determined by fitting sintering kinetic data to the general power-law expression (GPLE)

$$-\frac{d\left(\frac{D}{D_0}\right)}{dt} = k_s\left(\frac{D}{D_0} - \frac{D_{eq}}{D_0}\right)^m \quad (2)$$

which adds a term $-D_{eq}/D_0$ to account for the observed asymptotic approach of the typical dispersion *versus* time curve to a limiting dispersion D_{eq} at infinite time; m, the order of sintering, is found to be either 1 or 2. A recently compiled, comprehensive quantitative treatment of previous sintering rate data based on the GPLE with an order m of 2 [104–106] quantitatively addresses the effects of catalyst properties and reaction conditions on sintering rate. Some of these data are summarized in Table 10 [108,113–115]. These data show, for example, that the rate constant, and hence the rate of sintering, is less for Ni/Al_2O_3 than for Pt/Al_2O_3, an unexpected result in view of the lower heat of vaporization for Ni. This result is possibly explained by a greater metal support interaction for Ni with alumina.

Table 10. Comparison of Second-Order Sintering Rate Constants and Activation Energies for Pt, Ni, and Ag Catalysts [a].

Catalyst	Atm.	D_0 [b]	k_s [c] (400 °C)	k_s (650 °C)	k_s (700 °C)	k_s (750 °C)	E_{act}, [d] kJ/mol	Ref.
0.6% Pt/γ-Al_2O_3	H_2	~0.85	0.007	0.310	0.530	1.32	79	[113]
5% Pt/γ-Al_2O_3	H_2	0.10	0.420	0.76	0.84	0.97	13	[114]
15% Ni/γ-Al_2O_3	H_2	0.16	0.004	0.083	0.13	0.27	66	[108]
0.6% Pt/γ-Al_2O_3	Air	~0.85	0.024	0.29	0.41	0.75	52	[113]
5% Pt/γ-Al_2O_3	Air	0.10	0.014	1.46	2.79	8.51	97	[114]
1.8% Ag/η-Al_2O_3	Air	0.36	0.69	-	-	-	-	[115]

[a] Refs. [105,106]; [b] Initial metal dispersion or percentage exposed; [c] Second-order sintering rate constant from general power-law expression (GPLE) with units of h^{-1}; [d] Sintering activation energy for GPLE, $-d(D/D_0)/dt = k_s[D/D_0 - D_{eq}/D_0]^m$, where $m = 2$.

Sintering studies of supported metals are generally of two types: (1) studies of commercially relevant supported metal catalysts and (2) studies of model metal–support systems. The former type provides useful rate data that can be used to predict sintering rates, while the latter type provides insights into the mechanisms of metal particle migration and sintering, although the results cannot be quantitatively extrapolated to predict behavior of commercial catalysts. There is direct evidence from the previous studies of model-supported catalysts [104,107] for the occurrence of crystallite migration (mainly in well-dispersed systems early in the sintering process), atomic migration (mainly at longer

sintering times), and spreading of metal crystallites (mainly in oxygen atmosphere). There is also evidence that under reaction conditions, the surface is dynamic, *i.e.*, adsorbates and other adatoms rapidly restructure the surface and slowly bring about faceting; moreover, thermal treatments cause gradual changes in the distribution of coordination sites to minimize surface energy. There is a trend in increasing sophistication of spectroscopic tools used to study sintering and redispersion. In the next decade, we might expect additional insights into atomic and molecular processes during reaction at the atomic scale using STM, analytical high resolution transmission electron microscopy (HRTEM), and other such powerful surface science tools.

2.3.3. Sintering of Catalyst Carriers

Sintering of carriers (supports) has been reviewed by Baker and co-workers [103] and Trimm [116]. Single-phase oxide carriers sinter by one or more of the following processes: (1) surface diffusion, (2) solid-state diffusion, (3) evaporation/condensation of volatile atoms or molecules, (4) grain boundary diffusion, and (5) phase transformations. In oxidizing atmospheres, γ-alumina and silica are the most thermally stable carriers; in reducing atmospheres, carbons are the most thermally stable carriers. Additives and impurities affect the thermal properties of carriers by occupying defect sites or forming new phases. Alkali metals, for example, accelerate sintering; while calcium, barium, nickel, and lanthanum oxides form thermally stable spinel phases with alumina. Steam accelerates support sintering by forming mobile surface hydroxyl groups that are subsequently volatilized at higher temperatures. Chlorine also promotes sintering and grain growth in magnesia and titania during high temperature calcination. This is illustrated in Figure 19 [117]. By contrast, sulfuric acid treatment of hydrated alumina (gibbsite) followed by two-step calcination, results in a very stable transitional alumina with needle-like particle morphology [116]. Dispersed metals in supported metal catalysts can also accelerate support sintering; for example, dispersed nickel accelerates the loss of Al_2O_3 surface area in Ni/Al_2O_3 catalysts.

As an important example of support sintering through phase transformations, Al_2O_3 has a rich phase behavior as a function of temperature and preparation. A few among the many important phases that are stable or metastable, include boehmite, γ-alumina, and α-alumina [8,118,119]. Other phases are possible and the temperatures at which the phase transitions occur depend on crystal size and moisture content of the starting material, but as an example, as temperature is raised, boehmite, which is a hydrated or hydroxyl form of alumina, transforms to γ-alumina between 300 and 450 °C, then to δ-alumina at ~850°C, θ-alumina at ~1000°C, and finally α-alumina at ~1125 °C. The corresponding crystal structures for these five phases are orthorhombic, cubic defective spinel, orthorhombic, deformed monoclinic spinel, and hexagonal close pack (hcp with ABAB stacking) [8,118,119]. The approximate surface areas of these respective phases, as measured by nitrogen physisorption using Brunauer, Emmett, Teller (BET) analysis, are approximately 400, 200, 120, 50, and 1 m^2/g [8]. The dramatic drop in surface area during the transition from θ to α is associated with collapse of the microporous structure and formation of the dense hcp phase.

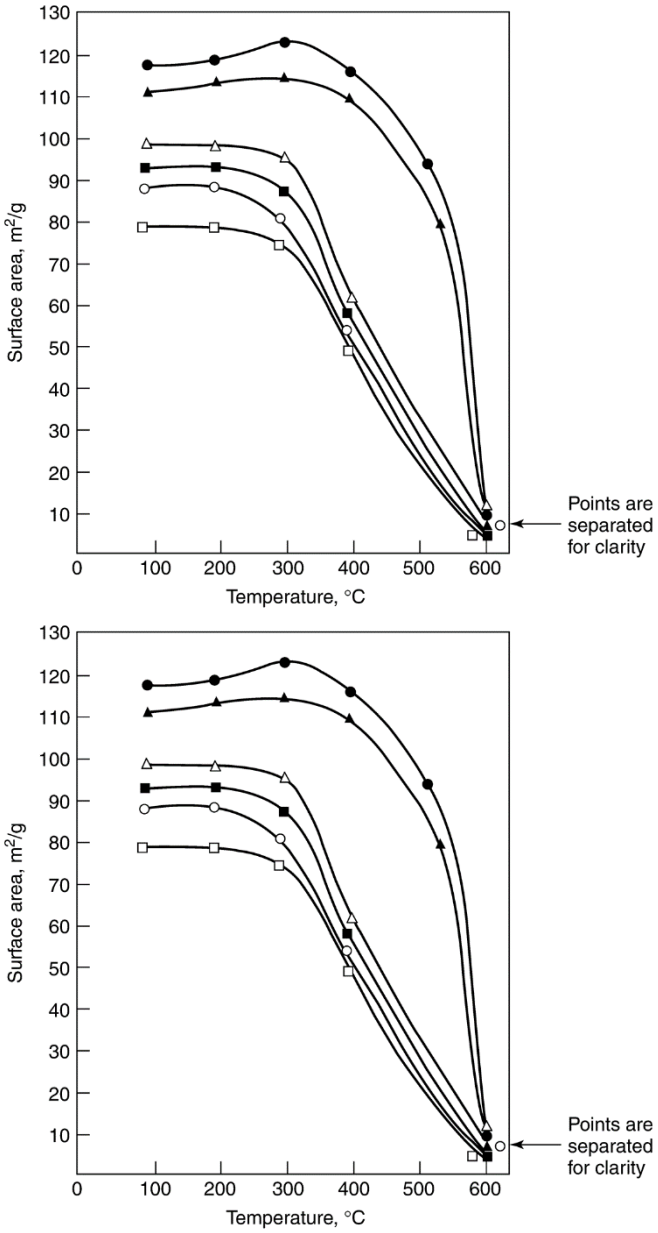

Figure 19. BET surface area of titania as a function of thermal treatment and chlorine content of fresh samples (before pretreatment). Samples were treated at the temperature indicated for 2 h. Reproduced from [117]. Copyright 1985, Elsevier. ● = Blank TiO_2; ▲ =TiO_2 soaked in H_2O; Δ = TiO_2 soaked in HCl/H_2O (2.06 wt% Cl); ■ = TiO_2 soaked in HCl/H_2O (2.40 wt% Cl);○ = TiO_2 soaked in HCl/H_2O (2.55 wt% Cl); □ = TiO_2 soaked in HCl/H_2O (2.30 wt% Cl).

2.3.4. Effects of Sintering on Catalyst Activity

Baker and co-workers [103] have reviewed the effects of sintering on catalytic activity. Specific activity (based on catalytic surface area) can either increase or decrease with increasing metal crystallite size during sintering if the reaction is structure-sensitive, or it can be independent of changes in metal crystallite size if the reaction is structure-insensitive. Thus, for a structure-sensitive reaction, the impact of sintering may be either magnified or moderated; while for a structure insensitive-reaction, sintering has in principle no effect on specific activity (per unit surface area). In the latter case, the decrease in mass-based activity is proportional to the decrease in metal surface area. Ethane hydrogenolysis and ethane steam reforming are examples of structure-sensitive reactions, while CO hydrogenation on supported cobalt, nickel, iron, and ruthenium is largely structure-insensitive in catalysts of moderate loading and dispersion.

2.4. Gas/Vapor–Solid and Solid-State Reactions

In addition to poisoning, there are a number of chemical routes leading to catalyst deactivation: (1) reactions of the vapor phase with the catalyst surface to produce (a) inactive bulk and surface phases (rather than strongly adsorbed species), (b) volatile compounds that exit the catalyst and reactor in the vapor phase, or (c) sintering due to adsorbate interactions, that we call chemical-assisted sintering to distinguish it from thermal sintering previously discussed; (2) catalytic solid-support or catalytic solid-promoter reactions, and (3) solid-state transformations of the catalytic phases during reaction. Each of these routes is discussed in some detail below.

2.4.1. Gas/Vapor–Solid Reactions

2.4.1.1. Reactions of Gas/Vapor with Solid to Produce Inactive Phases

Dispersed metals, metal oxides, metal sulfides, and metal carbides are typical catalytic phases, the surfaces of which are similar in composition to the bulk phases. For a given reaction, one of these catalyst types is generally substantially more active than the others, e.g., only Fe and Ru metals are active for ammonia synthesis, while the oxides, sulfides, and carbides are inactive. If, therefore, one of these metal catalysts is oxidized, sulfided, or carbided, it will lose essentially all of its activity. While these chemical modifications are closely related to poisoning, the distinction here is that rather than losing activity owing to the presence of an adsorbed species, the loss of activity is due to the formation of a new phase altogether.

Examples of vapor-induced chemical transformations of catalysts to inactive phases are listed in Table 11 [8,120–127]. These include the formation of $RhAl_2O_4$ in the three-way Pt–Rh/Al_2O_3 catalyst during high temperature operation in an auto exhaust; oxidation of Fe by low levels of O_2 during ammonia synthesis or by H_2O during regeneration; dealumination (migration of Al from the zeolite framework) of Y-zeolite during high temperature catalytic cracking and regeneration in steam; reaction of SO_3 with the alumina support to form aluminum sulfate leading to support breakdown and catalyst pore plugging in several processes, including CO oxidation in a gas turbine exhaust, conversion of CO and hydrocarbons in a diesel exhaust converter, and selective catalytic reduction (SCR) of NO_x in utility boiler flue gases [8,122–124,127]; oxidation of Fe_5C_2 to Fe_3O_4 and of Co metal supported on alumina or

silica to Co surface aluminates or silicates during Fischer–Tropsch synthesis at high conversions and hence high P_{H_2O}; and formation of $NiAl_2O_4$ during reaction and steam regeneration of Ni/Al_2O_3 in a slightly oxidizing atmosphere above about 500 °C, especially if more reactive aluminas, e.g., γ, δ, or θ forms, are used as supports. Because reaction of SO_3 with γ-Al_2O_3 to produce $Al_2(SO_4)_3$ is a serious cause of deactivation of alumina-supported catalysts in several catalytic processes (e.g., diesel exhaust abatement and SCR), TiO_2 or SiO_2 carriers are used rather than Al_2O_3 or in the diesel or automotive exhaust the alumina catalyst is stabilized by addition of BaO, SrO, or ZrO_2 [8,122–127].

Table 11. Examples of Reactions of Gases/Vapors with Catalytic Solids to Produce Inactive Phases.

Catalytic process	Gas/vapor composition	Catalytic solid	Deactivating chemical reaction	Ref.
Auto emissions control	N_2, O_2, HCs, CO, NO, H_2O, SO_2	Pt–Rh/Al_2O_3	2 Rh_2O_3 + γ-Al_2O_3→$RhAl_2O_4$ + 0.5 O_2	[120,121]
Ammonia synthesis and regeneration	H_2, N_2	Fe/K/Al_2O_3	Fe→FeO at >50 ppm O_2	[8]
	Traces O_2, H_2O		Fe→FeO at >0.16 ppm H_2O/H_2	
Catalytic cracking	HCs, H_2, H_2O	La-Y-zeolite	H_2O induced Al migration from zeolite framework causing zeolite destruction	[8]
CO oxidation, gas turbine exhaust	N_2, O_2, 400 ppm CO, 100–400 ppm SO_2	Pt/Al_2O_3	2 SO_3 + γ-Al_2O_3→$Al_2(SO_4)_3$ which blocks catalyst pores	[8]
Diesel HC/soot emissions control	N_2, O_2, HCs (gas and liquid), CO, NO, H_2O, soot, SO_2	Pt/Al_2O_3 and β-zeolite; oxides of CaCuFeVK on TiO_2	Formation of $Al_2(SO_4)_3$ or sulfates of Ca, Cu, Fe, or V, which block catalysts pores and lower activity for oxidation; Al_2O_3 stabilized by BaO	[122–124]
Fischer–Tropsch	CO, H_2, H_2O, CO_2, HCs	Fe/K/Cu/SiO_2	Fe_5C_2→Fe_3O_4 due to oxidation at high X_{CO} by product H_2O, CO_2	[125]
Fischer–Tropsch	CO, H_2, H_2O, HCs	Co/SiO_2	Co + SiO_2→$CoO{\cdot}SiO_2$ and collapse of SiO_2 by product H_2O	[126]
Selective catalytic reduction (SCR), stationary	N_2, O_2, NO, PM [a], H_2O, SO_2	$V_2O_5/WO_3/TiO_2$	Formation of $Al_2(SO_4)_3$ if Al_2O_3 is used	[127]
Steam reforming and regeneration in H_2O	CH_4, H_2O, CO, H_2, CO_2	Ni/Al_2O_3	Ni + Al_2O_3→$NiAl_2O_4$	[8]

[a] Particulate matter.

2.4.1.2. Reactions of Gas/Vapor with Solid to Produce Volatile Compounds

Metal loss through direct vaporization is generally an insignificant route to catalyst deactivation. By contrast, metal loss through formation of volatile compounds, e.g., metal carbonyls, oxides, sulfides, and halides in CO, O_2, H_2S, and halogen-containing environments, can be significant over a wide range of conditions, including relatively mild conditions. Classes and examples of volatile compounds are listed in Table 12. Carbonyls are formed at relatively low temperatures but high pressures of CO; halides can be formed at relatively low temperatures and low concentration of the halogens. However, the conditions under which volatile oxides are formed vary considerably with the metal; for example, RuO_3 can be formed at room temperature, while PtO_2 is formed at measurable rates only at temperatures exceeding about 500 °C.

Table 12. Types and Examples of Volatile Compounds Formed in Catalytic Reactions.

Gaseous environment	Compound type	Example of compound
CO, NO	Carbonyls and nitrosyl carbonyls	$Ni(CO)_4$, $Fe(CO)_5$ (0–300 °C) [a]
O_2	Oxides	RuO_3 (25 °C), PbO (>850 °C), PtO_2 (>700 °C)
H_2S	Sulfides	MoS_2 (>550 °C)
Halogens	Halides	$PdBr_2$, $PtCl_4$, PtF_6, $CuCl_2$, Cu_2Cl_2

[a] Temperatures of vapor formation are listed in parentheses.

While the chemical properties of volatile metal carbonyls, oxides, and halides are well known, there is surprisingly little information available on their rates of formation during catalytic reactions. There have been no reviews on this subject and relatively few reported studies to define the effects of metal loss on catalytic activity [28,128–141]. Most of the previous work has focused on volatilization of Ru in automotive converters [128–131]; nickel carbonyl formation in nickel catalysts during methanation of CO [133,139] or during CO chemisorption at 25 °C [28,135], and formation of Ru carbonyls during Fischer–Tropsch synthesis [136,137]; volatilization of Pt during ammonia oxidation on Pt–Rh gauze catalysts [140,141]; and volatilization of Cu from methanol synthesis and diesel soot oxidation catalysts, leading to sintering in the former and better catalyst–soot contact but also metal loss in the latter case [109].

Results of selected studies are summarized in Table 13. Bartholomew [131] found evidence of significant (50%) Ru loss after testing of a Pd–Ru catalyst in an actual reducing automobile exhaust for 100 h, which he attributed to formation of a volatile ruthenium oxide and which was considered responsible at least in part for a significant loss (20%) of NO reduction activity.

Table 13. Documented Examples of Reactions of Vapor with Solid to Produce Volatile Compounds.

Catalytic process	Catalytic solid	Vapor formed	Comments on deactivation process	Ref.
Automotive converter	Pd–Ru/Al_2O_3	RuO_4	50% loss of Ru during 100-h test in reducing automotive exhaust	[131]
Methanation of CO	Ni/Al_2O_3	$Ni(CO)_4$	P_{CO} > 20 kPa and T < 425 °C due to $Ni(CO)_4$ formation, diffusion and decomposition on the support as large crystallites	[133]
CO chemi-sorption	Ni catalysts	$Ni(CO)_4$	P_{CO} > 0.4 kPa and T > 0 °C due to $Ni(CO)_4$ formation; catalyzed by sulfur compounds	[134]
Fischer–Tropsch synthesis (FTS)	Ru/NaY zeolite, Ru/Al_2O_3, Ru/TiO_2	$Ru(CO)_5$, $Ru_3(CO)_{12}$	Loss of Ru during FTS (H_2/CO = 1, 200–250 °C, 1 atm) on Ru/NaY zeolite and Ru/Al_2O_3; up to 40% loss while flowing CO at 175–275 °C over Ru/Al_2O_3 for 24 h. Rate of Ru loss less on titania-supported Ru and for catalysts containing large metal crystallites (3 nm) relative to small metal crystallites (1.3 nm). Surface carbon lowers loss	[136,137]
Ammonia oxidation	Pt–Rh gauze	PtO_2	Loss: 0.05–0.3 g Pt/ton HNO_3; recovered with Pd gauze; loss of Pt leads to surface enrichment with inactive Rh	[8,142]
HCN synthesis	Pt–Rh gauze	PtO_2	Extensive restructuring and loss of mechanical strength	[8,143]
Methanol synthesis	CuZnO	$CuCl_2$, Cu_2Cl_2	Mobile copper chloride phase leads to sintering at reaction temperature (225 °C)	[109]
Diesel soot oxidation	Oxides of K, Cu, Mo, and trace Cl	$CuCl_2$, Cu_2Cl_2	Mobile copper chloride improves catalyst–soot contact; catalyst evaporation observed	[109]

Shen and co-workers [133] found that Ni/Al_2O_3 methanation catalysts deactivate rapidly during methanation at high partial pressures of CO (>20 kPa) and temperatures below 425 °C because of

$Ni(CO)_4$ formation, diffusion, and decomposition on the support as large crystallites; under severe conditions (very high P_{CO} and relatively low reaction temperatures) loss of nickel metal occurs. Thus, loss of nickel and crystallite growth could be serious problems at the entrance to methanation reactors where the temperature is low enough and P_{CO} high enough for metal carbonyl formation. Agnelli and co-workers [139] investigated kinetics and modeling of sintering due to formation and migration of nickel carbonyl species. They found that the initially sharp crystallite size distribution evolved during several hours of sintering under low temperature (230 °C) reaction conditions to a bimodal system consisting of small spherical crystallites and large faceted crystals favoring (111) planes. The sintering process was modeled in terms of an Ostwald-ripening mechanism coupled with mass transport of mobile subcarbonyl intermediates. Long-term simulations were found to predict reasonably well the ultimate state of the catalyst. On the basis of their work, they proposed two solutions for reducing loss of nickel: (1) increasing reaction temperature and decreasing CO partial pressure in order to lower the rate of carbonyl formation, and (2) changing catalyst composition, e.g., alloying nickel with copper or adding alkali to inhibit carbonyl species migration.

Of note, Kuo and Hwang have shown that the particle morphology itself affects the rate of Ostwald ripening due to different relative chemical potential energies of the surfaces [144]. Using silver nanoparticles, they found that atoms at sharp edges and corners were removed first, resulting in more rounded particles for all starting geometries. Thus, initial particle geometry appears to have an effect in addition to the chemical atmosphere experienced by the particles.

Loss of nickel metal during CO chemisorption on nickel catalysts at temperatures above 0 °C is also a serious problem; moreover, this loss is catalyzed by sulfur poisoning [28]. In view of the toxicity of nickel tetracarbonyl, the rapid loss of nickel metal, and the ill-defined adsorption stoichiometries, researchers are advised to avoid using CO chemisorption for measuring nickel surface areas; instead, hydrogen chemisorption, an accepted ASTM method with a well-defined adsorption stoichiometry, is recommended [145]. Figure 20 illustrates a mechanism for the formation of $Ni(CO)_4$ on a crystallite of nickel in CO atmosphere.

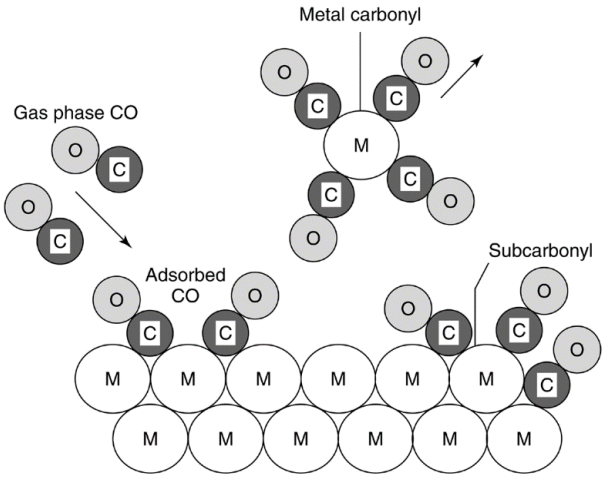

Figure 20. Formation of volatile tetra-nickel carbonyl at the surface of nickel crystallite in CO atmosphere. Reproduced from [8]. Copyright 2006, Wiley-Interscience.

Goodwin and co-workers [136,137] studied the influence of reaction atmosphere, support, and metal particle size on the loss of Ru due to carbonyl formation. They found that the loss of Ru during CO hydrogenation (H_2/CO = 1, 200–250 °C, 1 atm) on Ru/NaY zeolite and Ru/Al_2O_3 for extended periods of time was significant (e.g., up to 40% while flowing CO at 175–275 °C over Ru/Al_2O_3 for 24 h). The loss of Ru was significantly less on titania-supported Ru; moreover, the rate of loss was lower for catalysts containing large metal crystallites (3 nm) relative to those containing small metal crystallites (1.3 nm). Metal loss was inhibited in part at higher reaction temperatures as a result of carbon deposition. Thus, while it is clear that loss of ruthenium could be a serious problem in Fischer–Tropsch synthesis, there are measures in terms of catalyst design and choice of reaction conditions that can be taken to minimize loss.

One of the most dramatic examples of vapor phase loss of the catalyst occurs during NH_3 oxidation on Pt–Rh gauze, an important reaction in the manufacture of nitric acid [8,140,141]. At the high reaction temperature (~900 °C), formation of a volatile platinum oxide (PtO_2) occurs at a very significant rate; in fact, the rate of loss of 0.05–0.3 g Pt/ton of HNO_3 is high enough to provide a substantial economic incentive for Pt recovery [8]. The most effective recovery process involves placing a woven Pd-rich alloy gauze immediately below the Pt–Rh gauze to capture the Pt through formation of a Pd–Pt alloy. Pt loss is also the most significant cause of catalyst deactivation as the gauze surface becomes enriched in nonvolatile but inactive rhodium oxide [142], requiring shutdown and catalyst replacement every 3–12 months [8].

Decomposition of volatile platinum oxide species formed during high temperature reaction may (similar to the previously discussed formation of large crystallites of Ni from $Ni(CO)_4$) lead to formation of large Pt crystallites and/or substantial restructuring of the metal surface. For example, Wu and Phillips [146–148] observed surface etching, enhanced sintering, and dramatic surface restructuring of Pt thin films to faceted particles during ethylene oxidation over a relatively narrow temperature range (500–700 °C). The substantially higher rate of sintering and restructuring in O_2/C_2H_4 relative to that in nonreactive atmospheres was attributed to the interaction of free radicals such as HO_2, formed homogeneously in the gas phase, with the metal surface to form metastable mobile intermediates. Etching of Pt–Rh gauze in a H_2/O_2 mixture under the same conditions as Pt surfaces (600 °C, $N_2/O_2/H_2$ = 90/7.5/2.5) has also been reported [143]. A significant weight loss was observed in a laminar flow reactor with little change in surface roughness, while in an impinging jet reactor, there was little weight loss, but substantial restructuring of the surface to particle-like structures, 1–10 μm in diameter; these particles were found to have the same Pt–Rh composition as the original gauze. The nodular structures of about 10-μm diameter formed in these experiments are strikingly similar to those observed on Pt–Rh gauze after use in production of HCN at 1100 °C in 15% NH_3, 13% CH_4, and 72% air (see Figure 21). Moreover, because of the high space velocities during HCN production, turbulent rather than laminar flow would be expected, as in the impinging jet reactor. While little Pt is volatilized from the Pt–Rh gauze catalyst during HCN synthesis, the extensive restructuring leads to mechanical weakening of the gauze [8].

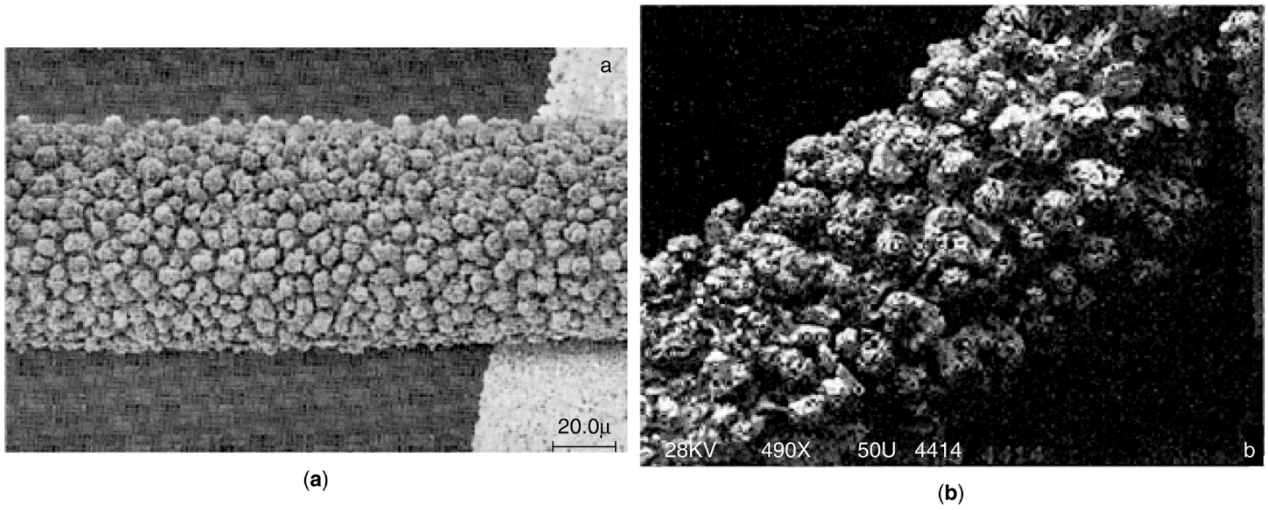

Figure 21. (**a**) SEM of Pt–Rh gauze after etching in $N_2/O_2/H_2$ = 90/7.5/2.5 at 875 K for 45 h. Reproduced from [143]. Copyright 1992, Elsevier. (**b**) SEM of Pt–Rh gauze after use in production of HCN (magnification 1000×). Photograph courtesy of Ted Koch at DuPont, personal correspondence to the author.

Other examples of catalyst deactivation due to volatile compound formation include (1) loss of the phosphorus promoter from the VPO catalyst used in the fluidized-bed production of maleic anhydride, with an attendant loss of catalyst selectivity [8], (2) vapor-phase loss of the potassium promoter from steam-reforming catalysts in the high temperature, steam-containing environment [8], and (3) loss of Mo from a 12-Mo-V-heteropolyacid due to formation of a volatile Mo species during oxydehydrogenation of isobutyric acid to methacrylic acid [138].

While relatively few definitive studies of deactivation by volatile compound formation have been reported, the previous work does provide the basis for enumerating some general principles. A generalized mechanism of deactivation by formation of volatile metal compounds can be postulated (see Figure 22). In addition, the roles of kinetics and thermodynamics can be stated in general terms:

(1) At low temperatures and partial pressures of the volatilization agent (VA), the overall rate of the process is limited by the rate of volatile compound formation.

(2) At intermediate temperatures and partial pressures of the VA, the rate of formation of the volatile compound exceeds the rate of decomposition. Thus, the rate of vaporization is high, the vapor is stable, and metal loss is high.

(3) At high temperatures and partial pressures of the VA, the rate of formation equals the rate of decomposition, *i.e.*, equilibrium is achieved. However, the volatile compound may be too unstable to form or may decompose before there is an opportunity to be transported from the system. From the previous work, it is also evident that besides temperature and gas phase composition, catalyst properties (crystallite size and support) can play an important role in determining the rate of metal loss.

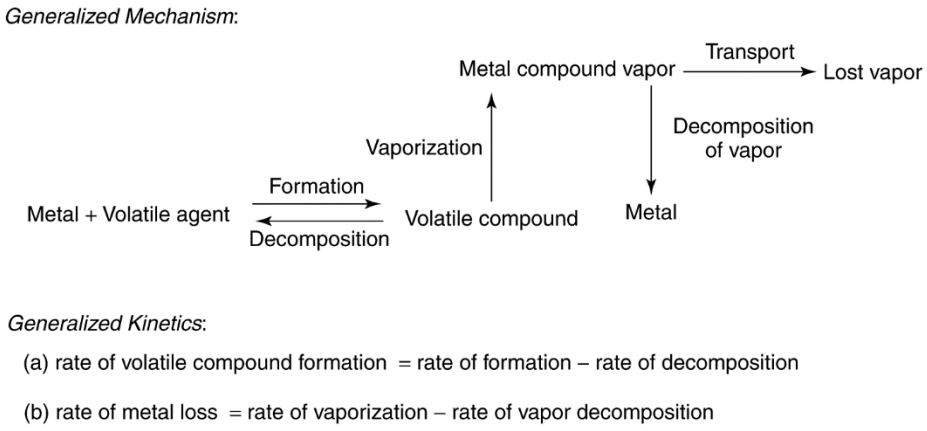

Figure 22. Generalized mechanisms and kinetics for deactivation by metal loss. Reproduced from [8]. Copyright 2006, Wiley-Interscience.

2.4.2. Solid-State Reactions

Catalyst deactivation by solid-state diffusion and reaction appears to be an important mechanism for degradation of complex multicomponent catalysts in dehydrogenation, synthesis, partial oxidation, and total oxidation reactions [8,149–160]. However, it is difficult in most of these reactions to know the extent to which the solid-state processes, such as diffusion and solid-state reaction, are affected by surface reactions. For example, the rate of diffusion of Al_2O_3 to the surface to form an aluminate may be enhanced by the presence of gas-phase oxygen or water or the nucleation of a different phase may be induced by either reducing or oxidizing conditions. Recognizing this inherent limitation, the focus here is nevertheless on processes in which formation of a new bulk phase (and presumably the attendant surface phase) leads to substantially lower activity. There is probably some overlap with some of the examples given under Gas/Vapor–Solid Reactions involving reactions of gas/vapor with solid to produce inactive phases.

Examples from the literature of solid-state transformations leading to catalyst deactivation are summarized in Table 14. They include (1) the formation of $KAlO_2$ during ammonia synthesis at the $Fe/K/Al_2O_3$ catalyst surface, (2) decomposition of the active phase PdO to inactive Pd metal during catalytic combustion on PdO/Al_2O_3 and PdO/ZrO_2 catalysts, (3) transformation of active carbides to inactive carbides in Fischer–Tropsch synthesis on Fe/K/Cu catalysts, (4) formation of inactive V(IV) compounds in SO_2 oxidation, and (5) reductive transformation of iron molybdate catalysts during partial oxidation of benzene, methanol, propene, and isobutene.

Table 14. Examples of Solid-State Transformations Leading to Catalyst Deactivation.

Catalytic process	Catalytic solid	Deactivating chemical reaction	Ref.
Ammonia synthesis	$Fe/K/Al_2O_3$	Formation of $KAlO_2$ at catalyst surface	[159]
Catalytic combustion	PdO/Al_2O_3, PdO/ZrO_2	PdO→Pd at $T > 800$ °C	[152]
Catalytic combustion	Co/K on MgO, CeO_2, or La_2O_3	Formation of CoO–MgO solid soln., $LaCoO_3$, or K_2O film on CeO_2	[160]

Table 14. *Cont.*

Catalytic process	Catalytic solid	Deactivating chemical reaction	Ref.
Dehydrogenation of ethyl benzene to styrene	$Fe_2O_3/Cr_2O_3/K_2O$	K migration to center of pellet caused by thermal gradient	[8]
Fischer–Tropsch	Fe/K, Fe/K/CuO	Transformation of active carbides to inactive carbides	[157,158]
Oxidation of SO_2 to SO_3	$V_2O_5/K_2O/Na_2O/$	Formation of inactive V(IV) compounds at $T < 420$–430 °C	[155]
Partial oxidation of benzene to maleic anhydride	V_2O_5–MoO_3	Decreased selectivity due to loss of MoO_3 and formation of inactive vanadium compounds	[149]
Partial oxidation of methanol to formaldehyde	$Fe_2(MoO_4)_3$ plus MoO_3	Structural reorganization to β-$FeMoO_4$; reduction of MoO_3	[150,156]
Partial oxidation of propene to acrolein	$Fe_2(MoO_4)_3$	Reductive transformation of $Mo_{18}O_{52}$ to Mo_4O_{11}	[153,156]
Partial oxidation of isobutene to methacrolein	$Fe_2(MoO_4)_3$	Reduction to $FeMoO_4$ and MoO_{3-x}	[151,154]

There are basic principles underlying most solid-state reactions in working catalysts that have been enumerated by Delmon [156]: (1) the active catalytic phase is generally a high-surface-area defect structure of high surface energy and as such a precursor to more stable, but less active phases and (2) the basic reaction processes may itself trigger the solid-state conversion of the active phase to an inactive phase; for example, it may involve a redox process, part of which nucleates the inactive phase.

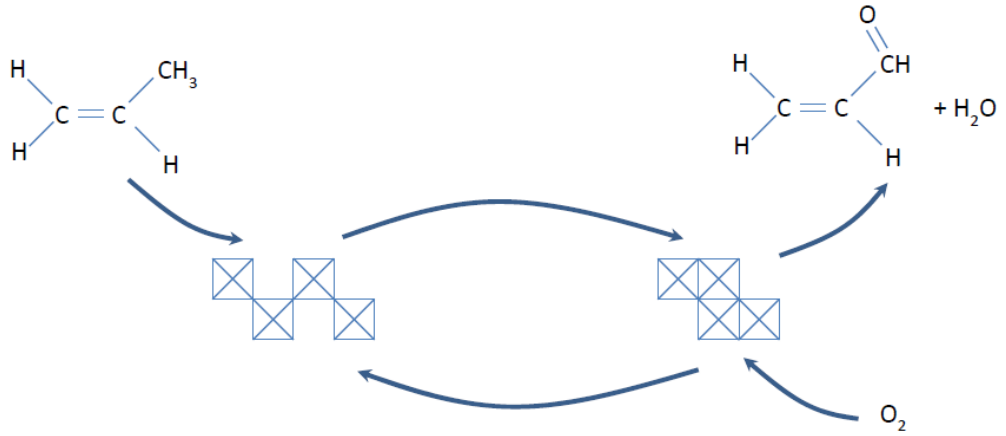

Figure 23. Schematic representation of the cyclic reduction/oxidation of twin pairs of MoO_6 octahedra between the corner and the edge-sharing arrangements (boxes represent MoO_6 octahedra with sharing of oxygen atoms at corners for MoO_3 or edges for MoO_2). The figure is not completely accurate, because it cannot take into account the fact that the arrangements are not perpendicular to the main axes of the lattice. Adapted from [156].

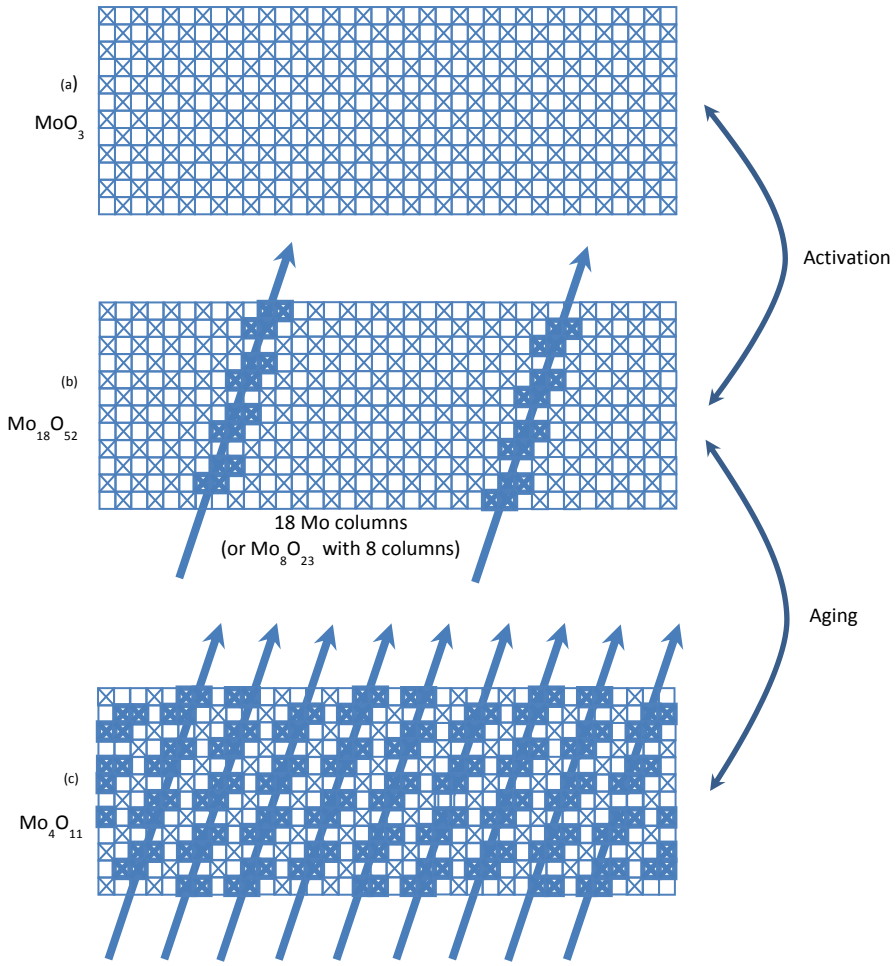

Figure 24. Schematic representation of the structure of MoO_3, $Mo_{18}O_{52}$, and Mo_4O_{11}. The shear planes in $Mo_{18}O_{52}$ and Mo_4O_{11} are represented by the oblique arrows (boxes with an "X" represent MoO_5 octahedra). Adapted from [156].

A well-documented example of these principles occurs in the partial oxidation of propene to acrolein on a $Fe_2(MoO_4)_3$ catalyst [153,156]. This oxidation occurs by the "*Mars van Krevelen*" *mechanism*, *i.e.*, a redox mechanism in which lattice oxygen reacts with the adsorbed hydrocarbon to produce the partially oxygenated product; the reduced catalyst is restored to its oxidized state through reaction with gaseous oxygen. In propene oxidation, two atoms of oxygen from the catalyst are used, one for removing two hydrogen atoms from the olefin and the other one in forming the unsaturated aldehyde. The fresh, calcined catalyst MoO_3 consists of corner-sharing MoO_6 octahedra (with Mo at the center and six oxygen atoms at the corners); but upon reduction to MoO_2, octahedra share edges as shown in Figure 23. However, it has been reported [153,156] that only slightly reduced (relative to MoO_3), open structures such as $Mo_{18}O_{52}$ and Mo_8O_{23} are the most active, selective phases; more complete reduction of either of these structures leads to formation of Mo_4O_{11} (see Figure 24) having substantially lower selectivity. Delmon and co-workers [154,156] have shown that addition of an oxygen donor such as Sb_2O_4 facilitates spillover of oxygen and thereby prevents overreduction and deactivation of the catalyst.

2.4.3. Reactions of Gas/Vapor with Solid to Restructure the Surface by Chemical Assisted Sintering

The surfaces of metallic catalysts can be greatly roughened by interactions with the reactants and/or products. However, as opposed to forming volatile species that are transported out of the reactor as discussed in the previous section, these interactions lead to a restructuring of the surface that is similar to that which occurs during thermal sintering, but at temperatures which are below the Tamman or Huttig temperatures, respectively defined as 0.5 and 0.3 of the melting point (T_m) of the material, at which thermal sintering might be expected. Therefore, this surface restructuring must be attributed to the interaction of the gas phase with the solid. The following three examples from the literature highlight the chemical-assisted sintering process caused by adsorbate-surface interactions on Ni, Co, and Pd surfaces.

Chemical sintering of Ni/alumina catalysts in methanation due to formation of volatile $Ni(CO)_4$ followed by its decomposition downstream to large Ni crystallites has been well documented [8,105]. Moreover, deactivation of Ni/alumina by Ni aluminate formation is also observed at the exit of methanators where temperature is moderately high (T = 450 °C) and steam partial pressure is maximum [105].

Wilson and de Groot [161] reported that under high pressure (4 bar, H_2/CO = 2) and moderate temperature (523 K) conditions, single crystal Co (0001) surfaces restructured significantly due to interaction with the CO, which they attributed to an etch-regrowth mechanism. The left hand panel of Figure 25a shows the scanning tunneling microscopy (STM) image of the single crystal surface, while Figure 25b shows the same location after exposure to the H_2/CO atmosphere for 1 h The surface restructuring and roughening is profound, with the peaks approximately four atoms high relative to the previously smooth surface that had only well-defined steps interrupting the (0001) planar surface.

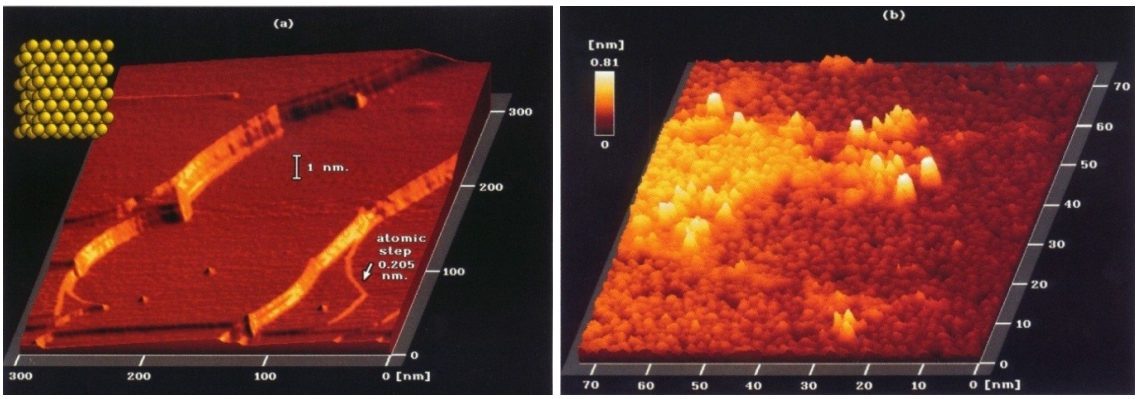

Figure 25. STM images of the Co (0001) surface (**a**) before and (**b**) after 1 h exposure to 4 MPa 2:1 H_2:CO atmosphere at 523 K. Reproduced from [161]. Copyright 1995, American Chemical Society.

More recently, Parkinson *et al.* [162] have shown that chemical-assisted sintering occurs at room temperature for palladium supported on magnetite under ultra high vacuum conditions with CO partial pressures of only 5×10^{-10} mbar. Figure 26 shows four STM images from a movie that demonstrates the surface mobility of the Pd at these low CO partial pressures. Figure 26a is the surface prior to CO exposure, while Figures 26b–d show the surface as a function of time up to about an hour of exposure. The authors note that hydroxyl-Pd groups (OH-Pd), identified by the ×'s in the images, serve as anchoring points for the coalescence of larger Pd clusters. The full movie, available with the

supplementary material for this article [162], is recommended to fully appreciate the unexpectedly high atomic mobility under these conditions.

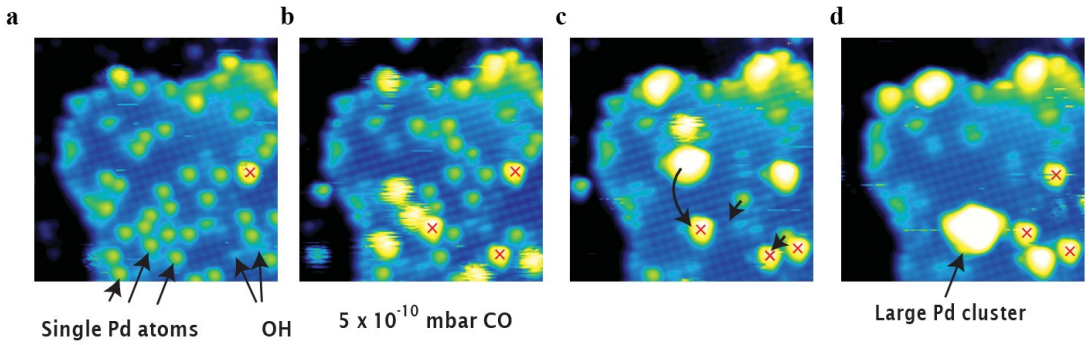

Figure 26. "The CO-induced formation of a large Pd cluster. a–d, Four STM images (14 × 14 nm^2, +1 V, 0.2 nA) selected from a 36-frame STM movie (duration 1 h 50 min) following the deposition of 0.2 ML Pd [on Fe_3O_4] at RT. Initially (**a**), isolated Pd atoms are present, together with hydroxyl groups and one OH–Pd (red cross). After three frames the background pressure of CO is raised to 5 × 10^{-10} mbar. Thirty minutes later (frame **b**), several mobile 'fuzzy' Pd carbonyl species, trapped at other Pd atoms, have formed. Shortly afterwards (**c**), three Pd carbonyls and four adatoms have formed a large cluster. Twenty-five minutes later (**d**), the cluster has captured another Pd carbonyl, and diffused to merge with an OH–Pd species.". Reproduced from [162]. Copyright 2013, MacMillan Publishers.

2.5. Mechanical Failure of Catalysts

2.5.1. Forms and Mechanisms of Failure

Mechanical failure of catalysts is observed in several different forms that depend on the type of reactor, including (1) crushing of granular, pellet, or monolithic catalyst forms due to a load in fixed beds; (2) attrition, the size reduction, and/or breakup of catalyst granules or pellets to produce fines, especially in fluid or slurry beds; and (3) erosion of catalyst particles or monolith coatings at high fluid velocities in any reactor design. Attrition is evident by a reduction in the particle size or a rounding or smoothing of the catalyst particle easily observed under an optical or electron microscope. Washcoat loss is observed by scanning a cross section of the honeycomb channel with either an optical or an electron microscope. Large increases in pressure drop in a catalytic process are often indicative of fouling, masking, or the fracturing and accumulation of attritted catalyst in the reactor bed.

Commercial catalysts are vulnerable to mechanical failure in large part because of the manner in which they are formed; that is, catalyst granules, spheres, extrudates, and pellets ranging in diameter from 50 μm to several millimeters are in general prepared by agglomeration of 0.02–2 μm aggregates of much smaller primary particles having diameters of 10–100 nm by means of precipitation or gel formation, followed by spray drying, extrusion, or compaction. These agglomerates have, in general, considerably lower strengths than the primary particles and aggregates of particles from which they are formed.

Two principal mechanisms are involved in mechanical failure of catalyst agglomerates: (1) fracture of agglomerates into smaller agglomerates of approximately $0.2d_0$–$0.8d_0$ and (2) erosion (or abrasion) from

the surface of the agglomerate of aggregates of primary particles having diameters ranging from 0.1 to 10 μm [163]. While erosion is caused by mechanical stresses, fracture may be due to mechanical, thermal, and/or chemical stresses. Mechanical stresses leading to fracture or erosion in fluidized or slurry beds may result from (1) collisions of particles with each other or with reactor walls or (2) shear forces created by turbulent eddies or collapsing bubbles (cavitation) at high fluid velocities. Thermal stresses occur as catalyst particles are heated and/or cooled rapidly; they are magnified by temperature gradients across particles and by differences in thermal expansion coefficients at the interface of two different materials, e.g., catalyst coating/monolith interfaces; in the latter case the heating or cooling process can lead to fracture and separation of the catalyst coating. Chemical stresses occur as phases of different density are formed within a catalyst particle via chemical reaction; for example, carbiding of primary iron oxide particles increases their specific volume and micromorphology leading to stresses that break up these particles [164]. A further example occurs in supported metal catalysts when large quantities of filamentous carbon (according to reaction mechanisms discussed earlier) overfill catalysts pores, generating enormous stresses that can fracture primary particles and agglomerates.

2.5.2. Role of Physical and Chemical Properties of Ceramic Agglomerates in Determining Strength and Attrition Resistance

2.5.2.1. Factors Affecting the Magnitude of Stress Required for Agglomerate Breakage and the Mechanisms by Which It Occurs

The extent to which a mechanism, *i.e.*, fracture or erosion, participates in agglomerate size reduction depends upon several factors: (1) the magnitude of a stress, (2) the strength and fracture toughness of the agglomerate, (3) agglomerate size and surface area, and (4) crack size and radius. Erosion (abrasion) occurs when the stress (e.g., force per area due to collision or cavitation pressure) exceeds the agglomerate strength, *i.e.*, the strength of bonding between primary particles. Erosion rate is reportedly [163] proportional to the external surface area of the catalyst; thus, erosion rate increases with decreasing agglomerate size.

2.5.2.2. Fracture Toughness of Ceramic Agglomerates

Most heterogeneous catalysts are complex, multiphase materials that consist, in large part, of porous ceramic materials, *i.e.*, are typically oxides, sulfides, or metals on an oxide carrier or support. When a tensile stress of a magnitude close to the yield point is applied, ceramics almost always undergo brittle fracture before plastic deformation can occur. Brittle fracture occurs through formation and propagation of cracks through the cross section of a material in a direction perpendicular to the applied stress. Agglomerate fracture due to a tensile stress occurs by propagation of internal and surface flaws; these flaws, created by external stresses or inherent defects, are stress multipliers, *i.e.*, the stress is multiplied by $2(a/r)^{0.5}$, where a is the crack length and r is the radius of curvature of the crack tip; since a/r can vary from 2 to 1000, the effective stress at the tip of a crack can be 4–60 times the applied stress. Tensile stress multipliers may be microcracks, internal pores, and grain corners.

The ability of a material to resist fracture is termed *fracture toughness*. The plane strain fracture toughness, K_{Ic}, is defined as

$$K_{Ic} = Y\sigma(\pi\alpha)^{0.5} \quad (3)$$

where Y is a dimensionless parameter (often close to 1.0–2.0), the magnitude of which depends upon both specimen and crack geometries, σ is the applied stress, and a is the length of a surface crack or half the length of an internal crack. Crack propagation and fracture are likely if the right hand side of Equation 3 exceeds the experimental value of plane strain fracture toughness (left-hand side of Equation 3). Plane strain fracture toughness values for ceramic materials are significantly smaller than for metals and typically below 10 MPa(m)$^{0.5}$; reported values for nonporous, crystalline alumina (99.9%), fused silica, and zirconia (3 mol% Y_2O_3) are 4–6, 0.8, and 7–12 MPa(m)$^{0.5}$, respectively; flexural strengths (analogous to yield strengths for metals) for the same materials are 280–550, 100, and 800–1500 MPa [165]. Thus, on the basis of both fracture toughness and flexural strength, nonporous, crystalline zirconia is much stronger toward fracture than alumina, which in turn is much stronger than fused silica.

2.5.2.3. Effects of Porosity on Ceramic Agglomerate Strength

The introduction of porosity to crystalline or polycrystalline ceramic materials will, on the basis of stress amplification, significantly decrease elastic modulus and flexural strength for materials in tension. This is illustrated by data in Figure 27, showing that elastic modulus and flexural strength of a ceramic alumina (probably alpha form) are reduced by 75 and 85% respectively as porosity is increased from 0 to 50% [166]. Thus, according to Figure 27b, the flexural strength of typical porous aluminas used as catalyst supports might lie in the range of 30–40 MPa. However, yield strengths for γ-Al_2O_3 (shown in the next section) are factors of 3–50 lower. Nevertheless, the data in Figure 27b suggest that higher strengths may be possible.

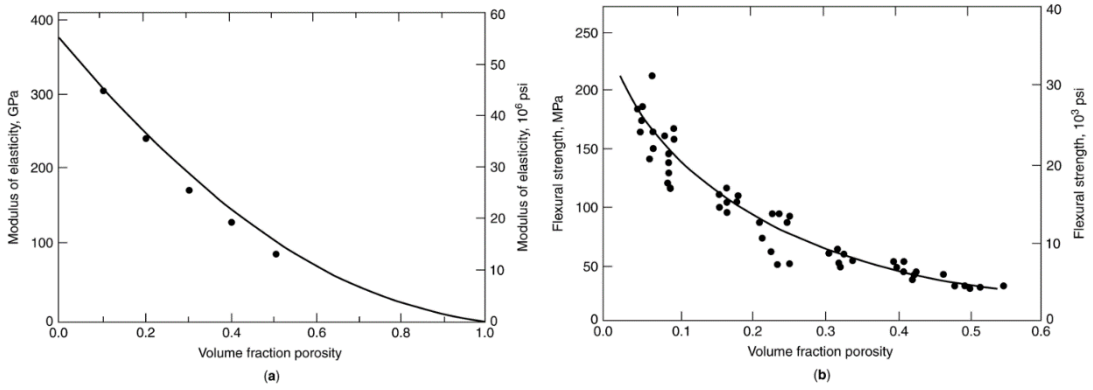

Figure 27. The influence of porosity on (**a**) the modulus of elasticity for aluminum oxide at room temperature and (**b**) the flexural strength for aluminum oxide at room temperature. Reproduced from [166]. Copyright 1956, Wiley.

2.5.2.4. Compressive Strengths of Ceramic Materials

Thus far, the discussion has focused mainly on tensile strength, the extent of which is greatly reduced by the presence of cracks or pores. However, for ceramic materials in compression, there is no stress amplification due to flaws or pores; thus ceramic materials (including catalytic materials) in compression are much stronger (approximately a factor of 10) than in tension. In addition, the strength of ceramic materials can be dramatically enhanced by imposing a residual compressive stress at the

surface through thermal or chemical tempering. Moreover, introduction of binders, such as graphite, enables agglomerates of ceramic powders to undergo significant plastic deformation before fracture.

2.5.3. Tensile Strengths and Attrition Resistance of Catalyst Supports and Catalysts

2.5.3.1. Tensile Strength Data for Catalyst Support Agglomerates

The strengths cited above for nonporous, annealed crystalline or polycrystalline materials do not necessarily apply to porous catalyst agglomerates, even under compression; rather, agglomerate strength is dependent upon the strengths of chemical and physical bonds, including the cohesive energy, between primary particles. Agglomerate strength would depend greatly on the preparation of the compact. Representative data for catalyst agglomerates (see Table 15) suggest they are generally substantially weaker than polycrystalline ceramic materials prepared by high temperature sintering, such as the alumina cited in Figure 27 [163,165,167–171]. For example, Pham and co-workers [163] found that the breaking strength of a VISTA B alumina agglomerate during uniaxial compaction is in the range of 5–10 MPa—substantially lower than the reported values for heat-treated polycrystalline alumina of 280–550 MPa [165]. A large part of this difference (about 85–95%) can be attributed to porosity; however, the remaining 5–15% must be due to differences in bonding between primary particles. In other words, the bonds between primary particles in catalyst agglomerates (and some ceramic agglomerates prepared by similar methods) are typically physical in nature (e.g., involve van der Waals forces) while those in sintered polycrystalline ceramic agglomerates are principally chemical because of solid bridging of primary particles. Thus, there appears to be considerable potential for strengthening catalyst agglomerates, since their strengths are typically factors of 3–50 lower than for conventional, heat-treated ceramics of similar porosity.

Table15. Mechanical Strengths and Attrition Rates of Catalyst Supports Compared to Those of Sintered Ceramic Agglomerates.

Catalyst support or ceramic	Preparation/pretreatment/properties	Strength, MPa	Attrition index, wt%/h	Ref.
High surface area catalyst supports				
γ-Al_2O_3, 1.2–4.25-mm spheres	Sol–gel granulation/dried 10 h at 40 °C, calcined 3 h at 450 °C/389 m^2/g, d_{pore} = 3.5 nm	11.6 ± 1.9	0.033	[167]
γ-Al_2O_3, 4.25-mm spheres	Alcoa LD-350	0.7	0.177	[167]
γ-Al_2O_3, 100 μm	VISTA-B-965-500C	6.2 ± 1.3	-	[163]
TiO_2 (anatase), 30 μm	Thermal hydrolysis/dried 110 °C, calcined 2 h at 500 °C/ 92 m^2/g, <10-nm primary crystallites	28[a]	-	[168]
TiO_2 (anatase), 90 μm	Basic precipitation/dried 110 °C, calcined 2 h at 500 °C/81 m^2/g, 10–14-nm primary crystallites	15[a]	-	[168]
TiO_2 (75% anatase, 25% rutile)	Degussa P25, fumed/4-mm extrudates/48 m^2/g, V_{pore} = 0.34 cm^3/g, d_{pore} = 21 nm	0.9	-	[169]

Table15. *Cont.*

Catalyst support or ceramic	Preparation/pretreatment/properties	Strength, MPa	Attrition index, wt%/h	Ref.
High surface area catalyst supports (cont.)				
TiO_2 (anatase)	Rhone-Poulenc DT51, ppt./4 mm extrudates/92 m^2/g, V_{pore} = 0.40 cm^3/g, d_{pore} = 8, 65 nm	0.9	-	[169]
Low surface area ceramics				
Al_2O_3	Spray dried with organic binder; plastic deformation observed	2.3	-	[170]
Al_2O_3	Heat treated (sintered), 99.9%	282–551	-	[165]
TiO_2 (Rutile)	Partially sintered	194	-	[170]
ZrO_2 (yttria additive)	Commercial samples from three companies, spray-dried	0.035–0.43	-	[171]
ZrO_2 (3% Y_2O_3)	Heat treated (sintered)	800–1500	-	[165]

[a]Rough estimates from break points on relative density *versus* log[applied pressure] curves; data are consistent with mass distribution *versus* pressure curves from ultrasonic tests.

2.5.3.2. Effects of Preparation and Pretreatment on Catalyst Agglomerate Strength

From the data in Table 15 it is evident that even subtle differences in preparation and pretreatment also affect agglomerate strength. For example, spheres of γ-Al_2O_3 prepared by sol–gel granulation are substantially (17 times) stronger than commercial γ-Al_2O_3 spheres [166]. Moreover, 30- and 90- μm diameter particles of TiO_2 prepared by thermal hydrolysis or basic precipitation are 30 and 15 times stronger than commercially available 4-mm extrudates [169].

2.5.4. Attrition of Catalyst Agglomerates: Mechanisms, Studies, and Test Methods

Catalyst attrition is a difficult problem in the operation of moving-bed, slurry-bed, or fluidized-bed reactors. Generally, stronger materials have greater attrition resistance; this conclusion is supported by representative data in Table 15 for γ-Al_2O_3, showing that the strength of the alumina prepared by sol–gel granulation is 17 times higher, while its attrition rates is 5 times lower.

The mechanism by which attrition occurs (erosion or fracture) can vary with catalyst or support preparation, crush strength, and with reactor environment; it can also vary with the mechanical test method. There is some evidence in the attrition literature, supporting the hypothesis that in the presence of a large stress, weaker oxide materials are prone to failure by fracture, while stronger materials tend to erode. For example, in the fluid catalytic cracking process, as new silica–alumina/zeolite catalyst in the form of 50–150-μm spherical agglomerates is added to replace catalyst lost by attrition, the weaker agglomerates break up fairly rapidly by fracture into smaller subagglomerates, following which the stronger agglomerates are slowly abraded to produce fine particles of 1–10 μm [172]. However, there is also contrary evidence from Thoma and co-workers [168], showing that fracture may be the preferred mechanism for strong TiO_2 agglomerates, while abrasion is favored for weaker agglomerates. That is, when subjected to ultrasonic stress, 30-μm-diameter agglomerates of amorphous anatase (TiO_2) prepared by thermal hydrolysis were observed to undergo fracture to 5–15-μm fragments, while 90-μm agglomerates of polycrystalline anatase prepared by basic precipitation were found to break down by

erosion to 0.1–5-μm fragments [168]; in this case, the amorphous anatase was apparently stronger by a factor of 2 (see Table 15). Supporting a third trend, data from Pham and co-workers [163] show that attrition mechanism and rate are independent of agglomerate strength, but depend instead on the type of material. That is, 100-μm-diameter agglomerates of precipitated Fe/Cu/K Fischer–Tropsch catalyst (prepared by United Catalyst Incorporated) and having nearly the same strength shown in Table 15 for Vista-B Al_2O_3 (6.3 *vs.* 6.2 MPa), were found to undergo substantial fracture to 5–30-μm fragments (an increase from 45 to 85%; see Figure 28) as well as substantial erosion to 1 μm or less fragments (increase from 2 to 50%). By comparison, under the same treatment conditions, 90-μm-diameter agglomerates of Vista-B Al_2O_3 underwent much less attrition, mainly by erosion (20% increase in 0.1–5-μm fragments). The very low attrition resistance of the Fe/Cu/K Universal Catalysts, Inc. (UCI) catalyst is further emphasized by the unsatisfactory outcome of a test of this catalyst by the U.S. Department of Energy (DOE) in a pilot-scale slurry-phase bubble-column reactor in LaPorte, TX.; following one day of operation, the filter system was plugged with catalyst fines, preventing catalyst–wax separation and forcing shutdown of the plant [173].

Thus, based on these three representative examples, it follows that which of the two attrition mechanisms predominates depends much more on material composition and type than on agglomerate strength. However, irrespective of mechanism, the rate of attrition is usually greater for the weaker material.

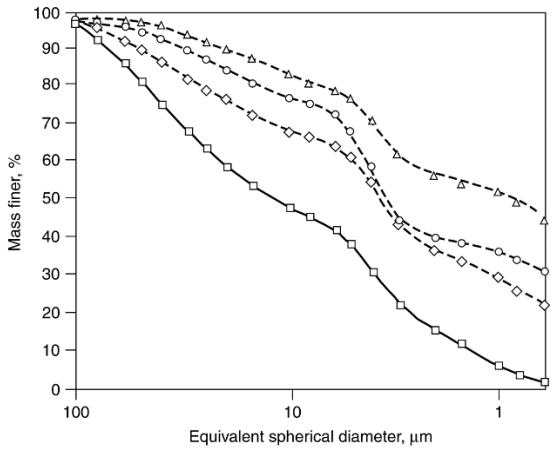

Figure 28. Sedigraph particle size distribution for a United Catalysts, Inc. (UCI) Fischer-Tropsch catalyst (designated as UCI-LAPI-COMP-DRUMC), used previously in Department of Energy (DOE) pilot-plant tests. There is considerable particle breakdown and generation of fine particles after 15 min of ultrasonic irradiation. Reproduced from [163]. Copyright 1999, Elsevier. —□— 0 min; – –◊– –5 min; - -○- - 10 min; – – Δ – –15 min.

Figure 29 illustrates the large effect that catalyst preparation method can have on the attrition resistance of an Fe/Cu Fischer–Tropsch catalyst [174]. This catalyst, prepared by precipitation, undergoes severe attrition during a 25-min treatment with ultrasonic radiation; indeed, the mass fraction finer than 0.1–5 μm increases from 0 to 65%. However, after a spray drying treatment of the same catalyst, an increase of only 0 to 10% in the same fractions is evident.

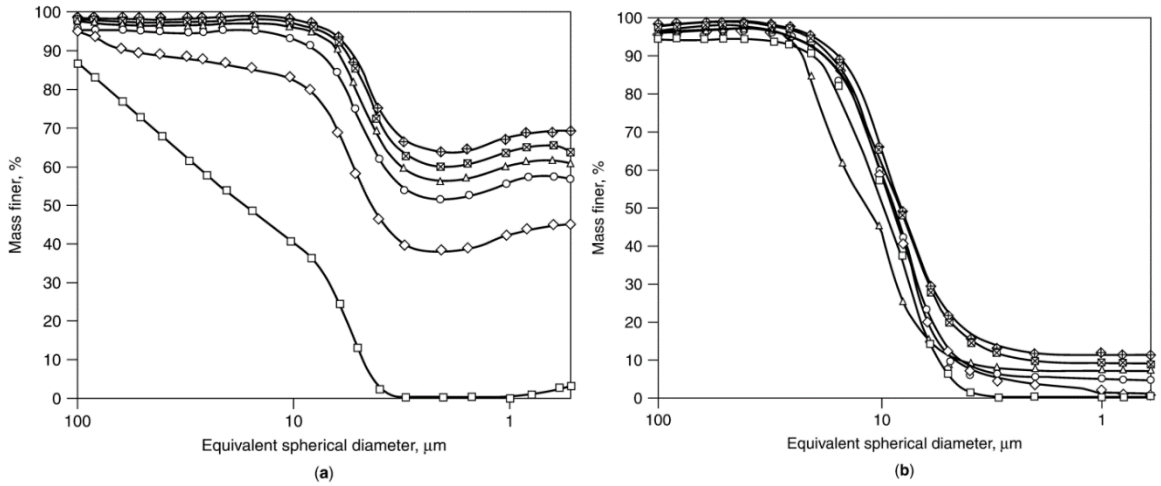

Figure 29. Sedigraph particle size distributions of a precipitated Fe–Cu catalyst, as-prepared and after spray-drying. The as-prepared catalyst (**a**) is weak and breaks down easily after 25 min of ultrasonic irradiation, while spray-drying (**b**) improves its attrition resistance. Reproduced from [174]. Copyright 2000, Elsevier. —□— 0 min; ♦ 5 min; —○— 10 min; —Δ— 15 min; —⊠— 20 min; — ⊕— 25 min.

In their review of attrition and attrition test methods, Bemrose and Bridgewater [175] discuss how attrition varies with reactor type, e.g., involves mainly particle–wall impacts in moving pellet bed reactors and particle–particle impacts in fluidized-bed reactors of high fluid velocity. In fact, jet attrition of catalyst particles in a gas fluidized-bed involving principally abrasion due to collision of high-velocity particles has been modeled in some detail [172,176]. Thus, given such important differences in attrition mechanism, realistic attrition test methods should attempt to model reactor operation as closely as possible. In addition, the ideal test would require only a small catalyst sample, a simple, inexpensive apparatus, and a few minutes to complete the test. Relatively quick, inexpensive single-particle crushing tests have been devised [175]; however, properties of a single particle are rarely representative of those for the bed; moreover, it is difficult to relate the results of this crushing test to the actual abrasion process. Realistic tests have been devised for two reactor types involving a moving catalyst, *i.e.*, an air-jet test for fluidized-bed catalysts [177,178], and a rotating drum apparatus for moving-bed catalysts [179]; however, the air-jet test requires a large quantity (e.g., 50 g) of catalyst, an expensive apparatus, and about 20 h to run. In the past decade, a new jet-cup test has been developed for testing of fluidized-bed catalysts [177,178], which requires only a 5-g sample and about 1 h to complete; comparisons of results for the jet-cup and air-jet tests indicate that the two tests give comparable results [177,178]. Nevertheless, the mechanisms for the two tests are different, *i.e.*, the air-jet (fluid-bed) test is abrasion- (erosion-) dominant, while the jet-cup test includes both abrasion and fracture mechanisms [178]. A 30-min, 10-g ultrasonic attrition test based on cavitation has also been developed in the past decade [168,174,180]; while it likewise involves both abrasion and fracture mechanisms, the results appear to correlate with other methods. For example, particle size distributions for the same Co/silica catalyst after ultrasonic, jet-cup, and laboratory-scale, slurry-bed column reactor (SBCR) tests are very similar (see Figure 30), indicating that both fracture and abrasion mechanisms operate in the small-scale SBCR. Moreover, the good agreement among the three methods suggests

that both the jet-cup and ultrasonic tests may provide data representative of the attrition process in laboratory-scale SBCR reactors. It is evident that these two small-scale methods are especially useful for screening of a series of catalysts to determine relative strength.

Nevertheless, the more realistic large-scale tests are probably needed for accurately determining design attrition rates of a commercial catalyst to be used in a full-scale process. The observation that attrition of a fluid catalytic cracking (FCC) catalyst initially involves fracture of weak agglomerates followed by abrasion of strong agglomerates emphasizes the need to collect and analyze the particle size distribution of attrited fines as a function of time in order to define which mechanism (or mechanisms) operates at startup as well as in the steady-state process. Because the mechanism may be time dependent, rapid, small-scale tests may produce misleading results.

While realistic laboratory-scale tests have been developed for simulating attrition in large moving-bed and fluidized-bed reactors, no such laboratory test has been developed and demonstrated yet for simulation of large-scale SBCR reactors, although recent research has focused on the development of such tests. For example, in laboratory-scale, SBCR tests of supported cobalt catalysts over several days [180], the attrition resistance decreases in the order Co/Al_2O_3 > Co/SiO_2 > Co/TiO_2 (especially the anatase form underwent attrition at a high rate); attrition resistance was observed to increase with increasing cobalt loading from 10 to 40 wt%.

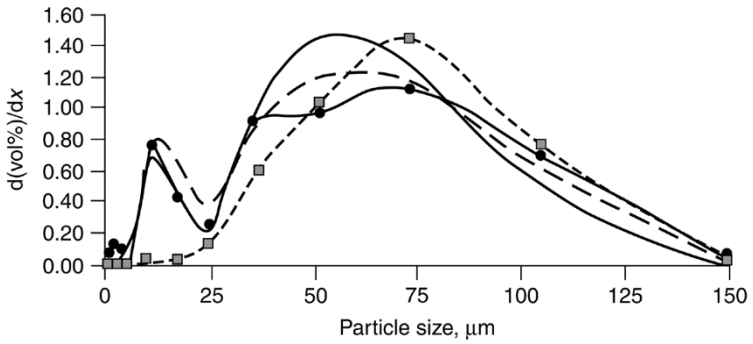

Figure 30. Particle size distributions of Co/SiO_2 catalyst. Adapted from [178]. ——— Ultrasound 250 W (>10 µm);- - - jet cup L/min (>10 µm); —●— Co/SiO_2 after SBCR; —■— Co/SiO_2 fresh.

2.5.5. Implications of Mechanistic Knowledge of Attrition for Catalyst Design

The understanding of mechanisms important in attrition of catalyst supports and catalysts, the relationship between strength and attrition rate for a given material, and test data can be used to great advantage in the design of attrition resistant catalysts. Several alternatives follow from the previous discussion for increasing attrition resistance: (1) increasing aggregate/agglomerate strength by means of advanced preparation methods, e.g., sol–gel granulation, spray drying, and carefully controlled precipitation methods (see Table 15 and Figure 29 for examples), (2) adding binders to improve strength and toughness, e.g., the addition of a polyvinylpyrrolidone binder to agglomerates of quartz sand increases agglomerate strength from 0.1 to 3 MPa [181], (3) coating aggregates with a porous but very strong material such as ZrO_2, e.g., embedding a fluidized-bed catalyst for partial oxidation of *n*-butane to maleic anhydride in a strong, amorphous matrix of zirconium hydrogen phosphate

significantly improves its attrition resistance [182], and (4) chemical or thermal tempering of agglomerates to introduce compressive stresses that increase strength and attrition resistance, e.g., heating and cooling particles rapidly by passing them through a low-residence-time, high-temperature furnace to harden the agglomerate exterior, while preventing significant sintering of or phase changes in the porous interior. The subject of preventing mechanical degradation and other forms of catalyst deactivation is addressed in greater detail under Prevention of Catalyst Decay.

2.6. Summary of Deactivation Mechanisms for Solid Catalysts

Causes of solid (heterogeneous) catalyst deactivation are basically threefold: (1) chemical, (2) mechanical, and (3) thermal. Mechanisms of heterogeneous catalyst deactivation can be classified into five general areas: (1) chemical degradation including volatilization and leaching, (2) fouling, (3) mechanical degradation, (4) poisoning, and (5) thermal degradation. Poisoning and thermal degradation are generally slow processes, while fouling and some forms of chemical and mechanical degradation can lead to rapid, catastrophic catalyst failure. Some forms of poisoning and many forms of fouling are reversible; hence, reversibly poisoned or fouled catalysts are relatively easily regenerated. On the other hand, chemical, mechanical, and thermal forms of catalyst degradation are rarely reversible.

3. Prevention of Catalyst Decay

It is often easier to prevent rather than cure catalyst deactivation. Many poisons and foulants can be removed from feeds using guard beds, scrubbers, and/or filters. Fouling, thermal degradation, and chemical degradation can be minimized through careful control of process conditions, e.g., lowering temperature to lower sintering rate or adding steam, oxygen, or hydrogen to the feed to gasify carbon or coke-forming precursors. Mechanical degradation can be minimized by careful choice of carrier materials, coatings, and/or catalyst particle forming methods.

While treating or preventing catalyst deactivation is facilitated by an understanding of the mechanisms, additional perspectives are provided by examining the route by which each of the mechanisms causes loss of catalytic activity, *i.e.*, how it influences reaction rate [109]. Thus, catalytic activity can be defined in terms of the observed site-based rate constant k_{obs}, which is equal to the product of the active site density σ (number of sites per area of surface), the site-based intrinsic rate constant k_{intr}, and the effectiveness factor η, *i.e.*,

$$k_{obs} = \sigma k_{intr} \eta \quad (4)$$

Loss of catalytic activity may be due to a decrease in any of the three factors in Equation 4, whose product leads to k_{obs}. Thus, catalyst deactivation can be caused by (1) a decrease in the site density σ, (2) a decrease in intrinsic activity (*i.e.*, decrease in k_{intr}), and/or (3) lowered access of reactants to active sites (decrease in η). Poisoning, for example, leads to a loss of active sites, *i.e.*, $\sigma = \sigma_0(1 - \alpha)$, where α is the fraction of sites poisoned; sintering causes loss of active sites through crystallite growth and reduction of active surface area. Fouling can cause both loss of active sites due to blocking of surface sites as well as plugging of pores, causing a decrease in the effectiveness η. Moreover, poisoning, as discussed earlier, can also lead to a decrease in intrinsic activity by influencing the

electronic structure of neighboring atoms. Thus, each of the deactivation mechanisms affects one or more of the factors comprising observed activity (see Table 16); all of the mechanisms, however, can effect a decrease in the number of catalytic sites.

Table 16. How Deactivation Mechanisms Affect the Rate of a Catalyzed Reaction and the Rapidity and Reversibility of Deactivation Process.

	Effects on reaction rate			Deactivation process	
Deactivation mechanism	**Decrease in number of active sites**	**Decrease in intrinisic activity (k_{intr})**	**Decrease in effectiveness factor (η)**	**Fast or slow [a]**	**Reversible**
Chemical degradation	×	×	× [b,c]	Varies	No
Fouling	×	×	-	Fast	Yes
Mechanical degradation	×	-	-	Varies	No
Poisoning	×	×	-	Slow	Usually
Thermal degradation/Sintering	×	× [b,d]	× [b,e]	Slow	Sometimes
Vaporization/leaching	×	× [b,f]	-	Fast	Sometimes

[a] Generally; [b] In some cases; [c] Chemical degradation can cause breakdown of support, pore plugging, and loss of porosity; [d] If the reaction is structure-sensitive, sintering could either increase or decrease intrinsic activity; [e] Sintering of the support may cause support collapse and loss of porosity; it may also increase average pore diameter. [f] Leaching of aluminum or other cations from zeolites can cause buildup of aluminum or other oxides in zeolite pores.

3.1. General Principles of Prevention

The age-old adage that says "an ounce of prevention is worth a pound of cure" applies well to the deactivation of catalysts in many industrial processes. The catalyst inventory for a large plant may entail a capital investment of tens of millions of dollars. In such large-scale processes, the economic return on this investment may depend on the catalyst remaining effective over a period of up to 3–5 years. This is particularly true of those processes involving irreversible or only partially reversible deactivation (e.g., sulfur poisoning or sintering). Some typical industrial catalysts, approximate catalyst lifetimes, and factors that determine their life are listed as examples in Table 17. It is evident that in many processes more than one mechanism limits catalyst life. Moreover, there is a wide variation in catalyst lifetimes among different processes, *i.e.*, from 10^{-6} to 15 years. While there is clearly greater interest in extending catalyst lifetimes in processes where life is short, it should be emphasized that great care must be exercised in protecting the catalyst in any process from process upsets (e.g., temperature runaway, short-term exposure to impure feeds, or changes in reactant composition) that might reduce typical catalyst life by orders of magnitude, e.g., from years to hours.

Table 17. Typical Lifetimes and Factors Determining the Life of Some Important Industrial Catalysts [a].

Reaction	Operating conditions	Catalyst	Typical life (years)	Process affecting life of catalyst charge	Catalyst property affected
Ammonia synthesis $N_2 + 3\ H_2 \rightarrow 2\ NH_3$	450–470 °C 200–300 atm	Fe with promoters (K_2O) and stabilizer (Al_2O_3)	10–15	Slow sintering	Activity
Methanation (ammonia and hydrogen plants) $CO/CO_2 + H_2 \rightarrow CH_4 + H_2O$	250–350 °C 30 atm	Supported nickel	5–10	Slow poisoning by S, As, K_2CO_3 from plant upsets	Activity and pore blockage
Acetylene hydrogenation ("front end") $C_2H_2 + H_2 \rightarrow C_2H_4$	30–150 °C 20–30 atm	Supported palladium	5–10	Slow sintering	Activity/selectivity and temperature
Sulfuric acid manufacturing $2\ SO_2 + O_2 \rightarrow 2\ SO_3$	420–600 °C 1 atm	Vanadium and potassium sulfates on silica	5–10	Inactive compound formation; pellet fracture; plugging by dust	Activity, pressure drop, and mass transfer
Methanol synthesis $CO + 2\ H_2 \rightarrow CH_3OH$	200–300 °C 50–100 atm	Copper on zinc and aluminum oxides	2–5	Slow sintering; poisoning by S, Cl, and carbonyls	Activity
Low temperature water gas shift $CO + H_2O \rightarrow CO_2 + H_2$	200–250 °C 10–30 atm	Copper on zinc and aluminum oxides	2–4	Slow poisoning and accelerated sintering by poisons	Activity
Hydrocarbon hydrodesulfurization $R_2S + 2\ H_2 \rightarrow H_2S + R_2$	300–400 °C 30 atm	Cobalt and molybdenum sulfides on aluminum oxide	1–10	Slow coking, poisoning by metal deposits in residuum	Activity, mass transfer, and pressure drop
High temperature water gas shift $CO + H_2O \rightarrow H_2 + CO_2$	350–500 °C 20–30 atm	Fe_3O_4 and chromia	1–4	Slow sintering, pellet breakage due to steam	Activity and pressure drop

Table 17. *Cont.*

Reaction	Operating conditions	Catalyst	Typical life (years)	Process affecting life of catalyst charge	Catalyst property affected
Steam reforming, natural gas $CH_4 + H_2O \rightarrow CO + 3\ H_2$	500–850 °C 30 atm	Nickel on calcium aluminate or α-alumina	1–3	Sintering, sulfur-poisoning, carbon formation, and pellet breakage due to plant upsets	Activity and pressure drop
Ethylene partial oxidation $2\ C_2H_4 + O_2 \rightarrow 2\ C_2H_4O$	200–270 °C 10–20 atm	Silver on α-alumina with alkali metal promoters	1–3	Slow sintering, poisoning by Cl, S	Activity and selectivity
Butane oxidation to maleic anhydride $C_4H_{10} + 3.5\ O_2 \rightarrow C_4H_2O_3 + 4\ H_2O$	400–520 °C 1–3 atm	Vanadium phosphorus oxide with transition metal additives	1–2	Loss of P; attrition or pellet breakage; S, Cl poisoning	Activity and selectivity
Reduction of aldehydes to alcohols $RCHO + H_2 \rightarrow RCH_2OH$	220–270 °C 100–300 atm	Copper on zinc oxide	0.5–1	Slow sintering, pellet breakage (depends on feedstock)	Activity or pressure drop
Ammonia oxidation $2\ NH_3 + 5/2\ O_2 \rightarrow 2\ NO + 3\ H_2O$	800–900 °C 1–10 atm	Pt–Rh alloy gauze	0.1–0.5	Surface roughness, loss of platinum	Selectivity, fouling by Fe
Oxychlorination of ethylene to ethylene dichloride $2\ C_2H_4 + 4\ HCl + O_2 \rightarrow 2\ C_2H_4Cl_2 + 2\ H_2O$	230–270 °C 1–10 atm	Copper chlorides on alumina (fluidized bed)	0.2–0.5	Loss by attrition and other causes resulting from plant upsets	Fluidized state and activity
Catalytic hydrocarbon reforming	460–525 °C 8–50 atm	Platinum alloys on treated alumina	0.01–0.5	Coking, frequent regeneration	Activity and mass transfer
Catalytic cracking of oils	500–560 °C 2–3 atm	Synthetic zeolites (fluidized bed)	0.000002	Very rapid coking, continuous regeneration	Activity and mass transfer

Adapted from Ref. [9].

While complete elimination of catalyst deactivation is not possible, the rate of damage can be minimized in many cases through understanding of the mechanisms, thereby enabling control of the deactivation process, *i.e.*, prevention is possible through control of catalyst properties, process conditions (*i.e.*, temperatures, pressures), feedstock impurities, methods of contacting, and process design. Figure 31 illustrates general approaches to eliminating or moderating deactivation through modifications in catalyst and/or process. Examples of how deactivation can be prevented are discussed below in connection with the most important causes of deactivation: chemical degradation, fouling by coke and carbon, poisoning, sintering, and mechanical degradation. Principles for preventing deactivation by these mechanisms are summarized in Table 18, while representative results from studies focusing on prevention or minimization of catalyst deactivation are summarized in Table 19.

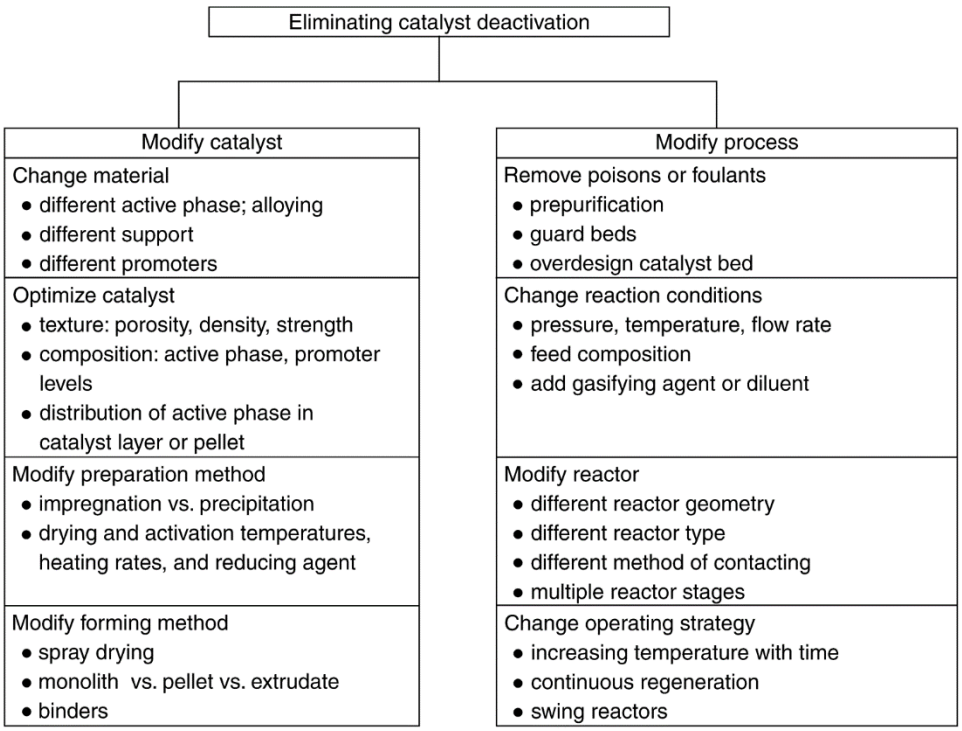

Figure 31. Approaches to eliminating catalyst deactivation.

Table 18. Methods for Preventing Catalyst Decay [8,41].

Basic mechanism	Problem	Cause	Methods of minimization
Chemical degradation	Oxidation of metal catalysts to inactive oxides	Oxidation of metal by contaminant O_2 or reactant/product water	(1) Purify feed of oxidants (2) Minimize reactant/product water by recycle/separation, staged reactors, and otherwise limiting conversion (3) Incorporate additives that facilitate resistance to oxidation
	Transformation of active phase to stable, inactive phase	Solid-state reaction of active phase with support or promoters	(1) Avoid conditions (e.g., oxidizing condition, high steam pressures, and high temperatures) that favor solid-state reactions (2) Select combinations of active phase and promoters/supports that are noninteracting
		Overreduction of active oxide phases	(1) Stabilize oxidation state using promoters that induce resistance to reduction or that serve as oxygen donors (2) Add steam to the reactants to prevent overreduction
Fouling by coke or carbon	Loss of catalytic surface sites due to formation of carbon or coke films	Free radical reactions in gas phase	(1) Avoid formation of free radicals, lower temperature (2) Minimize free space (3) Free radical traps, diluents (4) Add gasifying agents (e.g., H_2, H_2O)
		Free radical reactions at reactor walls	(1) Coat reactor with inert material
		Formation and growth on metal surfaces	(1) Avoid accumulation of coke precursors (e.g., atomic carbon, olefins) through careful choice of reactant conditions or membranes (2) Add gasifying agents (e.g., H_2, H_2O), diluents (3) Incorporate catalyst additives to increase rate of gasification or to change ensemble size (4) Passivate metal surfaces with sulfur (5) Decrease dispersion (6) Recycle inerts to flush surface of heavy oligomers and to moderate temperature

Table 18. *Cont.*

Basic mechanism	Problem	Cause	Methods of minimization
Fouling by coke or carbon (cont.)	Loss of catalytic surface sites due to formation of carbon or coke films	Formation and growth on metal oxides, sulfides	(1) Utilize measures 1, 2, 3, and 6 for metal surfaces (2) Design catalyst for optimum pore structure and acidity (3) Use shape-selective, coke-resistant molecular sieves
	Loss of catalyst effectiveness; plugging of pores; destruction of catalyst	Formation of gas phase coke, vermicular carbons, and liquid or solid cokes in massive quantities	(1) Minimize formation of free radicals or coke precursors as above (2) Use gasifying agents (3) Incorporate catalyst additives that lower solubility of carbon in metal or that change ensemble size (4) Use supports with large pores; large pellets
		Hot spots in pellet or bed	(1) Use wash coat or small pellets (2) Use slurry- or fluid-bed reactor, gas diluents
Mechanical failure	Crushing of granules, pellets, or monoliths in a fixed bed	Brittle fracture due to a mechanical load	(1) Minimize porosity of pellets or monoliths (2) Improve bonding of primary particles in agglomerates that make up pellets or monoliths using advanced forming methods, e.g., spray drying and controlled thermal treatments (3) Add binders such as carbon to the support material, which facilitate plastic deformation and thus protect against brittle fracture (4) Chemically or thermally temper agglomerates
	Attrition and/or erosion in fixed or moving beds	Abrasion of catalyst coatings or particles due to mechanical, thermal, or chemical stresses	(1) Avoid highly turbulent shear flows and/or cavitation, leading to high erosion rates (2) Avoid thermal stresses in the preparation and use of catalysts that lead to fracture or separation of coatings (3) Avoid formation of chemical phases of substantially different densities or growth of carbon filaments that cause fracture of primary particles and agglomerates. Choose supports, support additives, and coating materials, such as titanates, zirconia, and zirconates, having high fracture toughness

Table 18. *Cont.*

Basic mechanism	Problem	Cause	Methods of minimization
Poisoning	Loss of catalytic surface sites	Blockage of sites by strong adsorption of impurity	(1) Purify feed and/or use guard bed to adsorb poison (2) Employ additives that selectively adsorb poison (3) Choose reaction conditions that lower adsorption strength (4) Optimize pore structure and choose mass transfer regimes that minimize adsorption of poison on active sites (5) Apply coating that serves as diffusion barrier to poison
Thermal degradation, sintering	Loss of metal area	Metal particle or subparticle migration at high temperatures	(1) Lower or limit reaction temperature while facilitating heat transfer (2) Add thermal stabilizers to catalyst; and (3) avoid water
	Loss of support area	Crystallization and/or structural modification or collapse	Same as for avoiding loss of metal area

Table 19. Representative Results from Studies Focusing on Prevention/Minimization of Catalyst Deactivation.

Deactivation mechanism Process/Reaction Catalyst	Problem/cause	Method(s) of minimization	Ref.
Chemical degradation			
Auto emissions control Pt– or Pd–Rh/Al_2O_3	In three-way catalyst, Rh is very active for NO reduction, but it forms a solid solution with Al_2O_3 that has no activity and alloys with Pt or Pd that reduce its activity	Place Rh in a separate catalyst layer from Pt or Pd to prevent alloying; support Rh on ZrO_2, which is a noninteracting support for Rh. In general, multilayer strategies (up to 6 layers) are used to prevent undesirable interactions between different components of the catalyst	[183–185]

Table 19. *Cont.*

Deactivation mechanism Process/Reaction Catalyst	Problem/cause	Method(s) of minimization	Ref.
Chemical degradation			
Fischer–Tropsch synthesis Co supported on Al_2O_3, SiO_2, TiO_2, and Fe/Cu/K/SiO_2	Oxidation of active Co metal crystallites to inactive Co oxides, aluminates, and silicates and of active iron carbides to inactive Fe_3O_4 or Fe_3C in the presence of high pressure steam at high conversion	(1) Employ two- or three-stage process that enables lower conversion and lower concentrations of steam product in the first stage. Treat gaseous stream leaving the first or second stage to remove water and liquid hydrocarbons (2) Add noble metal promoters that facilitate and maintain high reducibility of the metal or metal carbide phases (3) Stabilize silica and alumina supports with coatings of hydrothermally stable materials such as ZrO_2 and $MgAl_2O_4$	[8,126,186,187]
Partial oxidation of isobutene to methacrolein $Fe_2(MoO_4)_3$, $Mo_{12}Bi_xCe_yO_z$	Overreduction of the catalyst during reaction leads to activity decrease	(1) Stabilize reduction state of iron molybdate catalyst using an oxygen donor such as α-Sb_2O_4; the oxygen donor dissociates molecular oxygen to atomic oxygen that readily spills over to the catalyst (2) $Mo_{12}Bi_xCe_yO_z$ catalyst promoted with Co, Mg, Rb, and/or Cs oxides is highly resistant to reduction, highly selective to methacrolein, and long-lived	[154,156,188]
Steam reforming and steam-oxygen conversion of propane Pd/Al_2O_3	In the absence of steam, PdO is reduced to less active, less thermally stable Pd metal	Adding steam to the reactants inhibits oxidation of propane at lower reaction temperatures while preventing reduction of PdO at higher temperatures (up to 700–900 °C)	[189]

Table 19. *Cont.*

Deactivation mechanism Process/Reaction Catalyst	Problem/cause	Method(s) of minimization	Ref.
Fouling by coke, carbon			
Alkene oligomerization Zeolites, esp. ZSM-5, –22, –23, beta-zeolite, ferrierite	Catalyst fouling by condensation of heavy oligomers to coke	(1) Recycle of heavy paraffins flushes the surface of heavy oligomers while moderating temperature, thereby decreasing the rate of coke formation (2) Addition of steam improves conversion and catalyst life—probably by cleaning the catalyst surface of coke precursors	[190–192]
Alkylation of isoparaffins on solid catalysts Sulfated zirconia, USY [a], Nafion	Rapid catalyst deactivation due to coke formation; unacceptable product quality, and thermal degradation of catalyst during regeneration	(1) Near critical operation favors desorption and removal of coke precursors from pores while enabling lower reaction temperature (2) Remove oxygen, oxygenates, diolefins, and aromatics from feed; passivate stainless steel surfaces with silicon or bases (3) Design catalyst for optimum pore structure and acidity (4) Use stirred-slurry or fluid-bed reactor while minimizing olefin concentration	[193,194]
Catalytic reforming of naphtha Pt/Al_2O_3 promoted with Re, Sn, Ge, or Ir	Poisoning and fouling by coke produced by condensation of aromatics and olefins	(1) Use bimetallic catalyst, e.g., sulfided $Pt–Re/Al_2O_3$, which is substantially more resistant to coke formation and longer-lived than is Pt/Al_2O_3. Re sulfide sites break up large Pt ensembles that produce coke. Sn and Ge have a similar effect; Sn and Ir also improve selectivity (2) Optimize reaction conditions and reactor design, e.g., moving bed and low pressure; maintain optimum Cl and S contents of catalyst throughout the bed (3) Near critical reaction mixtures provide an optimum combination of solvent and transport properties for maximizing isomerization rates while minimizing coking	[8,195–198]

Table 19. *Cont.*

Deactivation mechanism Process/Reaction Catalyst	Problem/cause	Method(s) of minimization	Ref.
Fouling by coke, carbon			
Dehydrogenation of propane and butane Cr_2O_3/Al_2O_3, Cr_2O_3/ZrO_2, FeO/K/MgO, Pt/Al_2O_3, Pt–Sn/Al_2O_3, Pt–Sn/KL-zeolite	Catalyst activity is low owing to equilibrium limitations and buildup of product H_2; rapid loss of activity occurs owing to coke formation	(1) Add Sn and alkali metals to Pt/Al_2O_3—additives reduce coke coverage of active sites; Sn decreases Pt ensemble size and enhances reactivity of hydrogen with coke (2) Use H_2-selective silica membrane to remove product H_2, which increases propane conversion; catalyst deactivation is slowed and catalyst life increases, probably due to a lowering of surface coverage of reaction intermediates, including coke precursors, thereby reducing the rate of coke formation	[8,199–203]
Hydrocracking of heavy naphtha CoMo, NiW, MoW on Al_2O_3 or SiO_2–Al_2O_3; Pt or Pd on Y-zeolite, mordenite or ZSM-5	Loss of activity due to poisoning of sites and blocking of small zeolite pores by coke	(1) Optimize metals loading and porosity of catalyst; use coke-resistant zeolites; incorporate amorphous silica–alumina, which prevents build up of bulky compounds in shape-selective zeolites (2) Design process to prevent build up of polynuclear aromatics, e.g., through distillation, bleeding, flashing, precipitation, and adsorption (3) Decouple aromatics saturation and hydrocracking reactions to improve selectivity, controllability, and catalyst life, while decreasing H_2 consumption	[8,198,204]

Table 19. *Cont.*

Deactivation mechanism Process/Reaction Catalyst	Problem/cause	Method(s) of minimization	Ref.
Fouling by coke, carbon			
Methane reforming CO_2/Co/SiO_2, Pt/SiO_2, Pt/ZrO_2, MgO-supported noble metals, NiO·MgO solid solution	High rates of carbon formation, which rapidly deactivate catalyst	(1) Add MgO or CaO to reduce carbon deposition on Co or Ni catalysts. CO_2 adsorbs strongly on these basic oxides, possibly providing oxygen atoms that gasify coke precursors (2) Adding Sn to Pt catalysts increases stability; ZrO_2 support promotes activity and selectivity by aiding dissociation of CO_2 (3) Add water or H_2 or increase pressure to decrease carbon deposition rate	[205–208]
Methanol to olefins or gasoline Silica–alumina, Y-zeolite, ZSM-5, other zeolites, and aluminophosphate molecular sieves	Severe coking and deactivation of silica–alumina and Y-zeolite catalysts observed during high conversions of MeOH; also substantial coking of ZSM-5, other zeolites, and alumino-phosphate molecular sieves	(1) Maintain a positive methanol concentration through the reactor (e.g., CSTR) to decrease olefin concentration, favor olefin–MeOH reaction to higher olefins over olefin–olefin reactions to coke precursors, substantially decrease coking and deactivation rates, and thereby greatly improve activity and selectivity (2) Increase concentration of water, which attenuates coke formation on SAPO-34 by competing with coke precursors for active sites (3) Treat SAPO-34 above 700 °C in steam to lower acidity, increase catalyst life, and increase selectivity for C_2–C_3 olefins. Addition of diluent to feed is also beneficial (4) Silanation decreases activity but improves life of zeolites, e.g., HY, HZSM-5	[209–236]

Table 19. *Cont.*

Deactivation mechanism Process/Reaction Catalyst	Problem/cause	Method(s) of minimization	Ref.
Fouling by coke, carbon			
Steam reforming of light hydrocarbons or naphtha Ni on MgO, $MgAl_2O_4$ or $CaAl_2O_4$ promoted with S, Cu, or Au	High rates of carbon and coke formation, which rapidly deactivate catalyst	(1) Use basic supports or oxide promoters, which lower carbon deposition rate by preventing hydrocracking and by facilitating adsorption of water, which facilitates gasification of surface carbon (2) Promote with S, Cu, or Au, which lower rate of graphite formation on Ni by decreasing ensemble size (since ensemble size for C-C bond breaking is smaller than for graphite formation)	[8,60,70,71]
Poisoning			
Auto emissions control $Pt–Rh/Al_2O_3$ or Pd/Al_2O_3	Poisoning of noble metal catalyst by P and S compounds and large hydrocarbons from lube oil	Optimize pore structure of alumina, deposit noble metals in layers below the support surface, or provide a diffusion barrier coating of zeolite or alumina; these measures prevent access of large poison molecules to catalyst layer	[18,212]
Fischer–Tropsch synthesis Co/Al_2O_3	100 ppb of HCN and NH_3 poisons cobalt slurry catalyst within 4 days	Remove HCN and NH_3 to less than 50 ppb total by (1) catalytic hydrolysis of HCN to NH_3, followed by scrubbing with water or (2) guard bed containing acidic solid absorbent	[213]
Fluidized catalytic cracking (FCC) USY or REO-Y [b] in silica matrix	(1) Poisoning of acid sites by *N*-containing compounds. (2) Deposition of Ni and V metals that change selectivity and decrease activity	(1) FCC matrix serves as a coating to remove *N*-containing compounds before they reach zeolites (2) Add Group 13–15 compounds to passivate metals (Sb and Bi for Ni and In for V) and/or trap V with MgO or SrO	[8,198]

Table 19. *Cont.*

Deactivation mechanism Process/Reaction Catalyst	Problem/cause	Method(s) of minimization	Ref.
		Poisoning	
Hydrotreating of gas oil; deep HDS Al_2O_3- supported CoMo, noble metals	Noble metal hydrogenation and high-activity HDS catalysts are poisoned by H_2S	(1) Two-stage operation with removal of H_2S between stages (2) Split feed into light and heavy streams; desulfurize light and hydrocrack heavy streams, combine, and conduct deep hydrogenation/HDS	[198]
Hydrotreating of residuum Al_2O_3- supported Mo and CoMo	Pore-mouth poisoning and blockage by Ni, V, and Fe sulfides present in feed as organometallics	(1) Use guard bed or multistage bed to remove metals with first stage containing large-pore, low-activity catalyst for removal of metals and subsequent stages containing progressively smaller-pore, higher-activity catalysts (2) Use catalysts with bimodal pore distributions	[8,214]
		Thermal degradation	
Auto emissions control PdO/δ- or θ-Al_2O_3 doped with BaO, La_2O_3, Pr_2O_3, CeO_2, and ZrO_2	In close-couple, fast-warm-up converters, exhaust temperatures reach 1000–1100 °C; conventional Pt–Rh/γ-Al_2O_3 catalysts sinter rapidly under these conditions; CeO_2 used as oxygen storage material also sinters rapidly	(1) Use δ- or θ-Al_2O_3 and Al_2O_3 spinels having a higher thermal stability than γ-alumina (2) Thermally stabilize Al_2O_3 with BaO, La_2O_3, Pr_2O_3, CeO_2, and ZrO_2; stabilize CeO_2 with ZrO_2 or Pr_2O_3 and ZrO_2 with Y (3) Employ PdO that interacts more strongly than Pt with oxide supports and is hence more stable against sintering	[8,215–222]
Catalytic combustion of methane and LNG PdO/La_2O_3, Pr_2O_3, CeO_2, and ZrO_2	Reaction temperatures ranging up to 1400 °C cause rapid sintering of most catalytic materials. Conversion above 800 °C of PdO to Pd metal is followed by rapid sintering of Pd and loss of activity	(1) Develop PdO/REO catalysts that resist sintering and decomposition of PdO to Pd up to 1300 °C (2) Maintain catalyst temperature below 1000 °C by (a) using lean mixtures, followed by post-catalyst injection of most of the fuel, or (b) employing a metal monolith with heat exchange and gradient of catalyst through bed	[8,224–227]

Table 19. *Cont.*

Deactivation mechanism Process/Reaction Catalyst	Problem/cause	Method(s) of minimization	Ref.
Thermal degradation			
Dehydrogenation of butene to butadiene Cr_2O_3/Al_2O_3, $Pt–Sn/Al_2O_3$	Permanent loss of catalytic activity by sintering at high reaction temperatures (550–650 °C)	Optimize the operation of staged catalytic reactors (cycle time between regenerations, temperature, and composition of the feed as variables) while placing a limit on the upper temperature	[8,228]
Fischer–Tropsch synthesis Co/Al_2O_3, Co/SiO_2, Co/TiO_2	Sintering in hot spots and loss of hydrocarbon selectivity at higher reaction temperatures due to highly exothermic reaction	(1) Employ two-stage process that enables lower conversion, better heat removal, and thereby a smaller temperature increase in the first reactor (2) Employ slurry reactor with superior heat transfer efficiency	[186,229]
Fluid catalytic cracking (FCC) USY, REO-Y	Dealumination and destruction of zeolite crystallinity and loss of surface area/pore volume during high-temperature (650–760 °C, 3 atm) regeneration in steam/air	(1) Carry out controlled dealumination or silanization of Y-zeolite to produce USY (2) Use of REO-Y to improve thermal stability (3) Limit steam partial pressure during regeneration	[8,198]
Methane steam reforming Ni on $MgAl_2O_4$ or $CaAl_2O_4$	Sintering of Ni and support during high-temperature reaction (800–1000 °C) in high-pressure steam (20 atm)	(1) Design relatively low surface area catalyst with rugged, hydrothermally stable spinel carrier of about 5 m^2/g (2) Form catalyst into rings to facilitate heat transfer and prevent overheating at the heated tube-wall	[8,70]

Table 19. *Cont.*

Deactivation mechanism Process/Reaction Catalyst	Problem/cause	Method(s) of minimization	Ref.
		Mechanical degradation	
Partial oxidation of n-butane to maleic anhydride VPO	Attrition in fluidized-bed process	Imbed catalyst particles in a strong, amorphous matrix of zirconium hydrogen phosphate	[182]
Fischer–Tropsch synthesis in a bubble-column slurry reactor Co/Al_2O_3, Co/SiO_2, Co/TiO_2	Attrition in bubble column slurry reactor	(1) Spray drying improves density and attrition resistance. (Attrition resistance improves with higher particle density; attrition resistance decreases in the order Co/Al_2O_3 > Co/SiO_2 > Co/TiO_2) (2) Addition of SiO_2 and/or Al_2O_3 to TiO_2 improves its attrition resistance; addition of TiO_2 or of La_2O_3 to Al_2O_3 improves its attrition resistance (3) Attrition resistance of Co/Al_2O_3 is improved when the γ-Al_2O_3 is formed from synthetic boehmite having a crystallite diameter of 4–5 nm and is pretreated in acidic solution having a pH of 1–3	[230–235]

[a] USY: ultrastable Y-zeolite. [b] REO-Y: rare-earth exchanged Y-zeolite.

3.2. Prevention of Chemical Degradation (by Vapor–Solid and Solid–Solid Reactions)

The most serious problems of oxidation of metal catalysts, overreduction of oxide catalysts, and reaction of the active catalytic phase with carrier or promoter, can be minimized or prevented by careful catalyst and process design (as enumerated in Table 18 and illustrated in Table 19). For example, the loss of Rh due to solid-state reaction with alumina in the automotive three-way catalyst can be prevented by supporting Rh on ZrO_2 in a separate layer from Pt and/or Pd on alumina [215–222] In Fischer–Tropsch synthesis, the oxidation of the active cobalt phase in supported cobalt catalysts to inactive oxides, aluminates, and silicates can be minimized by employing a two- or three-stage process in which product steam is moderated in the first stage by limiting conversion and in subsequent states by interstage removal of water [223] It can also be moderated by addition of noble metal promoters that facilitate and maintain high reducibility of the cobalt and by coating the alumina or silica support with materials such as ZrO_2 that are less likely to react with cobalt to form inactive phases.

3.3. Prevention of Fouling by Coke and Carbon

Rostrup-Nielsen and Trimm [57], Trimm [59], and Bartholomew [60] have discussed principles and methods for avoiding coke and carbon formation. General methods of preventing coke or carbon formation are summarized in Table 18. Most of these are based on one important fundamental principle: *carbon or coke results from a balance between the reactions that produce atomic carbon or coke precursors and the reactions of these species with H_2, H_2O, or O_2 that remove them from the surface*. If the conditions favor formation over gasification, these species accumulate on the surface and react further to form less active forms of carbon or coke, which either coat the surface with an inactive film or plug the pores, causing loss of catalyst effectiveness, pore plugging, or even destruction of the carrier matrix.

Methods to lower rates of formation of carbon or coke precursors relative to their rates of gasification vary with the mechanism of formation (*i.e.*, gas, surface, or bulk phase) and the nature of the active catalytic phase (e.g., metal or oxide). For example, gas phase formation can be minimized by choosing reaction conditions that minimize the formation of free radicals, by using free-radical traps, by introducing gasifying agents (e.g., H_2, H_2O) or gas diluents, and by minimizing the void space available for homogeneous reaction. Similarly, the formation and growth of carbon or coke species on metal surfaces is minimized by choosing reaction conditions that minimize the formation of atomic carbon or coke precursors and by introducing gasifying agents. Selective membranes or supercritical conditions can also be used to lower the gas-phase and surface concentrations of coke precursors. Since carbon or coke formation on metals apparently requires a critical ensemble of surface metal atoms and/or dissolution of carbon into the bulk metal, introduction of modifiers that change ensemble sizes (e.g., Cu or S in Ni or Ru) or that lower the solubility of carbon (e.g., Pt in Ni) can be effective in minimizing these forms of deactivation.

For example, in a detailed STM study of submonolayers of Au on Ni(111), Besenbacher and co-workers [71] found that the electron density of Ni atoms in the vicinity of Au atoms was increased; from density functional theory (DFT) calculations they concluded that the strength of carbon adsorption (and hence the tendency to form graphite) was decreased on next-nearest neighbor Ni

atoms; from studies of the effects of S adsorption on methane activation and graphite formation on pure Ni, they were able to infer that the ensemble size needed for methane dissociation is smaller than that for graphite formation. These fundamental insights were used in the design of a 0.3% Au-promoted 16% Ni/$MgAl_2O_4$ catalyst that loses no activity over 4000 h during steam reforming of *n*-butane, while the corresponding unpromoted Ni catalyst loses about 5% of its initial activity (see Figure 32). In contrast to the moderating effects of noble metal additives, addition of 0.5% Sn to cobalt substantially increases the rate of carbon filament formation from ethylene [72], an effect desirable in the commercial production of carbon filament fibers.

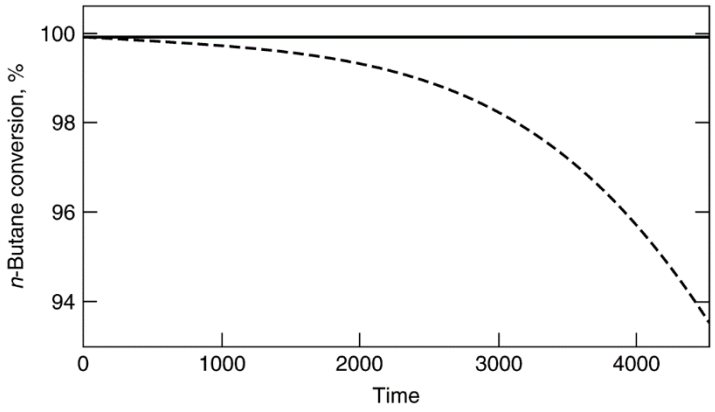

Figure 32. Conversion of *n*-butane as a function of time during steam reforming in a 3% *n*–butane–7% hydrogen–3% water in helium mixture at a space velocity of 1.2 h^{-1}. The dashed curve shows the *n*-butane conversion for the Ni catalyst (16.8% Ni) and the solid curve for the Au/Ni catalyst (16.4% Ni/0.3% Au). Reproduced from [71]. Copyright 1998, American Association for the Advancement of Science.

Coke deposition on oxide or sulfide catalysts occurs mainly on strongly acidic sites; accordingly the rate of coking can be lowered by decreasing the acidity of the support. For example, silanation of HY and HZSM-5 zeolites decreases their activities but improves catalyst life [236]. In steam reforming, certain catalyst additives, e.g., MgO, K_2O, or U_3O_8, facilitate H_2O or CO_2 adsorption and dissociation to oxygen atoms, which in turn gasify coke precursors [8,60,70].

Similarly, for steam reforming catalysts used for light alcohol and oxygenate conversion, the addition of partially reducible oxides, like ceria, in nickel perovskite ($La_{1-x}Ce_xNiO_3$) catalysts [237] or as a support for a cobalt catalyst [238], reduce the rate of carbon deposition. Alternatively, the reaction atmosphere may be modified to increase the gasification rate by adding oxidizing reactants (e.g., O_2 and/or CO_2) to reduce the rate of coke deposition [63]. This process is often described as autothermal reforming because it tends to balance the endothermic steam reforming reactions with exothermic reactions that make the process thermally neutral.

As in the case of poisoning (see below), there are certain reactor bed or catalyst geometries that minimize the effects of coking on the reaction. For example, specific film-mass transport or pore diffusion regimes favor coke or carbon deposition on either the outside or inside of the catalyst pellet [239,240]. Choosing supports with relatively large pores minimizes pore plugging; choice of large-diameter, mechanically-strong pellets avoids or delays reactor plugging. However, in view of the rapidity at

which coke and carbon can deposit on, plug, and even destroy catalyst particles, the importance of preventing the onset of such formation cannot be overemphasized.

Reforming of naphtha provides an interesting case study of catalyst and process designs to avoid deactivation by coking [8,196–198,241]. The classical Pt/Al_2O_3 catalyst is bifunctional; that is, the metal catalyzes dehydrogenation, while the acid sites of the Al_2O_3 catalyze isomerization and hydrocracking. Together, the two functions catalyze dehydrocylization and aromatization. Addition of Re, Sn, or Ge, to Pt and sulfiding of the Pt–Re catalyst substantially reduce coke formation by diluting large Pt ensembles that would otherwise produce large amounts of coke, while addition of Sn and Ir improves selectivity for dehydrogenation relative to hydrogenolysis, the latter of which leads to coke formation. Naphtha reforming processes are designed for (1) high enough H_2 pressure to favor gasification of coke precursors while minimizing hydrocracking, (2) maintenance of Cl and S contents throughout the bed to ensure optimum acidity and coke levels, and (3) low enough overall pressure to thermodynamically and kinetically favor dehydrogenation and dehydrocylization. Accordingly, optimal process conditions are a compromise between case 1 and case 3. The above-mentioned improvements in catalyst technologies, especially resistance to coking, have enabled important process improvements, such as optimal operation at lower pressure; thus, processes have evolved over the past two to three decades from conventional fixed-bed reactors at high pressure (35 bar) using nonregenerative Pt catalysts to low pressure (3.5 bar), slowly moving-bed, continuously regenerated units with highly selective Pt/Sn catalysts, resulting in substantial economic benefits [198,241].

3.4. Prevention of Poisoning

Since poisoning is generally due to strong adsorption of feed impurities and since poisoned catalysts are generally difficult or impossible to regenerate, it is best prevented by removal of impurities from the feed to levels that will enable the catalyst to operate at its optimal lifetime. For example, it is necessary to lower the feed concentration of sulfur compounds in conventional methanation and Fischer–Tropsch processes involving base metal catalysts to less than 0.1 ppm in order to ensure a catalyst lifetime of 1–2 years. This is typically accomplished using a guard bed of porous ZnO at about 200 °C. In cracking or hydrocracking reactions on oxide catalysts, it is important to remove strongly basic compounds, such as ammonia, amines, and pyridines, from the feed; ammonia in some feedstocks, for example, can be removed by aqueous scrubbing. The poisoning of catalysts by metal impurities can be moderated by selective poisoning of the unwanted metal. For example, in catalytic cracking of nickel-containing petroleum feedstocks, nickel sites, which would otherwise produce copious amounts of coke, are selectively poisoned by antimony [242]. The poisoning of hydrotreating catalysts by nickel and vanadium metals can be minimized by (1) using a guard bed of inexpensive Mo catalyst or graded catalyst bed with inexpensive, low-activity Mo at the top (bed entrance) and expensive, high-activity catalyst at the bottom (see Figure 33) and (2) by depositing coke prior to the metals, since these metal deposits can be physically removed from the catalyst during regeneration [243].

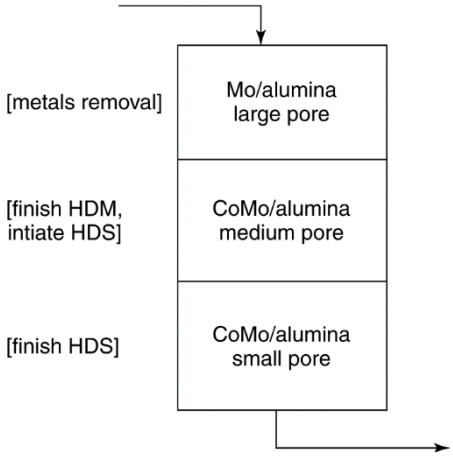

Figure 33. Staged reactor system with decreasing pore size strategy for hydrodemetalization (HDM)/hydrodesulfurization (HDS) of residuum. Reproduced from [214]. Copyright 1993, Marcel Dekker.

It may be possible to lower the rate of poisoning through careful choice of reaction conditions that lower the strength of poison adsorption [60] or by choosing mass-transfer-limiting regimes that limit deposits to the outer shell of the catalyst pellet, while the main reaction occurs uninterrupted on the interior of the pellet [239]. The manner in which the active catalytic material is deposited on a pellet (e.g., uniformly or in an eggshell or egg yolk pattern) can significantly influence the life of the catalyst [17,244].

An example of reducing catalyst poisoning (and oxidation) through process design has been reported in a process patent for staged hydrocarbon synthesis via the Fischer–Tropsch reaction [245]. While cobalt catalysts are favored because of their high activities and while it is desirable to achieve high conversions of CO in the process, the one-pass conversion for cobalt is limited by (1) its tendency to be oxidized at high partial pressures of product water observed at high CO conversions and (2) its tendency under these conditions to form the oxygenated products (e.g., alcohols and aldehydes) that poison or suppress its synthesis activity. One alternative is to separate products and recycle the unused CO and H_2, but this requires costly recompression and separation of the oxygenates. Costly separation and/or poisoning can be prevented by operating a first-stage reactor containing a cobalt catalyst to a moderately high conversion followed by reacting the remaining CO and H_2 in a second stage to above 95% conversion on an iron catalyst, which is not sensitive to the oxygenates and which shifts some of the product water to H_2 and CO_2, thus minimizing its hydrothermal degradation.

An example of reducing catalyst poisoning through catalyst design occurs in abatement of emissions for automotive and motorcycle engines [18,212]. Application of an alumina or zeolite coating, or alternatively preparing the active phase in a sublayer, provides a diffusion barrier that prevents or slows the access of poisons from the fuel or oil (e.g., phosphorus and/or zinc from lubricating oil or corrosion products) to the catalyst surface. The principle is to optimize the pore size distribution of the diffusion barrier to provide access to the catalytic phase of relatively small hydrocarbon, CO, NO, and O_2 molecules, while preventing access of larger molecules, such as from lubricating oil and/or particulates.

Finally, another strategy that has been employed to reduce the impact of poisoning, particularly for sulfur, is the inclusion of traps or "getters" as part of the catalyst. These species, including rare earth oxides of thulium (Tm) [50] or Ce [51] and simple zinc oxide, essentially act as sacrificial stoichiometric reactants to protect the active metal by preferentially adsorbing the poison. These traps can extend the catalyst life, but because they are not catalytic as they perform, they are necessarily temporary agents if the poison remains in the feed to the process.

3.5. Prevention of Sintering

Since most sintering processes are irreversible or are reversed only with great difficulty, it is important to choose reaction conditions and catalyst properties that avoid such problems. Metal growth is a highly activated process; thus, by choosing reaction temperatures lower than 0.3–0.5 times the melting point of the metal, rates of metal sintering can be greatly minimized. The same principle holds true in avoiding recrystallization of metal oxides, sulfides, and supports. Of course, one approach to lowering reaction temperature is to maximize activity and surface area of the active catalytic phase.

Although temperature is the most important variable in the sintering process, differences in reaction atmosphere can also influence the rate of sintering. Water vapor, in particular, accelerates the crystallization and structural modification of oxide supports. Accordingly, it is vital to minimize the concentration of water vapor in high temperature reactions on catalysts containing high surface area supports.

Besides lowering temperature and minimizing water vapor, it is possible to lower sintering rates through addition of thermal stabilizers to the catalyst. For example, the addition of higher melting noble metals (such as rhodium or ruthenium) to a base metal (such as nickel) increases the thermal stability of the base metal [106]. Addition of Ba, Zn, La, Si, and Mn oxide promoters improves the thermal stability of alumina [246]. These additives can affect product selectivity, but generally positively toward desired products, and always through extending the productive life of the catalysts [8].

Designing thermally stable catalysts is a particular challenge in high temperature reactions, such as automotive emissions control, ammonia oxidation, steam reforming, and catalytic combustion. The development of thermally stable automotive catalysts has received considerable attention, thus providing a wealth of scientific and technological information on catalyst design (e.g., Refs. [8,215–222]). The basic design principles are relatively simple: (1) utilize thermally and hydrothermally stable supports, e.g., high-temperature δ- or θ-aluminas or alkaline-earth or rare-earth oxides that form ultrastable spinels with γ-alumina; (2) use PdO rather than Pt or Pt–Rh for high temperature converters, since PdO is considerably more thermally stable in an oxidizing atmosphere because of its strong interaction with oxide supports; and (3) use multilayer strategies and/or diffusion barriers to prevent thermally induced solid-state reactions (e.g., formation of Rh aluminate) and to moderate the rate of highly exothermic CO and hydrocarbon oxidations. For example, a typical three-way automotive catalyst may contain alkaline-earth metal oxides (e.g., BaO) and rare-earth oxides (e.g., La_2O_3 and CeO_2), for stabilizing Pt and/or PdO on alumina, and ZrO_2 as a thermal stabilizer for the CeO_2 (an oxygen storage material) and as a noninteracting support for Rh in a separate layer or in a separate phase in a composite layer (see Figure 34).

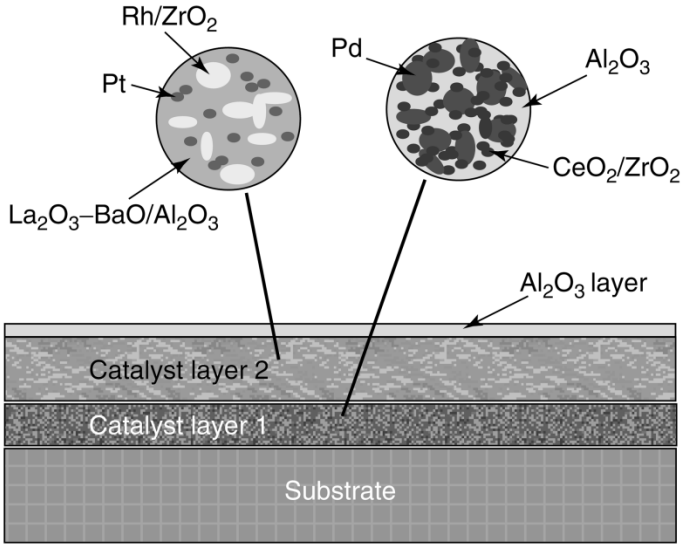

Figure 34. Conceptual design (by C. H. Bartholomew) of an advanced three-way catalyst for auto emissions control. Catalyst layer 1 is wash-coated first onto the monolithic substrate and consists of (**a**) well-dispersed Pd, which serves to oxidize CO/hydrocarbons and to reduce NO and (**b**) CeO_2/ZrO_2 crystallites (in intimate contact with Pd), which store/release oxygen respectively, thereby improving the performance of the Pd. Catalyst layer 2 (added as a second wash coat) is a particle composite of Rh/ZrO_2 (for NO reduction) and $Pt/La_2O_3–BaO/Al_2O_3$ (with high to moderately-high activity for oxidation of CO and hydrocarbons). A thin (50–80 μm) coat of Al_2O_3, deposited over catalyst layer 2, acts as a diffusion barrier to foulants and/or poisons. Both the Al_2O_3 layer and catalyst layer 2 protect the sulfur-sensitive components of catalyst layer 1 from poisoning by SO_2..

Often, ideal metal dispersions require metal nanoparticles to be distributed closely together, but these particles are thermodynamically unstable on the surface and undergo rapid sintering, as described in Section 2.3 above. Recently, in an attempt to reduce sintering rates, researchers have attempted to stabilize the metal nanoparticles by first dispersing them on a support, encapsulating them in the same or another metal oxide, and then opening porosity to the particles (e.g., [247,248]). These approaches have met with varying degrees of success, but point to promising new areas of synthesis techniques that have the potential to reduce or to eliminate deactivation by sintering.

3.6. Prevention of Mechanical Degradation

While relatively few studies have focused on this topic, there are nevertheless principles that guide the design of processes and catalysts in preventing or minimizing mechanical degradation (see Table 19). In terms of catalyst design, it is important to (1) choose supports, support additives, and coatings that have high fracture toughness, (2) use preparation methods that favor strong bonding of primary particles and agglomerates in pellets and monolith coatings, (3) minimize (or rather optimize) porosity (thus maximizing density), and (4) use binders, such as carbon, to facilitate plastic deformation and thus protect against brittle fracture. Processes (and to some extent preparation procedures) should be

designed to minimize (1) highly turbulent shear flows or cavitation that lead to fracture of particles or separation of coatings, (2) large thermal gradients or thermal cycling leading to thermal stresses, and (3) formation of chemical phases of substantially different densities or formation of carbon filaments leading to fracture of primary particles and agglomerates. Nevertheless, thermal or chemical tempering can be used in a controlled fashion to strengthen catalyst particles or agglomerates.

Examples of catalyst design to minimize attrition can be found in the recent scientific [230,231] and patent [232–235] literature focusing on the Fischer–Tropsch synthesis in slurry reactors. These studies indicate that (1) spray drying of particles improves their density and attrition resistance; (2) addition of silica and/or alumina into titania improves its attrition resistance, while addition of only 2000–3000 ppm of titania to γ-alumina improves alumina's attrition resistance; and (3) preformed alumina spheres promoted with La_2O_3 provide greater attrition resistance relative to silica. Increasing attrition resistance is apparently correlated with increasing density [230,231,235]. According to Singleton and co-workers [235], attrition resistance of Co/Al_2O_3 is improved when the γ-alumina support is (1) formed from synthetic boehmite having a crystallite diameter of 4–5 nm and (2) is pretreated in acidic solution having a pH of 1–3 (see Figure 35); moreover, attrition resistance decreases in the order $Co/Al_2O_3 > Co/SiO_2 > Co/TiO_2$ and is greater for catalysts prepared by aqueous *versus* nonaqueous impregnation.

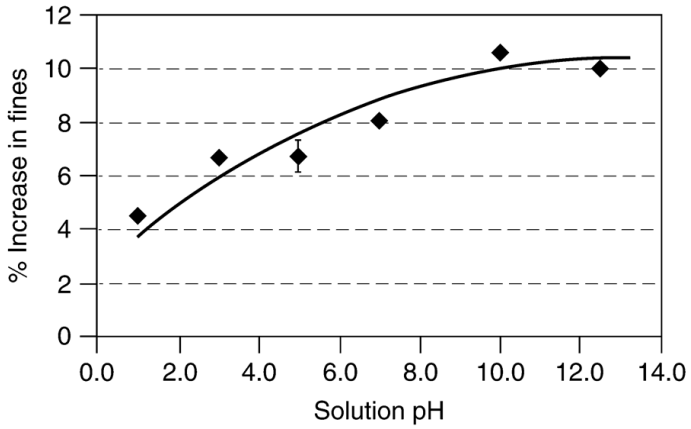

Figure 35. Effect of solution pH on the attrition resistance of 70-μm γ-Al_2O_3 particles measured in jet-cup tests [235]. The % increase in fines is defined at the % increase of particles of less than 11 μm.

4. Regeneration of Deactivated Catalysts

Despite our best efforts to prevent it, the loss of catalytic activity in most processes is inevitable. When the activity has declined to a critical level, a choice must be made among four alternatives: (1) restore the activity of the catalyst, (2) use it for another application, (3) reclaim and recycle the important and/or expensive catalytic components, or (4) discard the catalyst. The first alternative (regeneration and reuse) is almost always preferred; catalyst disposal is usually the last resort, especially in view of environmental considerations.

The ability to reactivate a catalyst depends upon the reversibility of the deactivation process. For example, carbon and coke formation is relatively easily reversed through gasification with hydrogen, water, or oxygen. Sintering on the other hand is generally irreversible, although metal redispersion is

possible under certain conditions in selected noble metal systems. Some poisons or foulants can be selectively removed by chemical washing, mechanical treatments, heat treatments, or oxidation [249,250]; others cannot be removed without further deactivating or destroying the catalyst.

The decision to regenerate/recycle or discard the entire catalyst depends largely on the rate of deactivation. If deactivation is very rapid, as in the coking of cracking catalysts, repeated or continuous regeneration becomes an economic necessity. Precious metals are almost always reclaimed where regeneration is not possible. Disposal of catalysts containing nonnoble heavy metals (e.g., Cr, Pb, or Sn) is environmentally problematic and should be a last resort; if disposal is necessary, it must be done with great care, probably at great cost. Accordingly, a choice to discard depends upon a combination of economic and legal factors [250]. Indeed, because of the scarcity of landfill space and an explosion of environmental legislation, both of which combine to make waste-disposal prohibitively expensive, there is a growing trend to regenerate or recycle spent catalysts [251,252]. A sizeable catalyst regeneration industry benefits petroleum refiners by helping to control catalyst costs and to limit liabilities [253,254]; it provides for *ex situ* regeneration of catalyst and recovery/recycling of metals, e.g., of cobalt, molybdenum, nickel, and vanadium from hydroprocessing catalysts [251].

Consistent with its importance, the scientific literature treating catalyst regeneration is significant and growing (includes nearly 1000 journal articles since 1990). Regeneration of sulfur-poisoned catalysts has been reviewed by Bartholomew and co-workers [28]. Removal of coke and carbon from catalysts has received attention in reviews by Trimm [59,250], Bartholomew [60], and Figueiredo [1]. Redispersion of sintered catalysts has been discussed by Ruckenstein and Dadyburjor [101], Wanke [102], and Baker and co-workers [103]. Useful case studies of regeneration of hydrotreating [255] and hydrocarbon-reforming catalysts [256] have also been reported. The proceedings of the 9th International Symposium on Catalyst Deactivation (2001) contains 12 papers treating catalyst regeneration [257]. Regeneration, recycling, and disposal of deactivated heterogeneous catalysts have been reviewed briefly by Trimm [250].

The patent literature treating catalyst regeneration/reactivation is enormous (more than 17,000 patents); the largest fraction of this literature describes processes for regeneration of catalysts in three important petroleum refining processes, *i.e.*, FCC, catalytic hydrocarbon reforming, and alkylation. However, a significant number of patents also claim methods for regenerating absorbents and catalysts used in aromatization, oligomerization, catalytic combustion, SCR of NO, hydrocracking, hydrotreating, halogenation, hydrogenation, isomerization, partial oxidation of hydrocarbons, carbonylations, hydroformylation, dehydrogenation, dewaxing, Fisher–Tropsch synthesis, steam reforming, and polymerization.

Conventional methods for regenerating (largely *in situ*) coked, fouled, poisoned, and/or sintered catalysts in some of these processes and representative examples thereof [258–297] are summarized in Table 20, while the basic principles and limitations involved in regeneration of coked, poisoned, and sintered catalysts are briefly treated in the subsections that follow.

Table 20. Conventional Methods for and Representative Examples of Catalyst Regeneration from Scientific and Patent Literatures.

Deactivation mechanism Process/Reaction Catalyst	**Problem/cause**	**Method(s) of regeneration/phenomena studied/conclusions**	**Ref.**
Deactivation by coke, carbon			
Alkene aromatization oligomerization Zeolites, esp. ZSM-5, -22, -23, beta-zeolite, ferrierite	Catalyst fouling by condensation of heavy oligomers to coke	(1) ZSM-5 catalyst for light olefin oligomerization containing 2–3% coke is treated in 8–10% steam/air mixture (1300 kPa, 93 °C inlet) in a fluidized bed (2) A coked crystalline alumogallosilicate is contacted with oxygen at a concentration of 0.05–10 vol%, 420–580 °C, and 300–4000 h^{-1}	[258,259]
Alkylation of isoparaffins on solid catalysts Sulfated zirconia, USY[a], Nafion, silicalite, ZSM-5	Rapid catalyst deactivation due to coke formation; unacceptable product quality, and thermal degradation of catalyst during regeneration	(1) Coked zeolite is regenerated in liquid phase (P > 3500 kPa) fluid bed with H_2 in two steps: (a) at reaction temperature (20–50 °C) and (b) at 25 °C above reaction temperature (2) Coked Pd- and Pt/Y-zeolite catalysts containing 10–13% coke are regenerated in either air or H_2; H_2 treatment enables removal of most of the coke at low to moderate temperatures; higher temperatures are required for air (3) USY and other zeolites are regenerated in supercritical isobutane	[260–263]

Table 20. *Cont.*

Deactivation mechanism Process/Reaction Catalyst	Problem/cause	Method(s) of regeneration/phenomena studied/conclusions	Ref.
Deactivation by coke, carbon			
Catalytic reforming of naphtha Pt/Al_2O_3 promoted with Re, Sn, Ge, or Ir	Poisoning and fouling by coke produced by condensation of aromatics and olefins	(1) Coke on Pt bimetallic reforming catalyst is removed off-stream in a fixed or moving bed at 300–600 °C, followed by oxychlorination (350–550 °C) (2) Coke on Pt/zeolite is removed in halogen-free oxygen-containing gas at $T < 415$ °C (3) Sintering during oxidation of coke on $Pt–Ir/Al_2O_3$ catalyst can be minimized by low regeneration temperatures (4) Study of influence of heating rate, temperature, and time on structural properties of regenerated $Pt–Sn/Al_2O_3$ (5) Study of effects of Cl, Sn content, and regeneration sequence on dispersion and selectivity of $Pt–Sn/Al_2O_3$ (6) Regenerated $Pt–Re/Al_2O_3$ is more stable than the fresh catalyst in *n*-heptane conversion and more selective for toluene	[264–269]
Dehydrogenation of propane and butane Cr_2O_3/Al_2O_3, Cr_2O_3/ZrO_2, FeO/K/MgO, Pt/Al_2O_3, $Pt–Sn/Al_2O_3$, Pt–Sn/KL-zeolite	Catalyst activity is low due to equilibrium limitations and build-up of product H_2; rapid loss of activity occurs due to coke formation	(1) Temperatures gradients were measured during burn off of coke formed on a chromia–alumina catalyst during butene dehydrogenation; data were used in developing a mathematical model for predicting temperatures and coke profiles (2) Coked supported palladium catalyst used in the dehydrogenation of dimethyltertrahydronaphthalenes to dimethylnaphthalenes is reactivated with an organic polar solvent at a temperature below 200 °C	[270,271]

Table 20. *Cont.*

Deactivation mechanism Process/Reaction Catalyst	Problem/cause	Method(s) of regeneration/phenomena studied/conclusions	Ref.
Deactivation by coke, carbon			
Fischer–Tropsch synthesis Co/Al_2O_3	Loss of activity due to blocking of sites by carbon overlayers and heavy hydrocarbons	(1) Carbidic surface carbon deposited on cobalt can be largely removed in hydrogen at 170–200 °C and in steam at 300–400 °C (2) Slurry-phase cobalt catalysts may lose 50% activity during reaction over a period of a few days; the activity can be rejuvenated *in situ* by injecting H_2 gas into vertical draft tubes inside the reactor	[272–274]
Fluid catalytic cracking (FCC) of heavy hydrocarbons USY or REO-Y[b] in silica matrix	Rapid loss of activity due to poisoning of acid sites and blocking of small zeolite pores by coke	(1) Process and apparatus for increasing the coke burning capacity of FCC regenerators; auxiliary regenerator partially burns off the coke at turbulent or fast fluidized-bed conditions (2) Multistage fluidized-bed regeneration of spent FCC catalyst in a single vessel by incorporating two relatively dense phase fluidized beds beneath a common dilute phase region	[275,276]
Hydrocracking of heavy naphtha CoMo, NiW, MoW on Al_2O_3 or SiO_2–Al_2O_3; Pt or Pd on Y-zeolite, mordenite, or ZSM-5	Loss of activity due to poisoning of acid sites and blocking of small zeolite pores by coke	(1) Regeneration of noble metal/zeolite via progressive partial removal of carbonaceous deposits under controlled oxidizing conditions to maximize sorption of a probe molecule while minimizing metal sintering (2) Regeneration of noble metal/zeolite in air at about 600 °C, followed by a mild treatment in aqueous ammonia to improve catalytic activity	[277,278]

Table 20. *Cont.*

Deactivation mechanism Process/Reaction Catalyst	Problem/cause	Method(s) of regeneration/phenomena studied/conclusions	Ref.
Deactivation by coke, carbon			
Hydrotreating of gas oil Al_2O_3-supported Mo and CoMo, NiMo, NiCoMo, MoW, NiW	Loss of activity due to formation of types I, II, and III coke on metal sulfide and alumina surfaces and in pores	(1) TPO studies of oxidative regeneration of CoMo and NiW HDS catalysts; sulfur is removed at 225–325 °C, carbon at 375–575 °C. Redispersion of NiW was observed by EXAFS (2) Physicochemical changes in CoMo and NiCoMo HDS catalysts during oxidative regeneration, including redispersion of Co, Ni, and Mo oxides and surface area loss, were examined (3) Changes in NiMo catalyst structure and coke composition during reaction and regeneration were examined and correlated (4) Properties of NiMo catalyst deactivated during shale oil hydrogenation and regenerated in O_2 or H_2 were examined. Regeneration in 1.6% O_2 was more effective than that in 5% H_2. Ni aluminate spinel was observed after burn off (5) Hard and soft cokes formed on CoMo catalysts during HDS of gas oil were characterized. At low coke levels, hard coke was more easily removed in H_2 than in O_2 (6) Spent catalysts are washed with solvent and contacted with steam at about 600 °C	[279,280, 294–297]
Methanol to olefins or gasoline Silica– alumina, Y-zeolite, ZSM-5, other zeolites, and aluminophosphate molecular sieves	Severe coking and deactivation of silica–alumina and Y-zeolite catalysts observed during high conversions of MeOH; also substantial coking of ZSM-5, other zeolites, and aluminophosphate molecular sieves	(1) Kinetics of coke burnoff from a SAPO-34 used in converting methanol to olefins were studied; kinetics are strongly dependent on the nature of the coke. Kinetics are slowed by strong binding of coke to acid sites (2) ZSM-34 catalyst used in conversion of methanol to light olefins is effectively regenerated in H_2-containing gas; this approach avoids the formation of catalyst-damaging products such as steam that would be formed during burn off in air	[281,282]

Table 20. *Cont.*

Deactivation mechanism Process/Reaction Catalyst	Problem/cause	Method(s) of regeneration/phenomena studied/conclusions	Ref.
		Poisoning	
FCC of residuum USY or REO-Y in silica matrix	(1) Poisoning of acid sites by *N*- containing compounds. (2) Deposition of Ni and V metals on acid sites which change selectivity and decrease activity	(1) Organometallic solutions of Sb and Bi are added to process stream to passivate Ni by forming inactive Ni–Sb and Ni–Bi species (2) V metal deposits are trapped by reaction with magnesium orthosilicate to form an unreactive magnesium vanadium silicate (3) Spent metal-contaminated catalyst is demetallized by chlorinating and washing, followed by contacting with NH_4F and one antimony compound (4) Metal-contaminated catalyst is contacted with an aqueous solution of a carboxylic acid (e.g., formic, acetic, citric, or lactic acid) (5) Metal-contaminated catalyst is contacted with HCl, HNO_3, or H_2SO_4 (6) Metal-contaminated catalyst is contacted with reducing CO gas to form gaseous metal carbonyls that are separated from the catalyst	[281,282,298–301]
Hydrogenation or dechlorination Ni/SiO_2, Pd/Al_2O_3	Poisoning of metal sites by arsenic, sulfur, and other poisons	(1) Regeneration of Ni/SiO_2 catalyst poisoned by thiophene using a sequence of oxidation–reduction treatments at low P_{O2} and 1 atm H_2 respectively (2) Regeneration in dilute hypochlorite solution of a Pd/Al_2O_3 catalyst deactivated during the aqueous-phase dechlorination of trichloroethylene in the presence of sulfite or HS^- ions present in ground water	[285,286]
Hydrotreating of residuum Al_2O_3-supported Mo and CoMo	Pore-mouth poisoning and blockage by Ni, V, and Fe sulfides present in feed as organometallics	(1) Regeneration of catalysts containing V, Ni, or Fe by contacting with H_2O_2 solution and organic acid (2) Following removal of coke by air or solvent wash, catalyst is acid leached to remove undesired metals	[287,288]

Table 20. *Cont.*

Deactivation mechanism Process/Reaction Catalyst	Problem/cause	Method(s) of regeneration/phenomena studied/conclusions	Ref.
Thermal degradation			
Catalytic reforming of naphtha Pt/Al_2O_3 promoted with Re, Sn, Ge, or Ir; Pt/KL-zeolite	Sintering of Pt causing formation of large metal crystallites and loss of active surface area	(1) Redispersion of Pt–Ir bimetallic catalysts using a wet HCl/air treatment, since the conventional oxychlorination is not effective (2) Redispersion of Pt/KL-zeolite using wet HCl/air treatment followed by brief calcination and reduction (*3*) Redispersion of $Pt–Re/Al_2O_3$ in Cl_2 and O_2 (*4*) Redispersion of supported Pt, other noble metals, and Ni in Cl_2 and O_2	[266,269,289,290]
Hydrocracking of heavy naphtha CoMo, NiW, MoW on Al_2O_3 or $SiO_2–Al_2O_3$; Pt or Pd on Y-zeolite, mordenite, or ZSM-5	Sintering of noble metal causing formation of large metal crystallites and loss of active surface area	Redispersion of noble metals on molecular sieves including silica-aluminates, ALPOS, SAPOS	[291]
Hydrotreating of gas oil and residuum Al_2O_3-supported Mo and CoMo	Sintering of Mo and Co sulfides causing formation of large sulfide crystals and loss of active surface area	(1) Oxidative regeneration of hydroprocessing catalyst at 600 °C optimizes surface area and Mo dispersion (2) Oxidative regeneration in several steps with a final oxidation at 500–600 °C to restore residual catalyst activity	[292,293]

[a] USY: ultrastable Y-zeolite. [b] REO-Y: rare-earth exchanged Y-zeolite.

4.1. Regeneration of Catalyst Deactivated by Coke or Carbon

Carbonaceous deposits can be removed by gasification with O_2, H_2O, CO_2, and H_2. The temperature required to gasify these deposits at a reasonable rate varies with the type of gas, the structure and reactivity of the carbon or coke, and the activity of the catalyst. Walker and co-workers [302] reported the following order (and relative magnitudes) for rates of uncatalyzed gasification at 10 kN/m^3 and 800 °C: O_2 (105) > H_2O (3) > CO_2 (1) > H_2 (3×10^{-3}). However, this activity pattern does not apply in general for other conditions and for catalyzed reactions [1]. Nevertheless, the order of decreasing reaction rate of $O_2 > H_2O > H_2$ can be generalized.

Rates of gasification of coke or carbon are greatly accelerated by the same metal or metal oxide catalysts upon which carbon or coke deposits. For example, metal-catalyzed coke removal with H_2 or H_2O can occur at a temperature as low as 400 °C [1]; β-carbon deposited in methanation can be removed with H_2 over a period of a few hours at 400–450 °C and with oxygen over a period of 15–30 min at 300 °C [60]. However, gasification of more graphitic or less reactive carbons or coke species in H_2 or H_2O may require temperatures as high as 700–900 °C [1], conditions, of course, that result in catalyst sintering.

Because catalyzed removal of carbon with oxygen is generally very rapid at moderate temperatures (e.g., 400–600 °C), industrial processes typically regenerate catalysts deactivated by carbon or coke in air. Indeed, air regeneration is used to remove coke from catalysts in catalytic cracking [81], hydrotreating processes [255], and catalytic reforming [256].

One of the key problems in air regeneration is avoiding hot spots or overtemperatures which could further deactivate the catalyst. The combustion process is typically controlled by initially feeding low concentrations of air and by increasing oxygen concentration with increasing carbon conversion [255,303]; nitrogen gas can be used as a diluent in laboratory-scale tests, while steam is used as a diluent in full-scale plant operations [303]. For example, in the regeneration of hydrotreating catalysts, McCulloch [255] recommends keeping the temperature at less than 450 °C to avoid the γ- to α-alumina conversion, MoO_3 sublimation, and cobalt or nickel aluminate formation, which occur at 815, 700, and 500–600 °C respectively.

Because coke burn-off is a rapid, exothermic process, the reaction rate is controlled to a large extent by film heat and mass transfer. Accordingly, burn-off occurs initially at the exterior surface and then progresses inward, with the reaction occurring mainly in a shrinking shell consistent with a "shell-progressive" or "shrinking-core" model, as illustrated in Figure 36 [304]. As part of this same work, Richardson [304] showed how experimental burn-off rate data can be fitted to various coking transport models, e.g., parallel or series fouling. Burn-off rates for coke deposited on SiO_2/Al_2O_3 catalysts were reported by Weisz and Goodwin [305]; the burning rate was found to be independent of initial coke level, coke type, and source of catalyst.

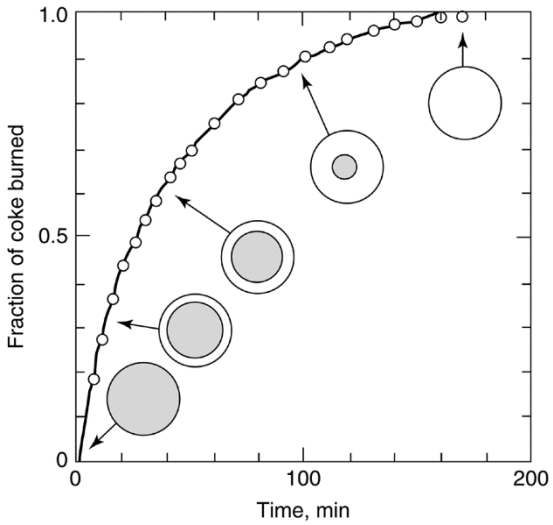

Figure 36. Shell-progressive regeneration of fouled pellet Reproduced from [304]. Copyright 1972, American Chemical Society.

4.2. Regeneration of Poisoned Catalysts

Much of the previous literature has focused on regeneration of sulfur-poisoned catalysts used in hydrogenations and steam reforming. Studies of regeneration of sulfur-poisoned Ni, Cu, Pt, and Mo with oxygen/air, steam, hydrogen, and inorganic oxidizing agents have been reported [28]. Rostrup-Nielsen [306] indicates that up to 80% removal of surface sulfur from Mg- and Ca-promoted Ni, steam reforming catalysts occurs at 700 °C in steam. The presence of both SO_2 and H_2S in the gaseous effluent suggests that the following reactions occur:

$$Ni\text{-}S + H_2O \rightarrow NiO + H_2S \quad (5)$$

$$H_2S + 2H_2O \rightarrow SO_2 + 3H_2 \quad (6)$$

Although this treatment is partially successful in the case of low-surface-area steam reforming catalysts, the high temperatures required for these reactions would cause sintering of most high-surface-area nickel catalysts.

Regeneration of sulfur-poisoned catalysts, particularly base metal catalysts, in air or oxygen has been largely unsuccessful. For example, the treatment of nickel steam-reforming catalysts in steam and air results in the formation of sulfates, which are subsequently reduced back to nickel sulfide upon contact with hydrogen. Nevertheless, sulfur can be removed as SO_2 at very low oxygen partial pressures, suggesting that regeneration is possible under carefully controlled oxygen atmospheres, including those provided by species such as CO_2 or NO that dissociate to oxygen. Apparently, at low oxygen pressures, the oxidation of sulfur to SO_2 occurs more rapidly than the formation of nickel oxide, while at atmospheric pressure the converse is true, *i.e.*, the sulfur or sulfate layer is rapidly buried in a nickel oxide layer. In the latter circumstance, the sulfur atoms diffuse to the nickel surface during reduction, thereby restoring the poisoned surface. Regeneration of sulfur-poisoned noble metals in air is more easily accomplished than with steam, although it is frequently attended by sintering. Regeneration of sulfur-poisoned nickel catalysts using hydrogen is impractical because (1) adsorption

of sulfur is reversible only at high temperatures at which sintering rates are also high and (2) rates of removal of sulfur in H_2 as H_2S are slow even at high temperature.

Inorganic oxidizing agents such as $KMnO_4$ can be used to oxidize liquid phase or adsorbed sulfur to sulfites or sulfates [16]. These electronically shielded structures are less toxic than the unshielded sulfides. This approach has somewhat limited application, *i.e.*, in partial regeneration of metal catalysts used in low temperature liquid-phase hydrogenation reactions or in liquid-phase destruction of chlorinated organic compounds. For example, Lowrey and Reinhard [286] reported successful regeneration in dilute hypochlorite solution of a Pd/Al_2O_3 catalyst deactivated during the aqueous-phase dechlorination of trichloroethylene (TCE) in the presence of sulfite or HS^- ions. These poisons are formed by sulfate-reducing bacteria present in natural groundwater and are apparently adsorbed on the alumina or Pd surfaces more strongly than sulfate ions. Figure 37 illustrates how readily the poisoned catalyst is regenerated by dilute hypochlorite solutions; indeed, it is evident in Figure 37b that regeneration every 5–10 days successfully maintains the catalytic conversion of TCE around 25% (a value only slightly less than that observed for reaction in distilled water).

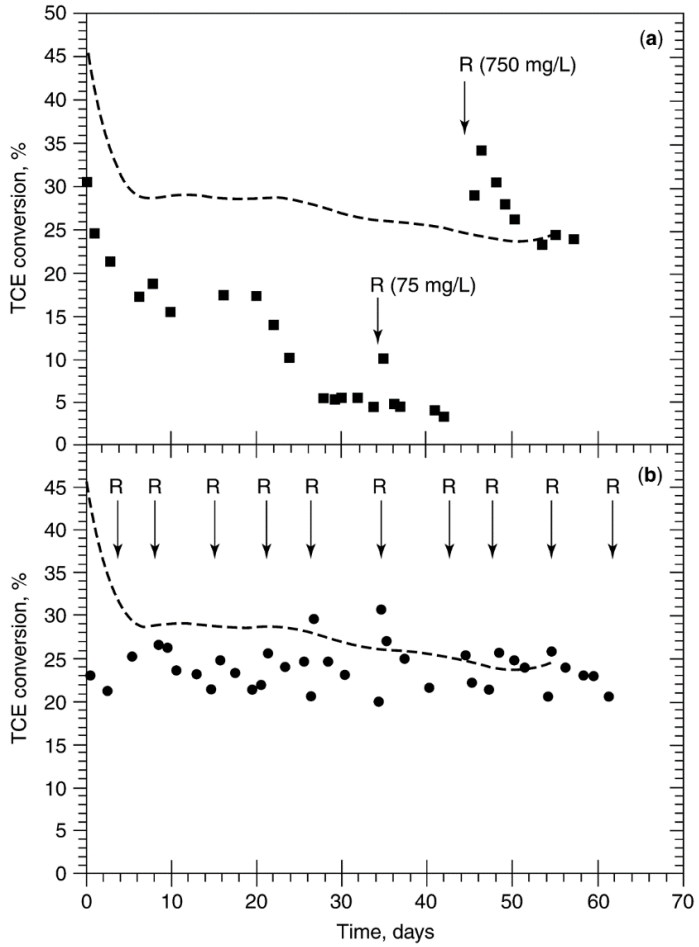

Figure 37. Effect of regeneration (R) with hypochlorite of Pd/Al_2O_3 catalysts used for aqueous phase dechlorination of trichloroethylene in the presence of HS^-/SO_3^2. Reproduced from [286]. Copyright 1992, American Chemical Society.

4.3. Detailed Case Study on Regeneration of Selective Catalytic Reduction (SCR) Catalysts

4.3.1. Introduction to SCR: Key to Abatement of NO_x from Coal Utility Boilers

NO_x, generally defined as NO and NO_2, emissions from coal utility boilers (approximately 30% of total NO_x emissions in the U.S.) contribute substantially to the formation of acid rain and photochemical smog, which in turn damage human health, property, agriculture, lakes, and forests. Selective catalytic reduction (SCR) technology has been used in utility boilers since the 1980s in Japan and Europe in response to stringent NO_x removal regulations. By 2000, SCR systems had been installed in coal-fired boilers totaling roughly 25 and 55 GW in Japan and Europe respectively [307,308]. Equivalent stringent NO_x abatement regulations were enacted later in the U.S. by the EPA, including

(1) the 1990 ARP and OTC mandates, requiring states to reduce NO_x emissions by 80%;
(2) the 1995 OTC-Phase 1 requiring Reasonably Available Control Technology (RACT);
(3) the 1998 NO_x SIP Call setting up a regional cap-and-trade program for 20 eastern states based on an equivalent NO_x emission rate of 0.15 lb/10^6-Btu; and
(4) the 2005 Clean Air Interstate Rule (CAIR) requiring all states to meet Best Available Retrofit Technology (BART) for existing plants, equivalent to emission rates of less than 0.05–0.10 lb/10^6-Btu [309,310].

By 2006, about 100 GW of coal-fired steam boilers in the U.S. used SCR. Presently, the U.S. has about 140 GW [309] of coal-boiler SCR capacity; world-wide, an estimated 300 GW of coal-boiler SCR is in operation.

Prior to the more recent stringent U.S. emissions regulations, boiler and engine manufacturers successfully reduced NO_x emissions by 30–60% using modifications to combustion processes, including reducing excess air, adding two-stage combustion features, altering burner design, *etc.* However, meeting the new reduction targets of 80–90% is, in general, only possible through catalytic after-treatment (SCR). Given ever more restrictive NO_x emission standards and the fact that worldwide power production from coal could double or triple in the next decade to an estimated 1500 GW [311], total installed SCR unit capacity is expected to grow commensurately, providing continued investment and design challenges in this area.

4.3.2. Selective Catalytic Reduction of NO_x

4.3.2.1. Reaction Chemistry and Preferred Catalysts

Selective catalytic reduction (SCR) is a process in which a reducing agent, typically NH_3, reacts selectively with the NO_x to produce N_2 without consumption of the excess O_2 present in the flue gas. Desirable stoichiometric reactions for SCR of NO and NO_2 (Equations 7 and 8) occur with high activity and selectivity to N_2 within a narrow temperature window of 300–400 °C on preferred commercial catalysts.

$$4NH_3 + 4NO + O_2 \rightarrow 4N_2 + 6H_2O \quad (7)$$

$$4NH_3 + 2NO_2 + O_2 \rightarrow 3N_2 + 6H_2O \quad (8)$$

Undesirable side reactions include oxidations of SO_2 (present in the flue gas) and the reducing agent NH_3. While only a small fraction of the SO_2 present in the flue gas is catalytically oxidized to SO_3, this acid precursor either corrodes downstream heat-exchange surfaces or reacts with NH_3 to form ammonium sulfates, which in turn can foul catalyst and/or heat exchange surfaces. Oxidation of NH_3 to either NO or N_2 may also occur at temperatures above 400 °C.

A typical commercial vanadia catalyst consists of 1 wt% V_2O_5 and 10 wt% WO_3 (alternatively 6 wt% MoO_3) supported on high-surface-area TiO_2 (mostly anatase, 60–80 m^2/g). TiO_2 has the decided advantage over Al_2O_3 as a support, since the former stabilizes the active vanadia species and does not form a bulk sulfate in the presence of SO_2-containing flue gases; thus TiO_2 promotes activity and extends catalyst life. WO_3 and MoO_3 prevent the transformation of anatase to rutile; they reside on basic sites of TiO_2, blocking adsorption of SO_3, thereby preventing sulfation of the support. Additionally, WO_3 and MoO_3 increase Brønsted acidity, promoting NO_x reduction while lowering SO_2 oxidation rate. Commercial vanadia-titania catalysts are typically supplied in the form of extruded monoliths or plates (see Figure 38), forms which minimize pressure drop [8].

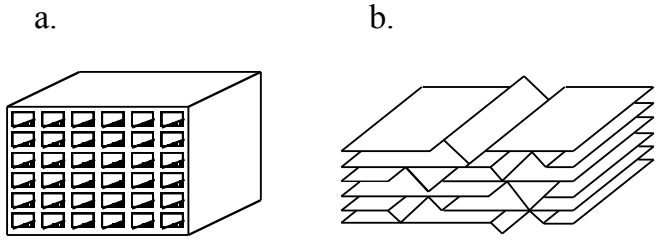

Figure 38. SCR catalyst support geometries: (**a**) extruded ceramic monolith; and (**b**) plate. Reproduced from [8]. Copyright 2006, Wiley-Interscience.

4.3.2.2. SCR Process Options

Two process options in terms of SCR reactant placement have found broad use for SCR units installed in coal-fired plants:

(1) the *high dust unit (HDU)* involving placement of the SCR unit after the economizer and prior to the air heater, particulate collector, and SO_2 scrubber; and
(2) the *tail end unit (TEU)* involving placement of the SCR unit following the SO_2 scrubber.

The HDU is used more widely in the U.S. and the TEU more frequently in Europe and Japan.

The HDU has the advantage of providing flue gas to the SCR unit at its ideal temperature range of 300–400 °C and disadvantages of

(1) deactivation of the catalyst due to erosion, fouling, and poisoning by fly ash thereby limiting its useful life to about 3–4 years;
(2) large monolith channel design to limit plugging by fly ash, but which also limits the amount of active catalyst per reactor volume; and
(3) requirement for a low activity catalyst to limit oxidation of SO_2 to SO_3 and the attendant formation of ammonium sulfates which foul and corrode downstream heat exchangers.

The TEU enables use of a smaller volume of high activity catalyst with small diameter channels, since particulates and SO_2 have already been removed upstream; moreover, since deactivation rate is much lower due to the absence of fly ash and other poisons, catalyst life is substantially extended (*i.e.*, to 15–20 years). A significant disadvantage is that the outlet scrubber gas, which is only about 120 °C, must be reheated to at least 200–250 °C for the SCR to occur at reasonable rates. The energy cost of reheating only 100 °C can be as much as 4–6% of the boiler capacity, unless a regenerative heat exchanger is used. In addition, the SCR catalyst must be designed to operate at significantly lower temperatures (200–290 °C relative to a typical 300–400 °C for an HDU).

Given the long life of the TEU catalyst, no regeneration is necessary. However, regeneration of the HDU catalyst is highly desirable, since the regeneration cost is significantly lower than the cost of a new catalyst. With this background, further discussion focuses on the deactivation and regeneration of the HDU catalyst.

4.3.3. Catalyst Deactivation, Rejuvenation, and Regeneration

4.3.3.1. Catalyst Deactivation

SCR catalysts have typical process lifetimes around 2–7 years, depending upon their application and placement in a power plant or other such facility. The principal causes of SCR catalyst deactivation [8,312] are fourfold:

(1) fouling/masking of (deposition of solids on) catalyst surfaces, pores, and channels by fly ash components (e.g., sulfates and phosphates of Ca, K, and Na) or ammonium bisulfate;
(2) chemical poisoning of active sites by elements present in upstream lubricants or originating in the fuel such as As, Se, and P and alkali and alkaline earth metals;
(3) hydrothermal sintering of the titania, especially as a result of high-temperature excursions; and
(4) abrasion or erosion by fly ash.

Erosion, fouling, and masking from fly ash and poisoning by As and alkali metals are specific to SCR catalysts installed near the hot, high-particulate side of a coal-fired boiler, accounting for the significantly lower catalyst life of 2–4 years for this configuration.

Formation of ammonium bisulfate depends on flue gas temperature, SO_3 concentration and NH_3 concentration [313]. Deposition of ammonium bisulfate is more likely to occur in catalyst pores at lower reactor temperatures in low-dust or tail-end (TEU) SCR units and on cooler surfaces of heat exchangers. Figure 39a shows typical activity loss *versus* time performance for a set of commercial V/Ti catalysts tested in a DOE pilot SCR unit installed in a slip-stream near the exit of a coal-fired boiler (HDU location) using high sulfur, Eastern U.S. coals; 20% of the initial catalyst activity is lost in about 14,000 h (1.6 years); however, the plant will not shut down until 50–60% of the initial activity has been lost (around 3–4 years). Activity and NH_3 slip are plotted against NH_3/NO ratio for the same catalysts in Figure 39b. To maintain NH_3 slip (exit NH_3 concentration) below a target maximum of 2–5 ppm (2 is highly preferred), the NH_3/NO ratio must be maintained near 0.8; under these conditions NO conversion is about 88%.

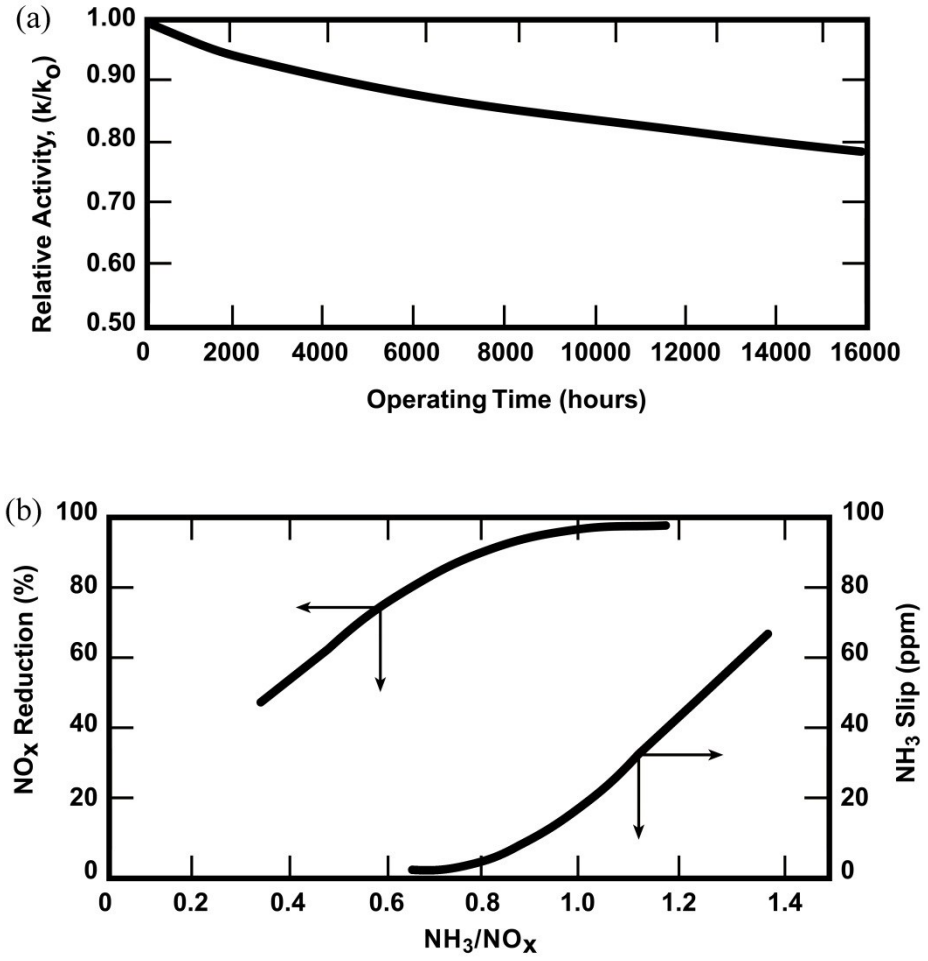

Figure 39. (**a**) Catalyst activity (k/k_o) *vs.* time; (**b**) Typical SCR performance. Reproduced from [313].

Prevention of deactivation requires optimal choices of catalyst design and process conditions. Abrasion, fouling, and/or poisoning by fly ash can be prevented by installation of a hot-side electrostatic precipitator or installing an active, low-temperature catalyst at the tail end of the process. Sintering is minimized by using catalyst promoters that enhance thermal stability and by maintaining reaction temperatures below critical values. The MoO_3 promoter extends catalyst life (in coal boilers) by preferentially adsorbing vapor-phase As which would otherwise adsorb on active V^{4+} sites. Free CaO in the fly ash (up to 3%) also scavenges As to low levels, forming calcium arsenide particles which are collected with the fly ash. Many U.S. coals contain adequate CaO; however, if the CaO content of the coal is too low, it can be added to the boiler or fuel. However, CaO levels above 3% of the fly ash are undesirable, since CaO reacts with SO_2 to form $CaSO_4$ which masks the exterior surface of the catalyst. Fouling by ammonium bisulfate is minimized by keeping exit SO_3 and NH_3 concentrations low and maintaining reaction temperatures above about 230 °C; SO_3 formation is minimized by keeping reaction temperatures below 350 °C or by using lower activity V_2O_5/TiO_2 or zeolite catalysts that have low selectivities for SO_3. Ultimately, however, extra catalyst volume is typically added to SCR reactors to extend periods between catalyst replacements.

For plants fueled by coal, substantial carry-over of inorganic ash occurs to HDU SCR units, a small, but significant fraction of which deposits on monolith walls, masks or blocks catalyst macropores, and

plugs flow channels [314]. Extensive fouling necessitates the use of air lancing to purge the ash out of the catalyst channels. Figure 40 reveals the extent of serious channel plugging and erosion of an SCR catalyst in a pilot plant following several thousand hours of operation in flue gas containing coal fly ash. Plugging and excessive pressure drop are avoided by keeping monolith cell width at or above 7 mm.

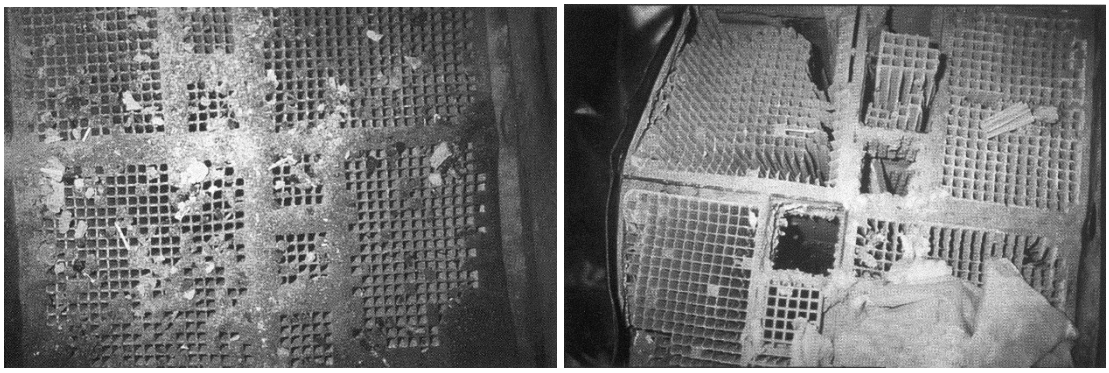

Figure 40. Catalyst channel plugging (**left**) and damage due to erosion (**right**) during operation in an SCR facility. Reproduced from [313].

The type and extent of chemical deactivation depends on operating conditions, fuel type, catalyst geometry, shut-downs for boiler maintenance, *etc.* Mini-pilot tests and subsequent full-scale SCR operating experience have provided little evidence of poisoning by basic minerals from Western United States coals; rather they indicate that deactivation occurs principally by masking of catalyst layers and plugging of catalyst pores by $CaSO_4$ and other fly ash minerals. Moreover, laboratory analysis of catalysts exposed to power plant slip streams indicates that mineral poisons do not penetrate deep into catalyst pores [315,316] nor do they adsorb on Brønsted acid sites unless plant conditions cause moisture to condense on the catalyst.

4.3.3.2. Plant Operating Strategy to Maximize Catalyst Life

A typical SCR unit consists of a series of two to four catalyst layers (three is most common for coal boiler cleanup) through which the flue gas usually flows downward (see Figure 41). A layer of fresh catalyst can be added as catalyst performance declines over time [317]. Two general schemes are followed for replacing the spent catalyst, both of which take into consideration the *relative activity* or *design activity level*, a parameter that is usually defined as the ratio of NO_x conversion at any time divided by that produced by the fresh catalyst. Once the NO_x reduction performance declines to the minimum design activity level (typically 65–75% of fresh activity), the catalyst can either be replaced entirely (*simultaneous* replacement scheme) or one layer can be replaced at a time (*sequential* replacement scheme), usually beginning at the top and working down [313,318]. The sequential method results in increased overall catalyst life (on a per-volume-replaced basis), while annual replacement cost would be 60% lower for the simultaneous scheme (see Figure 42 [319]). Thus, optimal, cost-effective design of an SCR unit requires considering both the initial capital and annual costs.

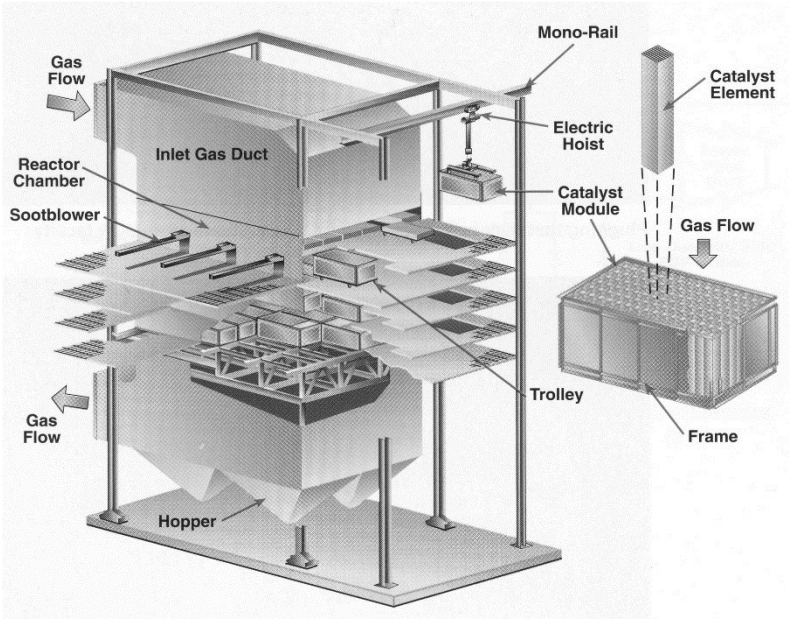

Figure 41. Vertical-flow fixed-bed SCR reactor. DOE SCR demonstration facility at Gulf Power Company's Plant Crist. Reproduced from [313].

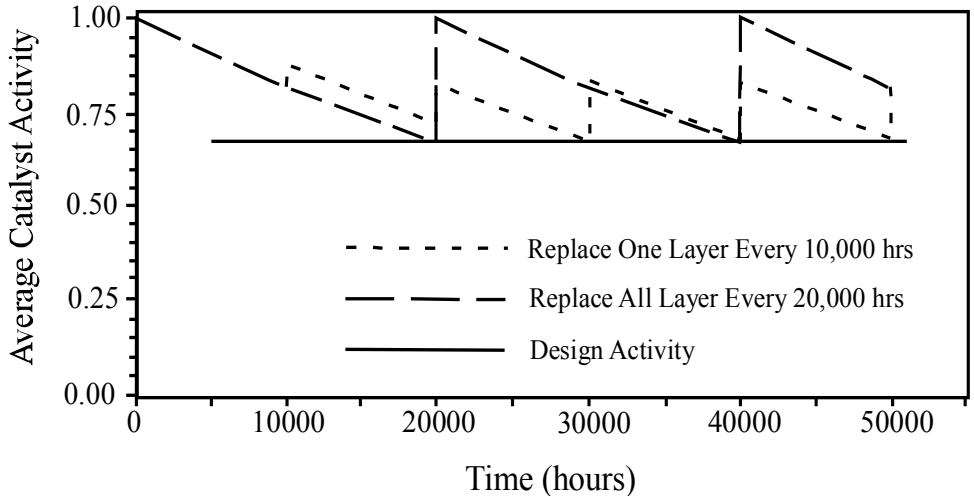

Figure 42. SCR replacement strategies: comparison of total replacement on a 20,000 h cycle relative to sequential replacement on a 10,000 h cycle while maintaining constant catalyst volume. Reproduced from [319].

Operating experience for commercial SCR installations has been better than anticipated. Catalyst lifetimes of 3–4 years at overall efficiencies of 75–90% for HDU's have been observed for electric boiler installations [312]. The principal contributors to operating cost include catalyst replacement cost, shutdown cost for catalyst replacement, and plant derating cost associated with catalyst pressure drop. Catalyst replacement or regeneration was typically required within 2–3 years and catalyst replacement times varied from 2–7 days. Pressure drop ranged from 0.8–15 cm of water for the various catalyst configurations and volumes. Pressure drops for plate type catalysts were significantly lower than for monolithic catalysts.

4.3.3.3. Catalyst Rejuvenation and Regeneration

While high-dust-catalyst life of 2–3 years is acceptable, advances in SCR catalyst regeneration technologies make it possible to extend life by several additional years. Recent experience indicates that even after long-term exposure to fly ash, foulants, and poisons, SCR catalysts may be successfully regenerated to the original performance or better [307,308,320–322].

4.3.3.4. Methods of Renewing Catalysts

Deactivated catalysts may be *cleaned*, *rejuvenated*, *and/or regenerated*. *Cleaning* commonly refers to removal of physical restrictions such as monolith channels plugged with fly ash or channel surfaces covered with a loose dust layer; these restrictions are easily removed *in situ* using compressed air, although cleaning will also be done as a first step in the other methods. *Rejuvenation* refers to relatively mild treatments that remove catalyst poisons or foulants inside the catalyst pores and restore part of the catalytic activity; these treatments are often done *in situ* or *on-site*. *Rejuvenation* involves removal of blinding layers and partial removal of some poisons; thus, activity is partly recovered, but none is added. *Regeneration* involves the *off-site*, complete restoration of catalytic activity through a series of relatively sophisticated treatments, some of which remove not only poisons and foulants, but also a part or much of the active catalytic materials from the support; hence, regeneration also involves restoration of the catalytically active materials bringing the catalyst to its original state or one of even higher activity. SCR catalysts are routinely and regularly cleaned or "blown out" during operation, while rejuvenation or regeneration is typically done after approximate 50–60% of the initial activity of the catalyst has been lost. *In situ rejuvenation* (ISR) *treatments* were practiced early (e.g., 1990s and early 2000s), while *off-site regeneration* (OSR) is now the *predominant practice* because of its greater effectiveness.

4.3.3.5. Rejuvenation or Regeneration?

According to McMahon [322], rejuvenating SCR catalyst may be more cost-effective than regenerating, if the catalyst is fairly new or the SCR system does not operate year around (as in the case of plants operating only during high pollutant levels, known as the "ozone season"). Otherwise, the choice between rejuvenation and regeneration depends largely on economics, *i.e.*,

(1) the plant's dispatch economics, including transportation costs;
(2) length of catalyst service;
(3) costs of removing and replacing the catalyst;
(4) the impact of the fuels combusted, *i.e.*, coal, oil, or gas; and
(5) the location of the catalyst in the plant, *i.e.*, HDU or TGU.

Examples of rejuvenation treatments are found in the scientific and patent literature. For example, work by Zheng and Johnsson [323] and others (e.g., [324,325]) indicates that activity of poisoned catalysts might be partially regenerated by washing with water, sulfuric acid, NH_4Cl, and/or catalyst precursor solutions (e.g., ammonium paratungstate and vanadyl sulfate), as well as a combination of

washing and treatment with gaseous SO_2. The extent to which these rejuvenation methods are effective in restoring a significant fraction of the original catalyst activity varies significantly.

4.3.3.5.1. Rejuvenation

On-site rejuvenation methods generally include the following procedural types: (i) removal of dust in the monolith channels with compressed air followed by (ii) washing catalyst in a tank containing agitated, deionized water to remove the $CaSO_4$ coating and alkali metal salts deposited by fly ash (the solution is generally mildly acidic due to impurities on the catalyst) or acidic aqueous solution (pH = 1–2 in either case) in a tank; (iii) rinsing vigorously with deionized water (usually in the same tank) to remove the dissolved and suspended deposits; and (iv) drying slowly in clean air at room temperature followed by drying gently in hot air. Examples of on-site regeneration methods include those developed and practiced in the time frame of 1995–2002 by SCR-Tech, SBW, Saar Energie, Steag, EnBW, HEW, BHK, and Integral [326–328]. The method described by Schneider and Bastuck [327] provided for adding catalytic materials, *i.e.*, vanadium and tungsten oxides (via impregnation of the V and W salts) to the cleaned catalyst.

The patent of Budin *et al.* [328] provides for more sophisticated treatments, including use of (i) nonionic surfactants and complex-forming or ion-exchange additives, (ii) washing with an acid or base, (iii) using acoustic radiation to remove fly-ash components, and (iv) addition of catalytic materials (oxides of V, W, Mo free of alkali and alkaline-earth metals, halogen, and sulfur) to restore activity, although few details or conditions of use are provided. In fact, no examples are provided in any of the patents cited directly above; accordingly, it is unclear to what extent and under what conditions the more sophisticated methods were used for on-site regeneration. The methods claimed by Budin *et al.* [328] are clearly more readily applied in off-site regeneration, as will be clear from the discussion below.

4.3.3.5.2. Regeneration

Bullock & Hartenstein [320], Cooper *et al.* [329], and McMahon [322] build a strong case for off-site regeneration and a comprehensive catalyst management program.

4.3.3.6. A Comprehensive Approach to Catalyst Management

The approach [320,322] includes

(1) strategies for extending catalyst life and reusability and planning for catalyst removal/rotation to coincide with power plant outages;
(2) catalyst inspection and testing before and following regeneration with replacement of badly damaged catalyst which is unregenerable;
(3) off-site regeneration using a series of robust washing and chemical treatments to remove channel blockages, deactivated catalyst metals, and poisons, followed by chemical treatments to restore active catalytic materials; and
(4) gentle drying/calcination in air to high temperatures to produce catalytically active oxides.

4.3.3.7. Common Regeneration Practices

Normal regeneration procedures [307,308,320,322,330–333] are designed to enhance removal of blockages, deactivated catalyst, and poisons and restore active catalytic material. These typically include the following steps:

(1) pressurized wet and dry treatments to remove channel blockages and outer dust layers;
(2) washing of catalyst units in tanks containing agitated water augmented with surfactants, dispersants, ion-exchange materials, emulsifiers, acid, base, and/or acoustic radiation to remove the outer $CaSO_4$ coating, alkali metal salts deposited in the catalyst pores, and deactivated (e.g., As-poisoned) catalyst;
(3) rinsing repeatedly in deionized water and repeating ultrasonic treatments between or in concert with chemical treatments, with a final rinse to finish removal of any catalyst or fouling residue;
(4) reimpregnation of the clean support with salts of the active catalytic materials (V, Mo, and W); and
(5) drying (calcining) at low heating rates to decompose the salts of the active catalytic materials to active metal oxides of V, Mo, and W.

4.3.3.8. Regeneration Process Profile: SCR-Tech Regeneration Process

SCR-Tech is the most prominent and experienced off-site regeneration company with 13 years of experience in the regeneration business and a documented record of research and development, going back to their German parent company ENVICA, who in 1997 began developing an offsite regeneration process. SCR-Tech was the first and until 2008 the only company in the U.S. to perform off-site regeneration. In September 2007, Evonik Energy Services (formerly Steag) opened an SCR catalyst regeneration facility in the U.S.

The SCR-Tech regeneration process involves a number of different process steps illustrated in Figure 43. Upon receipt of a shipment of catalyst, catalyst elements from several modules are inspected and analyzed; results of the analysis provide a basis for determining the precise protocol for treatment, *i.e.*, the number and order of processing steps [334,335]. A large catalyst module is then led through a protocol of soaking, washing, ultrasonic treatment, arsenic and/or phosphorus removal (as needed), replenishment of V and Mo, neutralization, and rinsing in various soaking pits, as shown in Figure 43; all of these wet chemical steps are performed at controlled pH and temperature. Finally, the catalyst is dried, inspected, and packaged for shipment. Performance guarantees are provided for complete removal of blinding layers, catalyst activity (typically higher after regeneration), SO_2 to SO_3 conversion rate (typically lower), mechanical stability (the same), and deactivation rate (the same) such that all properties of the regenerated catalyst are as good or better than the new catalyst.

A comparison of the physical appearances of SCR monoliths and plates before and after regeneration in Figure 44 reveals the rigor of the SCR-Tech cleaning process. The nearly complete removal of poisons originally in high concentrations by the regeneration process is demonstrated in Figure 45. Surface concentrations of CaO, P_2O_5, SiO_2, and SO_4 were also substantially reduced.

Table 21 compares the costs of regenerating *versus* buying a new catalyst [322]. This case is for a typical 500 MW unit with 650 m^3 of catalyst contained in 450 modules (150 modules in each of

3 layers). The purchase cost of new catalyst in 2006 was $3500 to 4500 per m^3. The cost to regenerate the catalyst is approximately 60% of this price. Thus, the purchase cost of one layer is $758,000 to $975,000 as compared to a regeneration cost of $455,000 to $585,000 resulting in savings per layer of $303,000 to $390,000 or $910,000 to $1.2 million for three layers. Assuming the SCR unit runs year around (as most do now) and catalyst life is three years, the annual savings due to regeneration is in the range of $300,000 to $600,000. The disposal cost for an SCR catalyst can range from $50 to $2,000/ton, the upper figure based on the cost of treating the vanadium as hazardous waste. Hence the disposal cost could be as high as $500,000 for a layer of catalyst. According to McMahon, SCR catalysts can be regenerated from 3 to 7 times.

Figure 43. SCR-Tech catalyst regeneration process. Reproduced from [322,335–337]. Reproduced with permission of Electric Power and CoaLogix, Inc.

(**a**) (**b**)

Figure 44. (**a**) Monolith and (**b**) plate SCR catalysts before and after SCR-Tech regenerative treatment. Reproduced from [334]. Courtesy CoaLogix, Inc.

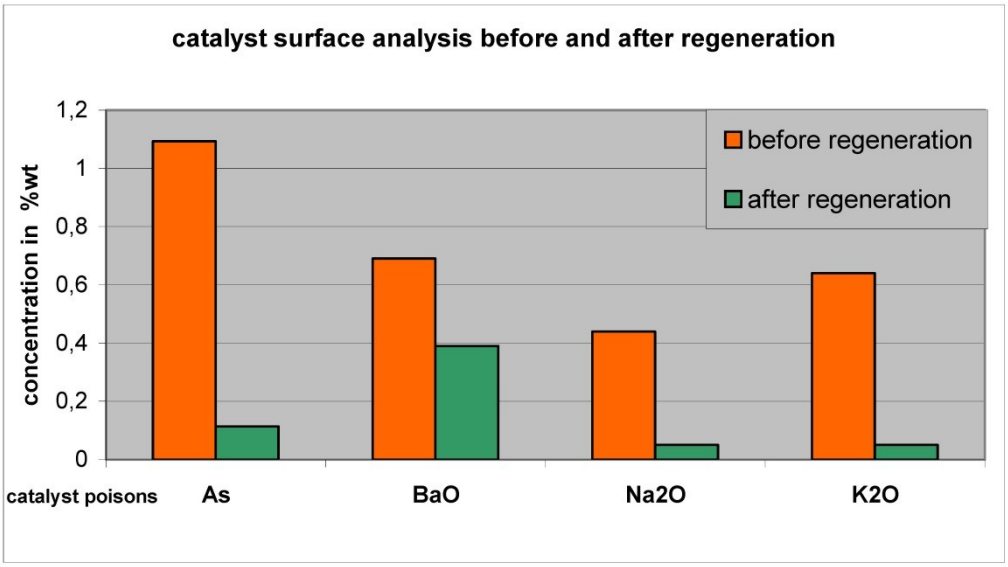

Figure 45. Concentration of principle poisons before and after regeneration. Reproduced from [320]. Courtesy CoaLogix, Inc.

Table 21. Cost per layer (217 m^3 or 150 modules) of new *versus* regenerated SCR catalyst. Adapted from [322]. Copyright 2006, Electric Power.

Catalyst Handling Step	**New**	**Regenerated**
Removal from SCR system	Comparable	Comparable
Transport out	Comparable	Comparable
Purchase price	$758,000–$975,000	$455,000–$585,000
Shipping	Comparable	Comparable
Installation	Comparable	Comparable
Net savings from regeneration	$303,000–$390,000 pls disposal cost	
Disposal cost	$20,000–$500,000	0

4.3.4. SCR Catalyst Case Study Summary Observations and Conclusions

1. Off-site regeneration processes are more sophisticated and demanding than on-site rejuvenation processes; the off-site regeneration processes provide significantly more efficient cleaning and reconstitution of the catalyst with full recovery of activity—sometimes greater than the fresh catalyst activity. Rejuvenation provides only partial (up to 85%) recovery of the original activity.

2. The development of offsite processes for regeneration of SCR catalysts is relatively new, having occurred largely over the past 10–15 years. SCR-Tech was the first and until 2008 the only company to operate an off-site regeneration facility in the U.S.

3. Because surface deposits are a primary deactivation mechanism, especially in HDU catalysts, extensive multi-step treatments are required, but rejuventation or regeneration appear to be a cost-effective method of catalyst management for SCR catalysts.

4.4. Redispersion of Sintered Catalysts

During catalytic reforming of hydrocarbons on platinum-containing catalysts, growth of 1-nm platinum metal clusters to 5–20-nm crystallites occurs. An important part of the catalyst regeneration procedure is the redispersion of the platinum phase by a high temperature treatment in oxygen and chlorine, generally referred to as "oxychlorination." A typical oxychlorination treatment involves exposure of the catalyst to HCl or CCl_4 at 450–550 °C in 2–10% oxygen for a period of 1–4 h (see details in Table 22). During coke burning, some redispersion occurs, e.g., dispersion (*D*) increases from 0.25 to 0.51, while during oxychlorination the dispersion is further increased, e.g., from 0.51 to 0.81 [256]. A mechanism for platinum redispersion by oxygen and chlorine is shown in Figure 46 [256]. It involves the adsorption of oxygen and chlorine on the surface of a platinum crystallite and formation of $AlCl_3$, followed by the formation of $PtCl_2(AlCl_3)_2$ complexes that dissociatively adsorb on alumina to oxychloro-platinum complexes. These latter complexes form monodisperse platinum clusters upon subsequent reduction.

Table 22. Typical Regeneration Procedure for Reforming Catalysts [a].

(*1*) *Preliminary operations:* cool the catalyst to about 200 °C and strip hydrocarbons and H_2 with N_2
(*2*) *Elimination of coke by combustion:* inject dilute air (0.5% O_2) at 380 °C and gradually increase oxygen content to about 2% by volume while maintaining temperature below 450–500 °C to prevent further sintering of the catalyst. To prevent excessive leaching of Cl_2, HCl or CCl_4 may be injected during the combustion step
(*3*) *Restoration of catalyst acidity:* restoration of acidity occurs at 500 °C by injection of a chlorinated compound in the presence of 100–200 ppm water in air
(*4*) *Redispersion of the metallic phase:* expose the catalyst to a few Torr of HCl or CCl_4 in 2–10% O_2 in N_2 at 510–530 °C for a period of about 4 h. After redispersion, O_2 is purged from the unit and the catalyst is reduced in H_2

[a] Ref. [255,256].

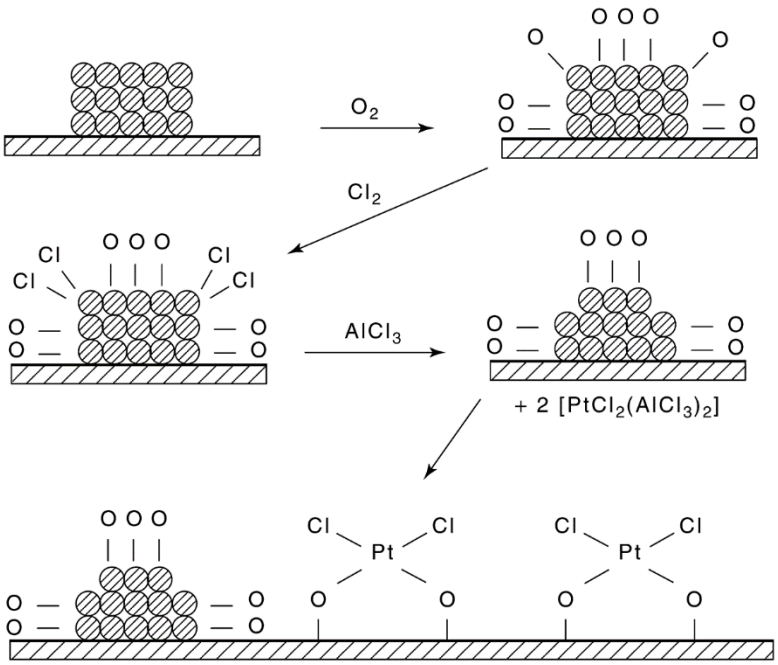

Figure 46. Proposed mechanism for redispersion by oxychlorination of alumina-supported platinum. Reproduced from [256]. Copyright 1982, Brill Nijhoff Publishers.

Some guidelines and principles regarding the redispersion process are worth enumerating:

(1) In cases involving a high degree of Pt sintering or poisoning, special regeneration procedures may be required. If large crystallites have been formed, several successive oxychlorinations are performed [256].

(2) Introducing oxygen into reactors in parallel rather than in series results in a significant decrease in regeneration time [101].

(3) Introduction of hydrocarbons present in the reactor recycle after regeneration is said to stabilize the catalyst; solvents such as ammonium acetate, dilute nitric acid containing lead nitrate, and EDTA and its diammonium salt are reported to dissolve out metal aggregates without leaching out the dispersed metal [101].

(4) The procedures for redispersion of Pt/alumina are not necessarily applicable to Pt on other supports or to other metals. For example, Pt/silica is redispersed at lower temperature and higher Cl_2 concentration (150–200 °C and 25% Cl_2). Pd/alumina can be redispersed in pure O_2 at 500 °C. While Pt–Re/alumina is readily redispersed by oxychlorination at 500 °C, Pt–Ir/alumina is not redispersed in the presence of O_2, unless the catalyst is pretreated with HCl [266].

An extensive scientific and patent literature of redisperson describes the use of chlorine, oxygen, nitric oxide, and hydrogen as agents for redispersion of sintered catalysts (summarized in Table 23). Most of the early literature shows positive effects for chlorine compounds in the presence of oxygen in redispersing alumina-supported platinum and other noble metals. Recent literature demonstrates the need for understanding the detailed surface chemistry in order to successfully develop and improve redispersion processes, especially in more complex catalyst systems such as alumina-supported

bimetallics. For example, on the basis of a fundamental study of the redispersion surface chemistry, Fung [266] developed a redispersion procedure for Pt–Ir bimetallic catalysts using a wet HCl/air treatment, since the conventional oxychlorination is not effective for this catalyst.

Table 23. Representative Patents Prior to 1990 Treating Catalyst Redispersion.

Dispersing agent class	Dispersing agent	Metals/support	Patent No.	Ref.
Chlorine-Containing				
	Cl_2, Cl + halogen	Pt/zeolite	U.S. 4,645,751	[338]
	Cl, H_2O, O_2	Pt/zeolite	U.S. 4,657,874	[339]
	HCl, Cl–O	Ir	U.S. 4,491,636	[340]
	Cl, O_2	Pt–Ir, Ir	U.S. 4,467,045	[341]
	HCl, Cl	Pt–Ir–Re, Pt–Ir/zeolites	U.S. 4,359,400	[342]
	Cl, halogen	Ir, Pt–Ir/Al_2O_3	U.S. 4,480,046	[343]
	Cl–H_2O	Pt–Ir–Se/Al_2O_3	U.S. 4,492,767	[344]
	HCl–O–He	Pt–Ir–Se/Al_2O_3	U.S. 4,491,635	[345]
	Cl, O_2	Pt/zeolite	U.S. 4,855,269	[346]
	HCl, Cl, H_2O, O	Pt/zeolite	U.S. 4,925,819	[347]
	HCl, O	Ir, Pt–Ir/Al_2O_3	U.S. 4,444,896	[348]
	Cl, halogen	Ir, Pt–Ir/Al_2O_3	U.S. 4,444,895	[349]
	HCl	Ir, Pt–Ir/Al_2O_3	U.S. 4,517,076	[350]
Oxygen				
	O_2	Pt, Re/Al_2O_3	U.S. 4,482,637	[351]
Oxygen/N_2				
	O_2, N_2	Cu/Cr, Mn, Ru, Pd, Zn, Si, Mg, Ca, Sr, Ba	U.S. 4,855,267	[352]
Other				
	NO, NO + halogen	Pt, Pd/zeolite	Eu 0,306,170	[353]
	Halogen	Ru, Os, Rh, Pd/Al_2O_3	U.S. 4,891,346	[354]
	Halide	Ir, Pt–Ir/Al_2O_3	U.S. 4,447,551	[355]
	Halide, halogen/H_2O	Ir, Pt–Ir/Al_2O_3	U.S. 4,472,514	[356]
	Halogen	Ir, Pt–Ir/Al_2O_3	U.S. 4,473,656	[357]
	NO, NO + halogen, Cl	Group VIII metals/Al_2O_3, SiO_2, zeolites	U.S. 4,952,543	[358]
	H_2-halides, O_2	Ir, Pt–Ir/Al_2O_3	U.S. 4,444,897	[359]
	Halogen, H_2O	Ir, Pt–Ir/Al_2O_3	U.S. 4,472,515	[360]

Redispersion of alumina-supported platinum and iridium crystallites is also possible in a chlorine-free oxygen atmosphere, if chlorine is present on the catalyst. The extent of redispersion depends on the properties of the Pt/Al_2O_3 catalyst and temperature; for example, the data in Figure 47 [102] for two different catalysts [catalyst 1 is a commercial Pt/Al_2O_3 (Engelhard); catalyst 2 is Pt/Al_2O_3 (Kaiser KA-201) impregnated with chloroplatinic acid] show that the maximum increases in dispersion occur at about 550 °C. The data also show that redispersion does not occur in a hydrogen environment. The question whether redispersion of platinum occurs only in oxygen without chlorine present on the catalyst remains controversial.

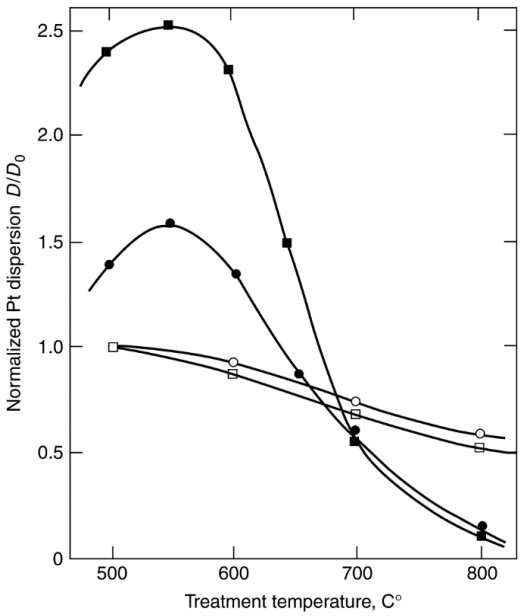

Figure 47. Effects of 1-h treatments in O_2 (closed symbols) and H_2 (open symbols) on the dispersion of Pt/Al_2O_3 catalysts: ○,● Pt/Al_2O_3 (Engelhard), □,■ Pt/KA-201 alumina (Kaiser). Reproduced from [102]. Copyright 1982, Brill Nijhoff Publishers.

Two models, "the thermodynamic redispersion model" and "the crystallite splitting model," have been advanced to explain the redispersion in oxygen [101,102,361]. The "thermodynamic" redispersion model hypothesizes the formation of metal oxide molecules that detach from the crystallite, migrate to active sites on the support, and form surface complexes with the support. Upon subsequent reduction, the metal oxide complexes form monodisperse metal clusters. In the "crystallite splitting" model, exposure of a platinum crystallite to oxygen at 500 °C leads to formation of a platinum oxide scale on the outer surface of the crystallite, which stresses and ultimately leads to splitting of the particle [361]. Dadyburjor hypothesizes that the crystallite splitting model is most applicable to the behavior of large crystallites and to all particles at relatively small regeneration times, while the thermodynamic migration model is useful for small particles and most particles after longer regeneration times.

4.4.1. Case Study: Cobalt based Fischer-Tropsch (FT) Catalyst Regeneration

Fischer-Tropsch (FT) synthesis is a catalytic process used to produce long chain hydrocarbons from synthesis gas consisting of carbon monoxide and hydrogen. Cobalt catalysts were initially developed by Franz Fischer and Hans Tropsch in the 1920s and similar cobalt-based catalysts are still in use today [8]. Although more expensive than iron based catalysts that are also used for FTS, supported cobalt FT catalysts are more active and selective for the desired liquid and wax products.

A recent review by the Davis group at the Center for Applied Energy Research at the University of Kentucky with Bukur at the University of Texas A&M in Qatar [362] focused on the results of studies using synchrotron radiation to characterize Co FT catalysts. The review includes a detailed consideration and analysis of the mechanisms and processes of sintering, oxidation, aluminate formation, and coking and carbide formation and under what operating conditions each is important. They summarize

their and others' previous findings that oxidation primarily occurs on small (<2 nm) cobalt crystallites and at high partial pressures of water [362–366]. Further, they highlight the potentially complicated transformations between CoO and aluminates [362,364,367]. These complications highlight a complex mechanism that may be related to chemical-assisted sintering of Co FTS catalysts through a combination of the effect of CoO reduction during the initial activation of the catalysts and water exposure during operation. First, CoO, present either due to incomplete reduction of the catalysts [368] or oxidation of the small (<2 nm) crystallites as suggested by Davis' group [369,370] can apparently increase the sintering rate due to mobility that allows them to aggregate into larger CoO clusters that are subsequently reduced to metallic Co, as inferred from evidence presented in a number of studies [79,362,368–371]. Primarily, X-ray absorption near edge (XANES) analysis shows simultaneous increasing extent of reduction and increasing Co-Co coordination, due both to removal of oxygen and increases in particle size. Second, water is believed to cause chemical-assisted sintering [80,367,372–374], especially at high partial pressures that occur at CO conversions above about 65% [223], although the exact mechanisms are debated. Minor surface oxidation [373,374] and surface wetting [375] have been proposed, although Saib *et al.* have shown that cobalt oxidation is not an important deactivation route [79] in catalysts with Co particles >~8 nm, which are typical in commercial FTS catalysts.

A number of articles by researchers at Sasol, Eindhoven University of Technology, and the University of South Africa detailed the causes of deactivation and demonstrated the regenerability of alumina-supported cobalt FT catalysts [79,368,371,376–382]. Through a combination of studies on single crystal [377] and actual catalysts from pilot plants operated under industrial FT conditions [368,371], they concluded that contrary to prior hypotheses, neither formation of cobalt aluminates nor oxidation of the cobalt were significant deactivation mechanisms. In fact, extent of Co oxidation actually decreased with time on stream [371]. However, Co sintering and carbon deposition were identified as the primary means of deactivation. In unpublished presentations by these authors, the relative contributions of carbon deposition and sintering to the deactivation were reported as roughly equal. More interestingly, both of these deactivation mechanisms could be largely reversed through high pressure oxidation treatment [376,378], which removes both inactive carbon and redisperses the cobalt. Through high resolution transmission electron micrographs (HRTEM), the mechanism of redispersion of the cobalt was identified as the Kirkendall effect, which results in the formation of spherical shells of cobalt oxide that during subsequent reduction disperse into smaller crystallites of cobalt (see Figure 48). Bezemer *et al.* have previously shown that unpromoted Co FT catalysts require Co crystallites of at least 6 nm in diameter to achieve maximum turnover frequency, but this is the optimum size because larger crystallites display the same surface activity as the 6 nm particles [383]. The oxidative regeneration and reduction process described by Hauman *et al.* [376] and Weststrate *et al.* [377] recovers ~95% of the fresh catalyst activity by removing the carbon deposits and returning the sintered cobalt particles to near the optimum 6 nm size. While the rate per mass of catalyst is nearly constant following regeneration, some smaller particles are produced on model catalysts because the rate on a turnover frequency basis decreases by roughly 1/3 compared to the fresh catalysts [376].

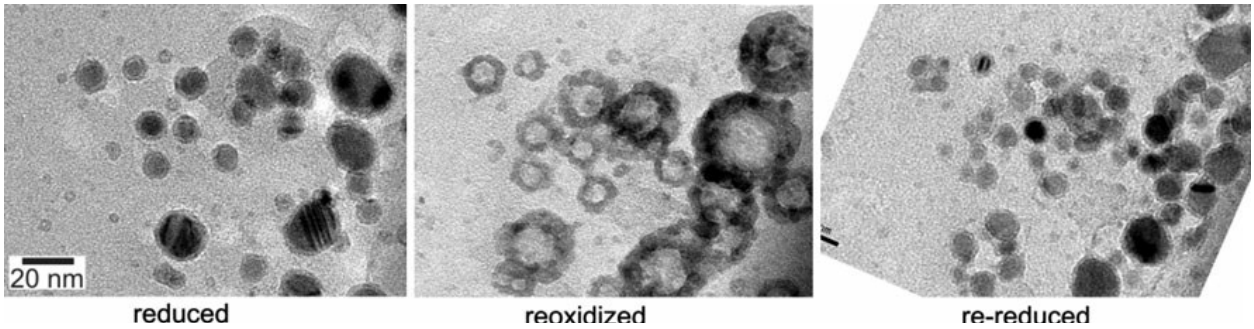

Figure 48. Bright field TEM images showing redispersion of cobalt particles supported on a flat model silica by oxidative treatment. The center image shows hollow spheres created by the Kirkendall effect, which form dispersed smaller particles upon re-reduction in the right hand image. Reproduced from [378]. Copyright 2011, Springer.

These results are significant because they show the power of careful evaluation of the root causes of deactivation in an important catalytic system and then show how proper choice of regeneration conditions can extend the life of the catalysts by redispersion of the active metal. However, promoters may not be redispersed as completely as the cobalt during repeated regeneration. Although traditional promoters, like Pt and Ru, appear to remain with the Co and maintain their effect, some promoters like Au tend to segregate and lose their promotion effect, as indicated by TPR peaks shifting to higher temperatures [384].

5. Summary

This article focuses on the causes, mechanisms, prevention, modeling, and treatment (experimental and theoretical) of deactivation. Several general, fundamental principles are evident:

(1) The causes of deactivation are basically of three kinds: chemical, mechanical, and thermal. The five intrinsic mechanisms of catalyst decay, (a) poisoning, (b) fouling, (c) thermal degradation, (d) chemical degradation, and (e) mechanical failure, vary in their reversibility and rates of occurrence. Poisoning and thermal degradation are generally slow, irreversible processes, while fouling with coke and carbon is generally rapid and reversible by regeneration with O_2 or H_2.

(2) Catalyst deactivation is more easily prevented than cured. Poisoning by impurities can be prevented through careful purification of reactants or mitigated to some extent by adding traps or "getters" as components of the catalyst. Carbon deposition and coking can be prevented by minimizing the formation of carbon or coke precursors through gasification, careful design of catalysts and process conditions, and by controlling reaction rate regimes, e.g., mass transfer regimes, to minimize effects of carbon and coke formation on activity. Sintering is best avoided by minimizing and controlling the temperature of reaction, although recent developments have focused on encapsulating metal crystallites to eliminate mobility, while still allowing access for reactants and products.

(3) Catalyst regeneration is feasible in some circumstances, especially to recover activity loss due to rapid coking or longer term deactivation associated with loss of active metal dispersion. Typically, regeneration or rejuvenation strategies are dictated by process or economic necessity to obtain desired process run lengths. Life cycle operating strategies are important considerations when evaluating catalyst regeneration/rejuvenation *versus* replacement decisions. Rejuvenation treatments can extend the useful life of catalysts. Selective catalytic reduction catalysts provide an example of rejuvenation practiced in a commercial process.

Acknowledgments

The authors wish to acknowledge Brigham Young University for its support and the employees of MDPI, for their untiring assistance in publishing this review.

Author Contributions

Calvin H. Bartholomew was the primary author of this review. Morris D. Argyle provided assistance in writing and revising the case studies and updating the article in response to the reviewers' comments.

Conflicts of Interest

The authors declare no conflict of interest.

References

1. Figueiredo, J.L. Carbon formation and gasification on nickel. In *Progress in Catalyst Deactivation; (NATO Advanced Study Institute Series E, No. 54)*; Martinus Nijhoff Publishers: Boston, MA, USA, 1982; pp. 45–63.
2. Hughes, R. *Deactivation of Catalysts*; Academic Press, London, UK, 1984.
3. Oudar, J.; Wise, H. *Deactivation and Poisoning of Catalysts*; Marcel Dekker: New York, NY, USA, 1985.
4. Butt, J.B.; Petersen, E.E. *Activation*, *Deactivation*, *and Poisoning of Catalysts*; Academic Press: San Diego, CA, USA, 1988.
5. Denny, P.J.; Twigg, M.V. Factors determining the life of industrial heterogeneous catalysts. In *Catalyst Deactivation 1980 (Studies in Surface Science and Catalysis)*; Delmon, B., Froment, G.F., Eds.; Elsevier: Amsterdam, The Nerthelands, 1980; Volume 6; pp. 577–599.
6. Bartholomew, C.H. Catalyst Deactivation. *Chem. Eng.* **1984**, *91*, 96–112.
7. Butt, J.B. Catalyst deactivation and regeneration. In *Catalysis—Science and Technology*; Anderson, J.R., Boudart, M., Eds.; Springer-Verlag: New York, NY, USA, 1984; Volume 6, pp. 1–63.
8. Bartholomew, C.H.; Farrauto, R.J. *Fundamentals of Industrial Catalytic Processes*, 2nd ed.; Wiley-Interscience: Hoboken, NJ, USA, 2006.

9. Delmon, B.; Froment, G.F. *Catalyst Deactivation 1980 (Studies in Surface Science and Catalysis)*; Elsevier: Amsterdam, The Nerthelands, 1980; Volume 6.
10. Delmon, B.; Froment, G.F. *Catalyst Deactivation 1987 (Studies in Surface Science and Catalysis)*; Elsevier: Amsterdam, The Nerthelands, 1987; Volume 34.
11. Bartholomew, C.H.; Butt, J.B. *Catalyst Deactivation 1991 (Studies in Surface Science and Catalysis*); Elsevier: Amsterdam, The Nerthelands, 1991; Volume 68.
12. Delmon, B.; Froment, G.F. *Catalyst Deactivation 1994 (Studies in Surface Science and Catalysis)*; Elsevier: Amsterdam, The Nerthelands, 1994; Volume 88.
13. Bartholomew, C.H.; Fuentes, G.A. *Catalyst Deactivation 1997 (Studies in Surface Science and Catalysis*); Elsevier: Amsterdam, The Nethelands, 1997; Volume 111.
14. Delmon, B.; Froment, G.F. *Catalyst Deactivation 1999 (Studies in Surface Science and Catalysis)*; Elsevier: Amsterdam, The Nethelands, 1999; Volume 126.
15. Moulijn, J.A. Catalyst Deactivation. *Appl. Catal. A* **2001**, *212*, 1–255.
16. Maxted, E.B. The poisoning of metallic catalysts. *Adv. Catal.* **1951**, *3*, 129–177.
17. Hegedus, L.L.; McCabe, R.W. Catalyst poisoning. In *Catalyst Deactivation 1980 (Studies in Surface Science and Catalysis)*; Delmon, B., Froment, G.F., Eds.; Elsevier: Amsterdam, The Nethelands, 1980; Volume 6, pp. 471–505.
18. Hegedus, L.L.; McCabe, R.W. *Catalyst Poisoning*; Marcel Dekker: New York, NY, USA, 1984.
19. Butt, J.B. Catalyst poisoning and chemical process dynamics. In *Progress in Catalyst Deactivation (NATO Advanced Study Institute Series E, No. 54)*; Figueiredo, J.L., Ed.; Martinus Nijhoff Publishers: Boston, MA, USA, 1982; pp. 153–208.
20. Barbier, J. Effect of poisons on the activity and selectivity of metallic catalysts. In *Deactivation and Poisoning of Catalysts*; Oudar, J., Wise, H., Eds.; Marcel Dekker: New York, NY, USA, 1985; pp. 109–150.
21. Bartholomew, C.H. Mechanisms of nickel catalyst poisoning. In *Catalyst Deactivation 1987 (Studies in Surface Science and Catalysis)*; Delmon, B., Froment, G.F., Eds.; Elsevier: Amsterdam, The Nethelands, 1987; Volume 34, pp. 81–104.
22. Rostrup-Nielsen, J.R. Promotion by poisoning. In *Catalyst Deactivation 1991 (Studies in Surface Science and Catalysis)*; Bartholomew, C.H., Butt, J.B., Eds.; Elsevier: Amsterdam, The Nethelands, 1991; Volume 68, pp. 85–101.
23. Inga, J.; Kennedy, P.; Leviness, S. A1 Fischer-tropsch process in the presence of nitrogen contaminants. WIPO Patent WO 2005/071044, 4 August 2005.
24. Völiter, V.J.; Hermann, M. Katalytische Wirksamkeit van reinem und von CO-vergiftetem Platin bei der p-H_2-Umwandlung. *Z. Anorg. Allg. Chem.* **1974**, *405*, 315.
25. Baron, K. Carbon monoxide oxidation on platinum-lead films. *Thin Solid Films* **1978**, *55*, 449–462.
26. Clay, R.D.; Petersen, E.E. Catalytic activity of an evaporated platinum film progressively poisoned with arsine. *J. Catal.* **1970**, *16*, 32–43.
27. Madon, R.J.; Seaw, H. Effect of Sulfur on the Fischer-Tropsch Synthesis. *Catal. Rev.—Sci. Eng.* **1977**, *15*, 69–106.
28. Bartholomew, C.H.; Agrawal, P.K.; Katzer, J.R. Sulfur poisoning of metals. *Adv. Catal.* **1982**, *31*, 135–242.

29. Rostrup-Nielsen, J.R. Sulfur Poisoning. In *Progress in Catalyst Deactivation (NATO Advanced Study Institute Series E, No. 54)*; Figueiredo, J.L., Ed.; Martinus Nijhoff Publishers: Boston, MA, USA, 1982; pp. 209–227.
30. Wise, H.; McCarty, J.; Oudar, J. Sulfur and carbon interactions with metal surfaces. In *Deactivation and Poisoning of Catalysts*; Oudar, J., Wise, H., Eds.; Marcel Dekker: New York, NY, USA, 1985; pp. 1–50.
31. Rostrup-Nielsen, J.R.; Nielsen, P.E.H. Catalyst deactivation in synthesis gas production, and important syntheses. In *Deactivation and Poisoning of Catalysts*; Oudar, J., Wise, H., Eds.; Marcel Dekker: New York, NY, USA, 1985; pp. 259–323.
32. Grossmann, A.; Erley, W.; Ibach, H. Adsorbate-induced surface stress and surface reconstruction: oxygen, sulfur and carbon on Ni(111). *Surf. Sci.* **1995**, *337*, 183–189.
33. Ruan, L.; Stensgaard, I.; Besenbacher, F.; Lægsgaard, E. Observation of a missing-row structure on an fcc (111) surface: The (5 √3 ×2)S phase on Ni(111) studied by scanning tunneling microscopy. *Phys. Rev. Lett.* **1993**, *71*, 2963–2966.
34. Kitajima, Y.; Yokoyama, T.; Ohta, T.; Funabashi, M.; Kosugi, N.; Kuroda, H. Surface EXAFS and XANES studies of (5v3× 2)S/Ni(111). *Surf. Sci.* **1989**, *214*, L261–L269.
35. Perdereau, M.; Oudar, J. Structure, mécanisme de formation et stabilité de la couche d'adsorption du soufre sur le nickel. *Surf. Sci.* **1970**, *20*, 80–98.
36. Oudar, J. Sulfur adsorption and poisoning of metallic catalysts. *Catal. Rev.—Sci. Eng.* **1980**, *22*, 171–195.
37. McCarroll, J.J.; Edmonds, T.; Pitkethly, R.C. Interpretation of a complex low energy electron diffraction pattern: Carbonaceous and sulphur-containing structures on Ni(111). *Nature* **1969**, *223*, 1260–1262.
38. Edmonds, T.; McCarroll, J.J.; Pitkethly, R.C. Surface structures formed during the interaction of sulphur compounds with the (111) face of nickel. *J. Vac. Sci. Technol.* **1971**, *8*, 68–74.
39. Bartholomew, C.H. Mechanisms of catalyst deactivation. *Appl. Catal. A* **2001**, *212*, 17–60.
40. Ruan, L.; Besenbacher, F.; Stensgaard, I.; Lægsgaard, E. Atom-resolved studies of the reaction between H_2S and O on Ni(110). *Phys. Rev. Lett.* **1992**, *69*, 3523–3526.
41. Hepola, J.; McCarty, J.; Krishnan, G.; Wong, V. Elucidation of behavior of sulfur on nickel-based hot gas cleaning catalysts. *Appl. Catal. B* **1999**, *20*, 191–203.
42. Erley, W.; Wagner, H. Sulfur poisoning of carbon monoxide adsorption on Ni(111). *J. Catal.* **1978**, *53*, 287–294.
43. Rendulic, K.D.; Winkler, A. The initial sticking coefficient of hydrogen on sulfur- and oxygen-covered polycrystalline nickel surfaces. *Surf. Sci.* **1978**, *74*, 318–320.
44. Goodman, D.W.; Kiskinova, M. Chemisorption and reactivity studies of H_2 and CO on sulfided Ni(100). *Surf. Sci.* **1981**, *105*, L265–L270.
45. Kiskinova, M.; Goodman, D.W. Modification of chemisorption properties by electronegative adatoms: H_2 and CO on chlorided, sulfided, and phosphided Ni(100). *Surf. Sci.* **1981**, *108*, 64–76.
46. Johnson, S.; Madix, R.S. Desorption of hydrogen and carbon monoxide from Ni(100), Ni(100)p(2 × 2)S, and Ni(100)c(2 × 2)S surfaces. *Surf. Sci.* **1981**, *108*, 77–98.

47. Madix, R.J.; Thornberg, M.; Lee, S.B. CO-sulfur interaction on Ni(110); evidence for local interactions, not long range electronic effects. *Surf. Sci.***1983**, *133*, L447–L451.
48. Hardegree, E.L.; Ho, P.; White, J.M. Sulfur adsorption on Ni(100) and its effect on CO chemisorption: I. TDS, AES and work function results. *Surf. Sci.* **1986**, *165*, 488–506.
49. Erekson, E.J.; Bartholomew, C.H. Sulfur poisoning of nickel methanation catalysts: II. Effects of H_2S concentration, CO and H_2O partial pressures and temperature on reactivation rates. *Appl. Catal.* **1983**, *5*, 323–336.
50. Jacobs, G.; Ghadiali, F.; Pisanu, A.; Padro, C.L.; Borgna, A.; Alvarez, W.E.; Resasco, D.E. Increased Sulfur Tolerance of Pt/KL Catalysts Prepared by Vapor-Phase Impregnation and Containing a Tm Promoter. *J. Catal.* **2000**, *191*, 116–127.
51. Jongpatiwut, S.; Sackamduang, P.; Rirksomboon, T.; Osuwan, S.; Alvarez, W.E.; Resasco, D.E. Sulfur- and water-tolerance of Pt/KL aromatization catalysts promoted with Ce and Yb. *Appl. Catal. A* **2002**, *230*, 177–193.
52. Jacobs, G.; Ghadiali, F.; Pisanu, A.; Borgna, A.; Alvarez, W.E.; Resasco, D.E. Characterization of the morphology of Pt clusters incorporated in a KL zeolite by vapor phase and incipient wetness impregnation. Influence of Pt particle morphology on aromatization activity and deactivation. *Appl. Catal. A* **1999**, *188*, 79–98.
53. McVicker, G.B.; Kao, J.L.; Ziemiak, T.J.J.; Gates, W.E.; Robbins, J.L.; Treacy, M.M.J.; Rice, S.B.; Vanderspurt, T.H.; Cross, V.R.; Ghosh, A.K. Effect of Sulfur on the Performance and on the Particle Size and Location of Platinum in Pt/KL Hexane Aromatization Catalysts. *J. Catal.* **1993**, *139*, 48–61.
54. Farbenindustrie, I.G. Improvements in the Manufacture and Production of Unsaturated Hydrocarbons of Low Boiling Point. British Patent 322,284, 5 December 1929.
55. Kritzinger, J.A. The role of sulfur in commercial iron-based Fischer–Tropsch catalysis with focus on C_2-product selectivity and yield. *Catal. Today* **2002**, *71*, 307–318.
56. Sparks, D.E.; Jacobs, G.; Gnanamani, M.K.; Pendyala, V.R.R.; Ma, W.; Kang, J.; Shafer, W.D.; Keogh, R.A.; Graham, U.M.; Gao, P.; *et al*. Poisoning of cobalt catalyst used for Fischer–Tropsch synthesis. *Catal. Today* **2013**, *215*, 67–72.
57. Rostrup-Nielsen, J.R.; Trimm, D.L. Mechanisms of carbon formation on nickel-containing catalysts. *J. Catal.* **1977**, *48*, 155–165.
58. Trimm, D.L. The Formation and Removal of Coke from Nickel Catalyst. *Catal. Rev.—Sci. Eng.* **1977**, *16*, 155–189.
59. Trimm, D.L. Catalyst design for reduced coking (review). *Appl. Catal.* **1983**, *5*, 263–290.
60. Bartholomew, C.H. Carbon deposition in steam reforming and methanation. *Catal. Rev.—Sci. Eng.* **1982**, *24*, 67–112.
61. Albright, L.F.; Baker, R.T.K. *Coke Formation on Metal Surfaces (ACS Symposium Series 202)*; American Chemical Society: Washington, DC, USA, 1982.
62. Menon, P.G. Coke on catalysts—harmful, harmless, invisible and beneficial types. *J. Mol. Catal.* **1990**, *59*, 207–220.
63. Rostrup-Nielsen, J.R. Conversion of hydrocarbons and alcohols for fuel cells. *Phys. Chem. Chem. Phys.* **2001**, *3*, 283–288.

64. Trane-Restrup, R.; Resasco, D.E.; Jensen, A.D. Steam reforming of light oxygenates. *Catal. Sci. Technol.* **2013**, *3*, 3292–3302.
65. De Lima, S.M.; da Silva, A.M.; da Costa, L.O.O.; Assaf, J.M.; Jacobs, G.; Davis, B.H.; Mattos, L.V.; Noronha, F.B. Evaluation of the performance of Ni/La_2O_3 catalyst prepared from $LaNiO_3$ perovskite-type oxides for the production of hydrogen through steam reforming and oxidative steam reforming of ethanol. *Appl. Catal. A* **2010**, *377*, 181–190.
66. Deken, J.D.; Menon, P.G.; Froment, G.F.; Haemers, G.; On the nature of carbon in Niα-Al_2O_3 catalyst deactivated by the methane-steam reforming reaction. *J. Catal.* **1981**, *70*, 225–229.
67. Durer, W.G.; Craig, J.H., Jr.; Lozano, J. Surface carbon and its effects on hydrogen adsorption on Rh(100). *Appl. Surf. Sci.* **1990**, *45*, 275–277.
68. Moeller, A.D.; Bartholomew, C.H. Deactivation by carbon of nickel and nickel-molybdenum methanation catalysts. *Prepr.—Am. Chem. Soc., Div. Fuel Chem.* **1980**, *25*, 54–70.
69. Marschall, K.-J.; Mleczko, L. Short-contact-time reactor for catalytic partial oxidation of methane. *Ind. Eng. Chem. Res.* **1999**, *38*, 1813–1821.
70. Rostrup-Nielsen, J.R. Catalytic steam reforming. In *Catalysis—Science and Technology*; Anderson, J.R., Boudart, M., Eds.; Springer-Verlag: New York, NY, USA, 1984; Volume 5, pp. 1–117.
71. Besenbacher, F.; Chorkendorff, I.; Clausen, B.S.; Hammer, B.; Molenbroek, A.M.; Nørskov, J.K.; Stensgaard, I. Design of a surface alloy catalyst for steam reforming. *Science* **1998**, *279*, 1913–1915.
72. Nemes, T.; Chambers, A.; Baker, R.T.K. Characteristics of carbon filament formation from the interaction of Cobalt−Tin particles with ethylene. *J. Phys. Chem. B* **1998**, *102*, 6323-6330.
73. Bartholomew, C.H.; Strasburg, M.V.; Hsieh, H. Effects of support on carbon formation and gasification on nickel during carbon monoxide hydrogenation. *Appl. Catal.* **1988**, *36*, 147–162.
74. Vance, C.K.; Bartholomew, C.H. Hydrogenation of carbon dioxide on group viii metals: III, Effects of support on activity/selectivity and adsorption properties of nickel. *Appl. Catal.* **1983**, *7*, 169–177.
75. Baker, R.T.K.; Chludzinski, J.J., Jr. Filamentous carbon growth on nickel-iron surfaces: The effect of various oxide additives. *J. Catal.* **1980**, *64*, 464–468.
76. Brown, D.E.; Clark, J.T.K.; Foster, A.I.; McCarroll, J.J.; Sims, M.L. Inhibition of coke formation in ethylene steam cracking. In *Coke Formation on Metal Surfaces (ACS Symposium Series 202)*; Albright, L.F., Baker, R.T.K., Eds.; American Chemical Society: Washington, DC, USA, 1982; pp. 23–43.
77. Bitter, J.H.; Seshan, K.; Lercher, J.A. Deactivation and coke accumulation during CO_2/CH_4 reforming over Pt catalysts. *J. Catal.* **1999**, *183*, 336–343.
78. Rostrup-Nielsen, J.R. Coking on nickel catalysts for steam reforming of hydrocarbons. *J. Catal.* **1974**, *33*, 184–201.
79. Saib, A.M.; Moodley, D.J.; Ciobica, I.M.; Hauman, M.M.; Sigwebela, B.H.; Weststrate, C.J.; Niemanstsverdriet, J.W.; van de Loosdrecht, J. Fundamental understanding of deactivation and regeneration of cobalt Fischer–Tropsch synthesis catalysts. *Catal. Today* **2010**, *154*, 271–282.
80. Tsakoumis, N.E.; Rønning, M.; Borg, O.; Rytter, E.; Holmen, A. Deactivation of cobalt based Fischer–Tropsch catalysts: A review. *Catal. Today* **2010**, *154*, 162–182.

81. Gates, B.C.; Katzer, J.R.; Schuit, G.C.A. *Chemistry of Catalytic Processes*; McGraw-Hill: New York, NY, USA, 1979.
82. Naccache, C. Deactivation of acid catalysts. In *Deactivation and Poisoning of Catalysts*; Oudar, J., Wise, H., Eds.; Marcel Dekker: New York, NY, USA, 1985; pp. 185–203.
83. Appleby, W.G.; Gibson, J.W.; Good, G.M. Coke Formation in Catalytic Cracking. *Ind. Eng. Chem. Process Des. Dev.* **1962**, *1*, 102–110.
84. Beuther, H.; Larson, O.H.; Perrotta, A.J. The mechanism of coke formation on catalysts. In *Catalyst Deactivation 1980 (Studies in Surface Science and Catalysis)*; Delmon, B., Froment, G.F., Eds.; Elsevier: Amsterdam, The Nerthelands, 1980; Volume 6, pp. 271–282.
85. Gayubo, A.G.; Arandes, J.M.; Aguayo, A.T.; Olazar, M.; Bilbao, J. Deactivation and acidity deterioration of a silica/alumina catalyst in the isomerization of cis-butene. *Ind. Eng. Chem. Res.* **1993**, *32*, 588–593.
86. Augustine, S.M.; Alameddin, G.N.; Sachtler, W.M.H. The effect of Re, S, and Cl on the deactivation of Pt γ-Al_2O_3 reforming catalysts. *J. Catal.* **1989**, *115*, 217–232.
87. Guisnet, M.; Magnoux, P. Coking and deactivation of zeolites: Influence of the Pore Structure. *Appl. Catal.* **1989**, *54*, 1–27.
88. Bauer, F.; Kanazirev, V.; Vlaev, C.; Hanisch, R.; Weiss, W. Koksbildung in ZSM-5-Katalysatoren. *Chem. Tech.* **1989**, *41*, 297–301.
89. Grotten, W.A.; Wojciechowski, B.W.; Hunter, B.K. On the relationship between coke formation chemistry and catalyst deactivation. *J. Catal.* **1992**, *138*, 343–350.
90. Bellare, A.; Dadyburjor, D.B. Evaluation of modes of catalyst deactivation by coking for cumene cracking over zeolites. *J. Catal.* **1993**, *140*, 510–525.
91. Uguina, M.A.; Serrano, D.P.; Grieken, R.V.; Vènes, S. Adsorption, acid and catalytic changes induced in ZSM-5 by coking with different hydrocarbons. *Appl. Catal. A* **1993**, *99*, 97–113.
92. Li, C.; Chen, Y.-W.; Yang, S.-J.; Yen, R.-B. *In-situ* FTIR investigation of coke formation on USY zeolite. *Appl. Surf. Sci.* **1994**, *81*, 465–468.
93. Buglass, J.G.; de Jong, K.P.; Mooiweer, H.H. Analytical studies of the coking of the zeolite ferrierite. *J. Chem. Soc. Abstr.* **1995**, *210*, 105-PETR.
94. Chen, D.; Rebo, H.P.; Moljord, K.; Holmen, A. Effect of coke deposition on transport and adsorption in zeolites studied by a new microbalance reactor. *Chem. Eng. Sci.* **1996**, *51*, 2687–2692.
95. Guisnet, M.; Magnoux, P.; Martin, D. Roles of acidity and pore structure in the deactivation of zeolites by carbonaceous deposits. In *Catalyst Deactivation 1997 (Studies in Surface Science and Catalysis)*; Bartholomew, C.H., Fuentes, G.A., Eds.; Elsevier: Amsterdam, The Nethelands, 1997; Volume 111, pp. 1–19.
96. Masuda, T.; Tomita, P.; Fujikata, Y.; Hashimoto, K. Deactivation of HY-type zeolite catalyst due to coke deposition during gas-oil cracking. In *Catalyst Deactivation 1999 (Studies in Surface Science and Catalysis)*; Delmon, B., Froment, G.F. Eds.; Elsevier: Amsterdam, The Nethelands, 1999; Volume 126, pp. 89–96.

97. Cerqueira, H.S.; Magnoux, P.; Martin, D.; Guisnet, M. Effect of contact time on the nature and location of coke during methylcyclohexane transformation over a USHY zeolite. In *Catalyst Deactivation 1999 (Studies in Surface Science and Catalysis)*; Delmon, B., Froment, G.F., Eds.; Elsevier: Amsterdam, The Nethelands, 1999; Volume 126, pp. 105–112.
98. Wanke, S.E.; Flynn, P.C. The sintering of supported metal catalysts. *Catal. Rev.—Sci. Eng.* **1975**, *12*, 93–135.
99. Wynblatt, P.; Gjostein, N.A. Supported metal crystallites. *Prog. Solid State Chem.* **1975**, *9*, 21–58.
100. Ruckenstein, E.; Pulvermacher, B. Kinetics of crystallite sintering during heat treatment of supported metal catalysts. *AIChE J.* **1973**, *19*, 356–364.
101. Ruckenstein, E.; Dadyburjor, D.B. Sintering and redispersion in supported metal catalysts. *Rev. Chem. Eng.* **1983**, *1*, 251–356.
102. Wanke, S.E. Sintering of commercial supported platinum group metal catalysts. In *Progress in Catalyst Deactivation (NATO Advanced Study Institute Series E, No. 54)*; Figueiredo, J.L., Ed.; Martin Nijhoff Publishers: Boston, MA, USA, 1982; pp. 315–328.
103. Baker, R.T.; Bartholomew, C.H.; Dadyburjor, D.B. Sintering and Redispersion: Mechanisms and Kinetics. In *Stability of Supported Catalysts: Sintering and Redispersion*; Horsley, J.A., Ed.; Catalytica: Mountain View, CA, USA, 1991; pp. 169-225.
104. Bartholomew, C.H. Model catalyst studies of supported metal sintering and redispersion kinetics. In *Catalysis (Specialist Periodical Report)*; Spivey, J.J., Agarwal, S.K., Eds.; Royal Society of Chemistry, Cambridge, UK, 1993; Volume 10, pp. 41–82.
105. Bartholomew, C.H. Sintering kinetics of supported metals: new perspectives from a unifying GPLE treatment. *Appl. Catal. A* **1993**, *107*, 1–57.
106. Bartholomew, C.H. Sintering kinetics of supported metals: perspectives from a generalized power law approach. In *Catalyst Deactivation 1994 (Studies in Surface Science and Catalysis)*; Delmon, B., Froment, G.F., Eds.; Elsevier: Amsterdam, The Nethelands, 1994; Volume 88, pp. 1–18.
107. Bartholomew, C.H. Sintering and redispersion of supported metals: Perspectives from the literature of the past decade. In *Catalyst Deactivation 1997 (Studies in Surface Science and Catalysis)*; Bartholomew, C.H., Fuentes, G.A., Eds.; Elsevier: Amsterdam, The Nethelands, 1997; Volume 111, pp. 585–592.
108. Bartholomew, C.H.; Sorenson, W. Sintering kinetics of silica- and alumina-supported nickel in hydrogen atmosphere. *J. Catal.* **1983**, *81*, 131–141.
109. Moulijn, J.A.; van Diepen, A.E.; Kapteijn, F. Catalyst deactivation: is it predictable?: What to do? *Appl. Catal. A* **2001**, *212*, 3–16.
110. Bridger, G.W.; Spencer, M.S. Methanol synthesis. In *Catalyst Handbook*, 2nd ed.; Twigg, M.V., Ed.; Manson Publishing: London, UK, 1996; pp. 441–468.
111. Fuentes, G.A. Catalyst deactivation and steady-state activity: A generalized power-law equation model. *Appl. Catal.* **1985**, *15*, 33–40.

112. Fuentes, G.A.; Ruiz-Trevino, F.A. Towards a better understanding of sintering phenomena in catalysis. In *Catalyst Deactivation 1991 (Studies in Surface Science and Catalysis)*; Bartholomew, C.H., Butt, J.B., Eds., Elsevier: Amsterdam, The Nethelands, 1991; Volume 68, pp. 637–644.
113. Bournonville, J.P.; Martino, G. Sintering of Alumina Supported Platinum. In *Catalyst Deactivation 1980 (Studies in Surface Science and Catalysis)*; Delmon, B., Froment, G.F., Eds., Elsevier: Amsterdam, The Nethelands, 1980; Volume 6, pp. 159–166.
114. Somorjai, G.A. Small-Angle X-Ray Scattering and Low Energy Electron Diffraction Studies on Catalyst Surfaces, In *X-ray and Electron Methods of Analysis* (*Progress in Analytical Chemistry)*; Van Olphen, H., Parrish, W., Eds., Plenum Press; New York, NY, USA, 1968; Volume 1, pp. 101–126.
115. Seyedmonir, S.R.; Strohmayer, D.E.; Guskey, G.J.; Geoffroy, G.L.; Vannice, M.A. Characterization of supported silver catalysts: III. Effects of support, pretreatment, and gaseous environment on the dispersion of Ag. *J. Catal.* **1985**, *93*, 288–302.
116. Trimm, D.L. Thermal stability of catalyst supports. In *Catalyst Deactivation 1991 (Studies in Surface Science and Catalysis)*; Bartholomew, C.H., Butt, J.B. Eds.; Elsevier: Amsterdam, The Nethelands, 1991; Volume 68, pp. 29–51.
117. Shastri, A.G.; Datye, A.K.; Schwank, J. Influence of chlorine on the surface area and morphology of TiO_2. *Appl. Catal.* **1985**, *14*, 119–131.
118. Oberlander, R.K. Aluminas for catalysts: Their preparations and properties. In *Applied Industrial Catalysis*; Leach, B.E., Ed.; Academic Press: Orlando, FL, USA, 1984; Volume 3, pp. 64–112.
119. Wefers, K.; Misra, C. *Oxides and Hydroxides of Aluminum*; Alcoa Technical Paper No. 19; Alcoa Laboratories: Pittsburg, PA, USA, 1987.
120. Hegedus, L.L.; Baron, K. Phosphorus accumulation in automotive catalysts. *J. Catal.* **1978**, *54*, 115–119.
121. Summers, J.; Hegedus, L.L. Modes of catalyst deactivation in stoichiometric automobile exhaust. *Ind. Eng. Chem. Prod. Res. Dev.* **1979**, *18*, 318–324.
122. Peter-Hoblyn, J.D.; Valentine, J.M.; Sprague, B.N.; Epperly, W.R. Methods for reducing harmful emissions from a diesel engine. U.S. Patent 6,003,303, 21 December 1999.
123. Manson, I. Self-regenerating diesel exhaust particulate filter and material. U.S. Patent 6,013,599, 11 January 2000.
124. Deeba, M.; Lui, Y.K.; Dettling, J.C. Four-way diesel exhaust catalyst and method of use. U.S. Patent 6,093,378, 25 July 2000.
125. Dry, M.E. The fischer-tropsch synthesis. In *Catalysis—Science and Technology*; Anderson, J., Boudart, M., Eds.; Springer-Verlag: New York, NY, USA, 1981; pp. 159–218.
126. Huber, G.W.; Guymon, C.G.; Stephenson, B.C.; Bartholomew, C.H. Hydrothermal stability of Co/SiO_2 Fischer-Tropsch synthesis catalysts. In *Catalyst Deactivation 2001 (Studies in Surface Science and Catalysis)*; Spivey, J.J., Roberts, G.W., Davis, B.H., Eds.; Elsevier: Amsterdam, The Netheland, 2001; Volume 139, pp. 423–430.
127. Busca, G.; Lietti, L.; Ramis, G.; Berti, F. Chemical and mechanistic aspects of the selective catalytic reduction of NO_x by ammonia over oxide catalysts: A review. *Appl. Catal. B* **1998**, *18*, 1–36.

128. Kobylinski, T.P.; Taylor, B.W.; Yong, J.E. Stabilized ruthenium catalysts For NO_x reduction. *Proc. SAE*, **1974**, Paper 740250.
129. Shelef, M.; Gandhi, H.S. The reduction of nitric oxide in automobile emissions: Stabilisation of catalysts containing ruthenium. *Platinum Met. Rev.* **1974**, *18*, 2–14.
130. Gandhi, H.S.; Stepien, H.K.; Shelef, M. Optimization of ruthenium-containing, stabilized, nitric oxide reduction catalysts. *Mat. Res. Bull.* **1975**, *10*, 837–845.
131. Bartholomew, C.H. Reduction of nitric oxide by monolithic-supported palladium-nickel and palladium-ruthenium alloys. *Ind. Eng. Chem. Prod. Res. Dev.* **1975**, *14*, 29–33.
132. Clark, R.W.; Tien, J.K.; Wynblatt, P. Loss of palladium from model platinum-palladium supported catalysts during annealing. *J. Catal.* **1980**, *61*, 15–18.
133. Shen, W.M.; Dumesic, J.A.; Hill, C.G. Criteria for stable Ni particle size under methanation reaction conditions: Nickel transport and particle size growth via nickel carbonyl. *J. Catal.* **1981**, *68*, 152–165.
134. Pannell, R.B.; Chung, K.S.; Bartholomew, C.H. The stoichiometry and poisoning by sulfur of hydrogen, oxygen and carbon monoxide chemisorption on unsupported nickel. *J. Catal.* **1977**, *46*, 340–347.
135. Lohrengel, G.; Baerns, M. Determination of the metallic surface area of nickel and its dispersion on a silica support by means of a microbalance. *Appl. Catal.* **1981**, *1*, 3–7.
136. Qamar, I.; Goodwin, J.G. Fischer-Tropsch Synthesis over Composite Ru Catalysts In Proceedings of 8th North American Catalysis Society Meeting, Philadelphia, PA, USA, 1983, Paper C-22.
137. Goodwin, J.G.; Goa, D.O.; Erdal, S.; Rogan, F.H. Reactive metal volatilization from Ru/Al_2O_3 as a result of ruthenium carbonyl formation. *Appl. Catal.* **1986**, *24*, 199–209.
138. Watzenberger, O.; Haeberle, T.; Lynch, D.T.; Emig, G. Deactivation of Heteropolyacid Catalysts. In *Catalyst Deactivation 1991 (Studies in Surface Science and Catalysis)*; Bartholomew, C.H., Butt, J.B., Eds.; Elsevier: Amsterdam, The Nethelands, 1991; Volume 68, pp. 441–448.
139. Agnelli, M.; Kolb, M.; Mirodatos, C. Co hydrogenation on a nickel catalyst: 1. Kinetics and modeling of a low-temperature sintering process. *J. Catal.* **1994**, *148*, 9–21.
140. Lee, H.C.; Farrauto, R.J. Catalyst deactivation due to transient behavior in nitric acid production. *Ind. Eng. Chem. Res.* **1989**, *28*, 1–5.
141. Farrauto, R.J.; Lee, H.C. Ammonia oxidation catalysts with enhanced activity. *Ind. Eng. Chem. Res.* **1990**, *29*, 1125–1129.
142. Sperner, F.; Hohmann, W. Rhodium-platinum gauzes for ammonia oxidation. *Platinum Met. Rev.* **1976**, *20*, 12–20.
143. Hess, J.M.; Phillips, J. Catalytic etching of Pt/Rh gauzes. *J. Catal.* **1992**, *136*, 149–160.
144. Kuo, C.L.; Hwang, K.C. Does morphology of a metal nanoparticle play a role in ostwald ripening processes? *Chem. Mater.* **2013**, *25*, 365–371.
145. Bartholomew, C.H. Hydrogen adsorption on supported cobalt, iron, and nickel. *Catal. Lett.* **1990**, *7*, 27–51.
146. Wu, N.L.; Phillips, J. Catalytic etching of platinum during ethylene oxidation. *J. Phys. Chem.* **1985**, *89*, 591–600.

147. Wu, N.L.; Phillips, J. Reaction-enhanced sintering of platinum thin films during ethylene oxidation. *J. Appl. Phys.* **1986**, *59*, 769–779.
148. Wu, N.L.; Phillips, J. Sintering of silica-supported platinum catalysts during ethylene oxidation. *J. Catal.* **1988**, *113*, 129–143.
149. Bielanski, A.; Najbar, M.; Chrzaoszcz, J.; Wal, W. Deactivation of the V_2O_5-MoO_3, catalysts in the selective oxidation of eenzene to maleic anhydride and the changes in its morphology and chemical composition. In *Catalyst Deactivation 1980 (Studies in Surface Science and Catalysis)*; Delmon, B., Froment, G.F., Eds.; Elsevier: Amsterdam, The Nethelands, 1980; Volume 6, pp. 127–140.
150. Burriesci, N.; Garbassi, F.; Petrera, M.; Petrini, G.; Pernicone, N. Solid state reactions in Fe-Mo oxide catalysts for methanol oxidation during aging in industrial plants. In *Catalyst Deactivation 1980 (Studies in Surface Science and Catalysis)*; Delmon, B., Froment, G.F., Eds.; Elsevier: Amsterdam, The Nethelands, 1980; Volume 6, pp. 115–126.
151. Xiong, Y.L.; Castillo, R.; Papadopoulou, C.; Dada, L.; Ladriere, J.; Ruiz, P.; Delmon, B. The protecting role of antimony oxide against deactivation of iron molybdate in oxidation catalysts. In *Catalyst Deactivation 1991 (Studies in Surface Science and Catalysis)*; Bartholomew, C.H., Butt, J.B., Eds.; Elsevier: Amsterdam, The Nethelands, 1991; Volume 68, pp. 425–432.
152. Farrauto, R.J.; Hobson, M.; Kennelly, T.; Waterman, E. Catalytic chemistry of supported palladium for combustion of methane. *Appl. Catal. A* **1992**, *81*, 227–237.
153. Gai-Boyes, P.L. Defects in Oxide Catalysts: Fundamental Studies of Catalysis in Action. *Catal. Rev.—Sci. Eng.* **1992**, *34*, 1–54.
154. Delmon, B. Solid-state reactions in catalysts during ageing: Beneficial role of spillover. In *Catalyst Deactivation 1994 (Studies in Surface Science and Catalysis, Volume 88)*; Delmon, B., Froment, G.F.; Eds., Elsevier: Amsterdam, The Nethelands, 1994, pp. 113–128.
155. Erickson, K.M.; Karydis, D.A.; Boghosian, S.; Fehrmann, R. Deactivation and compound formation in sulfuric-acid catalysts and model systems. *J. Catal.* **1995**, *155*, 32–42.
156. Delmon, B. Solid state reactions in catalysts: An approach to real active systems and their deactivation. In *Catalyst Deactivation 1997 (Studies in Surface Science and Catalysis)*; Bartholomew, C.H., Fuentes, G.A., Eds.; Elsevier: Amsterdam, The Nethelands, 1997; Volume 111, pp. 39–51.
157. Jackson, N.B.; Datye, A.K.; Mansker, L.; O'Brien, R.J.; Davis, B.H. Deactivation and attrition of iron catalysts in synthesis gas. In *Catalyst Deactivation 1997 (Studies in Surface Science and Catalysis)*; Bartholomew, C.H., Fuentes, G.A., Eds.; Elsevier: Amsterdam, The Nethelands, 1997; Volume 111, pp. 501–516.
158. Eliason, S.A.; Bartholomew, C.H. Temperature-programmed reaction study of carbon transformations on iron fischer-tropsch catalysts during steady-state synthesis. In *Catalyst Deactivation 1997 (Studies in Surface Science and Catalysis)*; Bartholomew, C.H., Fuentes, G.A., Eds.; Elsevier: Amsterdam, The Nethelands, 1997; Volume 111, pp. 517–526.

159. Baranski, A.; Dziembaj, R.; Kotarba, A.; Golebiowski, A.; Janecki, Z.; Pettersson, J.B.C. Deactivation of iron catalyst by water-potassium thermal desorption studies. In *Catalyst Deactivation 1999 (Studies in Surface Science and Catalysis)*; Delmon, B., Froment, G.F., Eds.; Elsevier: Amsterdam, The Nethelands, 1999; Volume 126, pp. 229–236.
160. Querini, C.A.; Ravelli, F.; Ulla, M.; Cornaglia, L.; Miró, E. Deactivation of Co, K catalysts during catalytic combustion of diesel soot: Influence of the support. In *Catalyst Deactivation 1999 (Studies in Surface Science and Catalysis)*; Delmon, B., Froment, G.F., Eds.; Elsevier: Amsterdam, The Nethelands, 1999; Volume 126, pp. 257–264.
161. Wilson, J.; de Groot, C. Atomic-scale restructuring in high-pressure catalysis. *J. Phys. Chem.* **1995**, *99*, 7860–7866.
162. Parkinson, G.S.; Novotny, Z.; Argentero, G.; Schmid, M.; Pavelec, J.; Kosak, R.; Blaha, P.; Diebold, U. Carbon monoxide-induced adatom sintering in a Pd–Fe_3O_4 model catalyst. *Nat. Mater.* **2013**, *12*, 724–728.
163. Pham, H.N.; Reardon, J.; Datye, A.K. Measuring the strength of slurry phase heterogeneous catalysts. *Powder Technol.* **1999**, *103*, 95–102.
164. Kalakkad, D.S.; Shroff, M.D.; Kohler, S.; Jackson, N.; Datye, A.K. Attrition of precipitated iron Fischer-Tropsch catalysts. *Appl. Catal. A* **1995**, *133*, 335–350.
165. Callister, W.D. *Materials Science and Engineering: An Introduction*; John Wiley, & Sons, Inc.: New York, NY, USA, 2000.
166. Coble, R.L.; Kingery, W.D. Effect of porosity on physical properties of sintered alumina. *J. Am. Ceram. Soc.* **1956**, *39*, 377–385.
167. Deng, S.G.; Lin, Y.S. Granulation of sol-gel-derived nanostructured alumina. *AIChE J.* **1997**, *43*, 505–514.
168. Thoma, S.G.; Ciftcioglu, M.; Smith, D.M. Determination of agglomerate strength distributions: Part 1. Calibration via ultrasonic forces. *Powder Technol.* **1991**, *68*, 53–61.
169. Bankmann, M.; Brand, R.; Engler, B.H.; Ohmer, J. Forming of high surface area TiO_2 to catalyst supports. *Catal. Today* **1992**, *14*, 225–242.
170. Kenkre, V.M.; Endicott, M.R. A theoretical model for compaction of granular materials. *J. Am. Ceram. Soc.* **1996**, *79*, 3045–3054.
171. Song, H.; Evans, J.R.G. A die pressing test for the estimation of agglomerate strength. *J. Am. Ceram. Soc.* **1994**, *77*, 806–814.
172. Werther, J.; Xi, W. Jet attrition of catalyst particles in gas fluidized beds. *Powder Technol.* **1993**, *76*, 39–46.
173. Bhatt, B.L.; Schaub, E.S.; Hedorn, E.C.; Herron, D.M.; Studer, D.W.; Brown, D.M. Liquid phase Fischer-Tropsch synthesis in a bubble column. In *Proceedings of Liquefaction Contractors Review Conference*; Stiegel, G.J., Srivastava, R.D., Eds.; U.S. Department of Energy: Pittsburgh, PA, USA, 1992; pp. 402–423.
174. Pham, H.N.; Datye, A.K. The synthesis of attrition resistant slurry phase iron Fischer-Tropsch catalysts. *Catal. Today* **2000**, *58*, 233–240.
175. Bemrose, C.R.; Bridgewater, J. A review of attrition and attrition test methods. *Powder Technol.* **1987**, *49*, 97–126.

176. Ghadiri, M.; Cleaver, J.A.S.; Tuponogov, V.G.; Werther, J. Attrition of FCC powder in the jetting region of a fluidized bed. *Powder Technol.* **1994**, *80*, 175–178.
177. Weeks, S.A.; Dumbill, P. Method speeds FCC catalyst attrition resistance determinations. *Oil Gas J.* **1990**, *88*, 38–40.
178. Zhao, R.; Goodwin, J.G.; Jothimurugesan, K.; Spivey, J.J.; Gangwal, S.K. Comparison of attrition test methods: ASTM standard fluidized bed vs jet cup. *Ind. Eng. Chem. Res.* **2000**, *39*, 1155–1158.
179. Doolin, P.K.; Gainer, D.M.; Hoffman, J.F. Laboratory testing procedure for evaluation of moving bed catalyst attrition. *J. Test. Eval.* **1993**, *21*, 481.
180. Oukaci, R.; Singleton, A.H.; Wei, D.; Goodwin, J.G. Attrition resistance of Al_2O_3-supported cobalt F-T catalysts. In Proceedings of the 217th National Meeting, ACS Division of Petroleum Chemistry, Anaheim, CA, USA, 21–25 March 1999; p. 91.
181. Adams, M.J.; Mullier, M.A.; Seville, J.P.K. Agglomerate strength measurement using a uniaxial confined compression test. *Powder Technol.* **1994**, *78*, 5–13.
182. Emig, G.; Martin, F.G. Development of a fluidized bed catalyst for the oxidation of *n*-butane to maleic anhydride. *Ind. Eng. Chem. Res.* **1991**, *30*, 1110–1116.
183. Silver, R.G.; Summers, J.C.; Williamson, W.B. *Catalysis and Automotive Pollution Control II*, Elsevier: Amsterdam, The Nethelands, 1991; p. 167.
184. Fisher, G.B.; Zammit, M.G.; LaBarge, J. *Investigation of Catalytic Alternatives to Rhodium in Emissions Control*; SAE Report 920846; SAE International: Warrendale, PA, USA, 1992.
185. Farrauto, R.J.; Heck, R.M. Catalytic converters: state of the art and perspectives. *Catal. Today* **1999**, *51*, 351–360.
186. Beer, G.L. Extended catalyst life two stage hydrocarbon synthesis process. U.S. Patent 6,169,120, 2 January 2001.
187. Bartholomew, C.H.; Stoker, M.W.; Mansker, L.; Datye, A. Effects of pretreatment, reaction, and promoter on microphase structure and Fischer-Tropsch activity of precipitated iron catalysts. In *Catalyst Deactivation 1999 (Studies in Surface Science and Catalysis)*; Delmon, B., Froment, G.F., Eds.; Elsevier: Amsterdam, The Nethelands, 1999; Volume 126, pp. 265–272.
188. Nagano, O.; Watanabe, T. Method for producing methacrolein. U.S. Patent 5,728,894, 17 March 1998.
189. Maillet, T.; Barbier, J.; Duprez, D. Reactivity of steam in exhaust gas catalysis III. Steam and oxygen/steam conversions of propane on a Pd/Al_2O_3 catalyst. *Appl. Catal. B* **1996**, *9*, 251–266.
190. Mathys, G.M.K.; Martens, L.R.M.; Baes, M.A.; Verduijn, J.P.; Huybrechts, D.R.C. Alkene oligomerization. WIPO Patent WO 1993/016020 (A3), 16 September 1993.
191. Mathys, G.M.K.; Martens, L.R.M.; Baes, M.A.; Verduijn, J.P.; Huybrechts, D.R.C. Alkene oligomerization. U.S. Patent 5,672,800, 30 September 1997.
192. Stine, L.O.; Muldoon, B.S.; Gimre, S.C.; Frame, R.R. Process for oligomer production and saturation. U.S. Patent 6,080,903, 26 June 2000.
193. Subramaniam, B.; Arunajatesan, V.; Lyon, C.J. Coking of solid acid catalysts and strategies for enhancing their activity. In *Catalyst Deactivation 1999 (Studies in Surface Science and Catalysis)*; Delmon, B., Froment, G.F., Eds.; Elsevier: Amsterdam, The Nethelands, 1999; Volume 126, pp. 63–77.

194. Ginosar, D.M.; Fox, R.V.; Kong, P.C. Solid catalyzed isoparaffin alkylation at supercritical fluid and near-supercritical fluid conditions. WIPO Patent WO 1999/033769 (A1), 8 July 1999.
195. Ribeiro, F.H.; Bonivardi, A.L.; Kim, C. Transformation of platinum into a stable, high-temperature, dehydrogenation-hydrogenation catalyst by ensemble size reduction with rhenium and sulfur. *J. Catal.* **1994**, *150*, 186–198.
196. Ginosar, D.; Subramaniam, B. Coking and activity of a reforming catalyst in near-critical and dense supercritical reaction mixtures. In *Catalyst Deactivation 1994 (Studies in Surface Science and Catalysis)*; Delmon, B., Froment, G.F., Eds.; Elsevier: Amsterdam, The Nethelands, 1994; Volume 88, pp. 327–334.
197. Petersen, E.E. Catalyst deactivation: Opportunity amidst woe. In *Catalyst Deactivation 1997 (Studies in Surface Science and Catalysis)*; Bartholomew, C.H., Fuentes, G.A., Eds.; Elsevier: Amsterdam, The Nethelands, 1997; Volume 111, pp. 87–98.
198. Gosselink, J.W.; Veen, J.A.R.V. Coping with catalyst deactivation in hydrocarbon processing. In *Catalyst Deactivation 1999 (Studies in Surface Science and Catalysis)*; Delmon, B., Froment, G.F., Eds.; Elsevier: Amsterdam, The Nethelands, 1999; Volume 126, pp. 3–16.
199. Lin, L.; Zao, T.; Zang, J.; Xu, Z. Dynamic process of carbon deposition on Pt and Pt–Sn catalysts for alkane dehydrogenation. *Appl. Catal.* **1990**, *67*, 11–23.
200. Resasco, D.E.; Haller, G.L. Catalytic dehydrogenation of lower alkanes. In *Catalysis (Specialist Periodiodical Report*; Spivey, J.J., Agarwal, S.K., Eds.; Royal Society of Chemistry, Cambridge, UK, 1994; Volume 11, pp. 379–411.
201. Cortright, R.D.; Dumesic, J.A. Microcalorimetric, Spectroscopic, and Kinetic Studies of Silica Supported Pt and Pt/Sn Catalysts for Isobutane Dehydrogenation. *J. Catal.* **1994**, *148*, 771–778.
202. Weyten, H.; Keizer, K.; Kinoo, A.; Luyten, J.; Leysen, R. Dehydrogenation of propane using a packed-bed catalytic membrane reactor. *AIChE J.* **1997**, *43*, 1819–1827.
203. Praserthdam, P.; Mongkhonsi, T.; Kunatippapong, S.; Jaikaew, B.; Lim, N. Determination of coke deposition on metal active sites of propane dehydrogenation catalysts. In *Catalyst Deactivation 1997 (Studies in Surface Science and Catalysis)*; Bartholomew, C.H., Fuentes, G.A., Eds.; Elsevier: Amsterdam, The Nethelands, 1997; Volume 111, pp. 153–158.
204. Rose, B.H.; Kiliany, T.R. Dual catalyst system. WIPO Pat. App. WO 2000/069993 (A1), 12 May 2000.
205. Guerrero-Ruiz, A.; Sepulveda-Escribano, A.; Rodriguez-Ramos, I. Cooperative action of cobalt and MgO for the catalysed reforming of CH_4 with CO_2. *Catal. Today* **1994**, *21*, 545–550.
206. Qin, D.; Lapszewicz, J. Study of mixed steam and CO_2 reforming of CH_4 to syngas on MgO-supported metals. *Catal. Today* **1994**, *21*, 551–560.
207. Stagg, S.; Resasco, D. Effects of promoters and supports on coke formation on Pt catalysts during CH_4 reforming with CO_2. In *Catalyst Deactivation 1997* (Studies in Surface Science and Catalysis); Bartholomew, C.H., Fuentes, G.A., Eds.; Elsevier: Amsterdam, The Nethelands, 1997; Volume 111, pp. 543–550.
208. Fujimoto, K.; Tomishige, K.; Yamazaki, O.; Chen, Y.; Li, X. Development of catalysts for natural gas reforming: Nickel-magnesia solid solution catalyst. *Res. Chem. Intermed.* **1998**, *24*, 259–271.

209. Marshall, C.L.; Miller, J.T. Process for converting methanol to olefins or gasoline. U.S. Patent 5,191,142, 2 March 1993.
210. Gayubo, A.G.; Aguayo, A.T.; Campo, A.E.S.D.; Benito, P.L.; Bilbao, J. The role of water on the attenuation of coke deactivation of a SAPO-34 catalyst in the transformation of methanol into olefins. In *Catalyst Deactivation 1999 (Studies in Surface Science and Catalysis)*; Delmon, B., Froment, G.F., Eds.; Elsevier: Amsterdam, The Nethelands, 1999; Volume 126, pp. 129–136.
211. Barger, P.T. SAPO catalysts and use thereof in methanol conversion processes. U.S. Patent 5,248,647, 28 Sepetember 1993.
212. Cox, J.P.; Evans, J.M. Exhaust gas catalyst for two-stroke engines. WIPO Patent WO 1999/042202 (A1), 20 February 1998.
213. Leviness, S.C.; Mart, C.J.; Behrmann, W.C.; Hsia, S.J.; Neskora, D.R. Slurry hydrocarbon synthesis process with increased catalyst life. WIPO Patent WO 1998/050487 (A1), 2 May 1997.
214. Bartholomew, C.H. Catalyst deactivation in hydrotreating of residua: A review. In *Catalytic Hydroprocessing of Petroleum and Distillates*; Oballa, M., Shih, S. Eds.; Marcel Dekker: New York, NY, USA, 1993; pp. 1–32.
215. Summers, J.; Williamson, W.B. Palladium-only catalysts for closed-loop control. In *Environmental Catalysis 1993*; Armor, J.N., Ed.; American Chemical Society: Washington, DC, USA, 1993; Volume 552, pp. 94–113.
216. Dettling, J.; Hu, Z.; Lui, Y.K.; Smaling, R.; Wan, C.Z.; Punke, A. Smart Pd TWC technology to meet stringent standards. In *Studies in Surface Science and Catalysis*; Elsevier: Amsterdam, The Nethelands, 1995; Volume 96, pp. 461–472.
217. Berndt, M.; Ksinsik, D. Catalyst and process for its preparation. U.S. Patent 4,910,180, 20 March 1990.
218. Prigent, M.; Blanchard, G.; Phillippe, P. Catalyst supports/catalysts for the treatment of vehicular exhaust gases. U.S. Patent 4,985,387, 15 January 1991.
219. Williamson, W.B.; Linden, D.G.; Summers, J.C., II. High-temperature three-way catalyst for treating automotive exhaust gases. U.S. Patent 5,041,407, 20 August 1991.
220. Williamson, W.B.; Linden, D.G.; Summers, J.C., II. High durability and exhuast catalyst with low hydrogen sulfide emissions. U.S. Patent 5,116,800, 26 May 1992.
221. Narula, C.K.; Watkins, W.L.H.; Chattha, M.S. Binary La-Pd oxide catalyst and method of making the catalyst. U.S. Patent 5,234,881, 10 August 1993.
222. Wan, C.-Z.; Tauster, S.J.; Rabinowitz, H.N. Catalyst composition containing platinum and rhodium components. U.S. Patent 5,254,519, 19 October 1993.
223. Argyle, M.D.; Frost, T.S.; Bartholomew, C.H. Modeling cobalt fischer tropsch catalyst deactivation with generalized power law expressions. *Top. Catal.* **2014**, *57*, 415–429.
224. Furuya, T.; Yamanaka, S.; Hayata, T.; Koezuka, J.; Yoshine, T.; Ohkoshi, A. Hybrid catalytic combustion for stationary gas turbine—Concept and small scale test results. In Proceedings of Gas Turbine Conference and Exhibition, Anaheim, CA, USA, 31 May–4 June, 1987; ASME Paper 87-GT-99.
225. Kawakami, T.; Furuya, T.; Sasaki, Y.; Yoshine, T.; Furuse, Y.; Hoshino, M. Feasibility study on honeycomb ceramics for catalytic combustor. In Proceedings of Gas Turbine and Aeroengine Congress and Exposition, Toronto, ON, Canada, 4–8 June 1989; ASME Paper 89-GT-41.

226. Betta, R.D.; Ribeiro, F.; Shoji, T.; Tsurumi, K.; Ezawa, N.; Nickolas, S. Catalyst structure having integral heat exchange. U.S. Patent 5,250,489, 5 October 1993.
227. Fujii, T.; Ozawa, Y.; Kikumoto, S. High pressure test results of a catalytic combustor for gas turbine. *J. Eng. Gas Turbines Power* **1998**, *120*, 509–513.
228. Borio, D.O.; Schbib, N.S. Simulation and optimization of a set of catalytic reactors used for dehydrogenation of butene into butadiene. *Comput. Chem. Eng.***1995**, *19*, S345–S350.
229. Fiato, R.A. Two stage process for hydrocarbon synthesis. U.S. Patent 5,028,634, 2 July 1991.
230. Zhao, R.; Goodwin, J.G., Jr.; Jothimurugesan, K.; Gangwal, S.K.; Spivey, J.J. Spray-dried Iron Fischer-Tropsch catalysts. 1. Effect of structure on the attrition resistance of the catalysts in the calcined state. *Ind. Eng. Chem. Res.* **2001**, *40*, 1065–1075.
231. Zhao, R.; Goodwin, J.G., Jr.; Jothimurugesan, K.; Gangwal, S.K.; Spivey, J.J. Spray-dried iron Fischer-Tropsch catalysts. 2. Effect of carburization on catalyst attrition resistance. *Ind. Eng. Chem. Res.* **2001**, *40*, 1320–1328.
232. Singleton, A.H.; Oukaci, R.; Goodwin, J.G. Processes and catalysts for conducting fischer-tropsch synthesis in a slurry bubble column reactor. U.S. Patent 5,939,350, 17 August 1999.
233. Plecha, S.; Mauldin, C.H.; Pedrick, L.E. Titania catalysts, their preparation and use in Fischer-Tropsch synthesis. U.S. Patent 6,087,405, 11 July 2000.
234. Plecha, S.; Mauldin, C.H.; Pedrick, L.E. Titania catalysts, their preparation and use in fischer-tropsch synthesis. U.S. Patent 6,124,367, 26 September 2000.
235. Singleton, A.H.; Oukaci, R.; Goodwin, J.G. Reducing fischer-tropsch catalyst attrition losses in high agitation reaction systems. WIPO Patent WO 2000/071253 (A3), 30 November 2000.
236. Seitz, M.; Klemm, E.; Emig, G. Poisoning and regeneration of NOx adsorbing catalysts for automotive applications. In *Catalyst Deactivation 1999 (Studies in Surface Science and Catalysis)*; Delmon, B., Froment, G.F. Eds.; Elsevier: Amsterdam, The Nethelands, 1999; Volume 126, pp. 211–218.
237. de Lima, S.M.; da Silva, A.M.; da Costa, L.O.O.; Assaf, J.M.; Mattos, L.V.; Sarkari, R.; Venugopal, A.; Noronha, F.B. Hydrogen production through oxidative steam reforming of ethanol over Ni-based catalysts derived from $La_{1-x}Ce_xNiO_3$ perovskite-type oxides. *Appl. Catal. B* **2012**, *121–122*, 1–9.
238. Song, H.; Ozkan, U.S. Ethanol steam reforming over Co-based catalysts: Role of oxygen mobility. *J. Catal.* **2009**, *261*, 66–74.
239. Masamune, S.; Smith, J.M. Performance of fouled catalyst pellets. *AIChE J.* **1966**, *12*, 384–394.
240. Murakami, Y.; Kobayashi, T.; Hattori, T.; Masuda, M. Effect of intraparticle diffusion on catalyst fouling. *Ind. Eng. Chem. Fundam.* **1968**, *7*, 599–605.
241. Stork, W.H.J. Molecules, catalysts and reactors in hydroprocessing of oil fractions. In *Hydrotreatment and Hydrocracking of Oil Fractions (Studies in Surface Science and Catalysis)*; Froment, G.F., Delmon, B., Grange, P., Eds.; Elsevier: New York, NY, USA, 1997; Volume 106, pp. 41–67.
242. Parks, G.D.; Schaffer, A.M.; Dreiling, M.J.; Shiblom, C.M. Surface Studies on the Interaction of Nickel and Antimony on Cracking Catalysts. *Prepr.—Am. Chem. Soc., Div. Petr. Chem.* **1980**, *25*, 335.

243. Trimm, D.L. Introduction to Catalyst Deactivation. In *Progress in Catalyst Deactivation (NATO Advanced Study Institute Series E, No. 54)*; Figueiredo, J.L., Ed.; Martinus Nijhoff Publishers: Boston, MA, USA,1982; pp. 3–22.
244. Becker, E.R.; Wei, J.J. Nonuniform distribution of catalysts on supports: I. Bimolecular Langmuir reactions. *J. Catal.* **1977**, *46*, 365–381.
245. Long, D.C. Staged hydrocarbon synthesis process. U.S. Patent 5,498,638, 12 March 1996.
246. Powell, B.R., Jr. Stabilitzation of high surface area aluminas. In Proceedings of the Materials Research Society Annual Meeting, Boston, MA, USA, 16–21 November 1980; Paper H9.
247. Dai, Y.; Lim, B.; Yang, Y.; Cobley, C.M.; Li, W.; Cho, E.C.; Grayson, B.; Fanson, P.T.; Campbell, C.T.; Sun, Y.; *et al*. A sinter-resistant catalytic system based on platinum nanoparticles supported on TiO_2 nanofibers and covered by porous silica. *Angew. Chem. Int. Ed.* **2010**, *49*, 8165–8168.
248. Shang, L.; Bian, T.; Zhang, B.; Zhang, D.; Wu, L.-Z.; Tung, C.-H.; Yin, Y.; Zhang, T. Graphene-supported ultrafine metal nanoparticles encapsulated by mesoporous silica: Robust catalysts for oxidation and reduction reactions. *Angew. Chem. Int. Ed.* **2014**, *53*, 250–254.
249. Heck, R.; Farrauto, R. *Catalytic Air Pollution Control: Commercial Technology*; Van Nostrand Reinhold: New York, NY, USA, 1995.
250. Trimm, D.L. The regeneration or disposal of deactivated heterogeneous catalysts. *Appl. Catal. A* **2001**, *212*, 153–160.
251. Berrebi, G.; Dufresne, P.; Jacquier, Y. Recycling of spent hydroprocessing catalysts: EURECAT technology. *Environ. Prog.* **1993**, *12*, 97–100.
252. D'Aquino, R.L. For catalyst regeneration, incentives anew. *Chem. Eng.* **2000**, *107*, 32–33, 35.
253. Chang, T. Regeneration industry helps refiners control costs, limit liabilities. *Oil Gas J.* **1998**, *96*, 49.
254. Blashka, S.R.; Duhon, W. Catalyst regeneration. *Int. J. Hydrocarbon Eng.***1998**, *4*, 60–64.
255. McCulloch, D.C. Catalytic hydrotreating in petroleum refining. In *Applied Industrial Catalysis*; Leach, B.E., Ed.; Academic Press: New York, NY, USA, 1983; pp. 69–121.
256. Franck, J.P.; Martino, G. Deactivation and Regeneration of Catalytic-Reforming Catalysts. In *Progress in Catalyst Deactivation* (NATO Advanced Study Institute Series E., No. 54); Figueiredo, J.L., Ed.; Martinus Nijhoff Publishers: Boston, MA, USA, 1982; pp. 355–397.
257. Spivey, J.J.; Roberts, G.W.; Davis, B.H. *Catalyst Deactivation 2001 (Studies in Surface Science and Catalysis*; Elsevier: Amsterdam, The Nethelands, 2001; Volume 139.
258. Haddad, J.H.; Harandi, M.N.; Owen, H. Upgrading light olefin fuel gas in a fluidized bed catalyst reactor and regeneration of the catalyst. U.S. Patent 5,043,517, 27 August 1991.
259. Ueda, M.; Murakami, T.; Shibata, S.; Hirabayashi, K.; Kondoh, T.; Adachi, K.; Hoshino, N.; Inoue, S. Process for the regeneration of coke-deposited, crystalline silicate catalyst. U.S. Patent 5,306,682, 26 April 1994.
260. Zhang, S.Y.-F.; Gosling, C.D.; Sechrist, P.A.; Funk, G.A. Dual regeneration zone solid catalyst alkylation process. U.S. Patent 5,675,048, 7 October 1997.

261. Panattoni, G.; Querini, C.A. Isobutane alkylation with C_4 olefins: regeneration of metal-containing catalysts. In *Catalyst Deactivation 2001 (Studies in Surface Science and Catalysis)*; Spivey, J.J., Roberts, G.W., Davis, B.H., Eds.; Elsevier: Amsterdam, The Nethelands, 2001; Volume 139, pp. 181.
262. Thompson, D.N.; Ginosar, D.M.; Burch, K.C. Regeneration of a deactivated USY alkylation catalyst using supercritical isobutene. *Appl. Catal. A* **2005**, *279*, 109–116.
263. Petkovic, L.M.; Ginosar, D.M.; Burch, K.C. Supercritical fluid removal of hydrocarbons adsorbed on wide-pore zeolite catalysts. *J. Catal.* **2005**, *234*, 328–339.
264. Dufresne, P.; Brahma, N. Offsite regeneration process for a catalyst containing at least one precious metal. U.S. Patent 5,854,162, 29 December 1998.
265. Innes, R.A.; Holtermann, D.L.; Mulaskey, B.F. Low temperature regeneration of coke deactivated reforming catalysts. U.S. Patent 5,883,031, 16 March 1999.
266. Fung, S.C. Regenerating a reforming catalyst—this bimetallic noble-metal catalyst is used in a refining process to convert saturated-hydrocarbons to aromatics - simply burning off the carbon was not enough—a procedure had to be found for redispersing the metals on the alumina support as well. *Chemtech* **1994**, *24*, 40–44.
267. Alfonso, J.C.; Aranda, D.A.G.; Schmal, M.; Frety, R. Regeneration of a Pt-Sn/Al_2O_3 catalyst: Influence of heating rate, temperature and time of regeneration. *Fuel Proc. Technol.* **1997**, *50*, 35–48.
268. Arteaga, G.J.; Anderson, J.A.; Rochester, C.H. Effects of Catalyst Regeneration with and without Chlorine on Heptane Reforming Reactions over Pt/Al_2O_3 and Pt–Sn/Al_2O_3. *J. Catal.* **1999**, *187*, 219–229.
269. Pieck, C.L.; Vera, C.R.; Parera, J.M. Study of industrial and laboratory regeneration of Pt-Re/Al_2O_3 catalysts. In *Catalyst Deactivation 2001 (Studies in Surface Science and Catalysis)*; Spivey, J.J., Roberts, G.W., Davis, B.H., Eds.; Elsevier: Amsterdam, The Nethelands, 2001; Volume 139, pp. 279–286.
270. Acharya, D.R.; Hughes, R.; Kennard, M.A.; Liu, Y.P. Regeneration of fixed beds of coked chromia—alumina catalyst. *Chem. Eng. Sci.* **1992**, *47*, 1687–1693.
271. Sikkenga, D.L.; Zaenger, I.C.; Williams, G.S. Palladium catalyst reactivation. U.S. Patent 4,999,326, 12 March 1991.
272. Ekstrom, A.; Lapszewicz, J. On the role of metal carbides in the mechanism of the Fischer-Tropsch reaction. *J. Phys. Chem.* **1984**, *88*, 4577–4580.
273. Ekstrom, A.; Lapszewicz, J. The reactions of cobalt surface carbides with water and their implications for the mechanism of the Fischer-Tropsch reaction. *J. Phys. Chem.* **1987**, *91*, 4514–4619.
274. Pedrick, L.E.; Mauldin, C.H.; Behrmann, W.C. Draft tube for catalyst rejuvenation and distribution. U.S. Patent 5,268,344, 7 December 1993.
275. Owen, H.; Schipper, P.H. Process and apparatus for regeneration of FCC catalyst with reduced NOx and or dust emissions. U.S. Patent 5,338,439,16 August 1994.
276. Raterman, M.F. Two-stage fluid bed regeneration of catalyst with shared dilute phase. U.S. Patent 5,198,397, 30 March 1993.

277. Apelian, M.R.; Fung, A.S.; Hatzikos, G.H.; Kennedy, C.R.; Lee, C.-H.; Kiliany, T.R.; Ng, P.K.; Pappal, D.A. Regeneration of noble metal containing zeolite catalysts via partial removal of carbonaceous deposits. U.S. Patent 5,393,717, 28 February 1995.
278. Clark, D.E. Hydrocracking process using a reactivated catalyst. U.S. Patent 5,340,957, 23 August 1994.
279. Yoshimura, Y.; Sato, T.; Shimada, H.; Matsubayashi, N.; Imamura, M.; Nishijima, A.; Yoshitomi, S.; Kameoka, T.; Yanase, H. Oxidative regeneration of spent molybdate and tungstate hydrotreating catalysts. *Energy Fuels* **1994**, *8*, 435–445.
280. Oh, E.-S.; Park, Y.-C.; Lee, I.-C.; Rhee, H.-K. Physicochemical changes in hydrodesulfurization catalysts during oxidative regeneration. *J. Catal.* **1997**, *172*, 314–321.
281. Aquavo, A.T.; Gayubo, A.G.; Atutxa, A.; Olazar, M.; Bilbao, J. Regeneration of a catalyst based on a SAPO-34 used in the transformation of methanol into olefins. *J. Chem. Tech. Biotech.* **1999**, *74*, 1082–1088.
282. Forbus, N.P.; Wu, M.M.-S. Regeneration of methanol/methyl ether conversion catalysts. U.S. Patent 4,777,156, 11 October 1988.
283. Krishna, A.; Hsieh, C.; English, A.E.; Pecoraro, T.; Kuehler, C. Additives improve FCC process; increase catalyst life, lower regeneration temperatures and improve yield and quality of products cost effectively. *Hydrocarbon Processing* 1991, 59–66.
284. Altomare, C.; Koermer, G.; Schubert, P.; Suib, S.; Willis, W. A designed fluid cracking catalyst with vanadium tolerance. *Chem. Mater.* **1989**, *1*, 459–463.
285. Aguinaga, A.; Montes, M. Regeneration of a nickel/silica catalyst poisoned by thiophene. *Appl. Catal. A* **1992**, *90*, 131–144.
286. Lowry, G.V.; Reinhard, M. Pd-Catalyzed TCE Dechlorination in Groundwater: Solute Effects, Biological Control, and Oxidative Catalyst Regeneration. *Environ. Sci. Technol.* **2000**, *34*, 3217–3223.
287. Trinh, D.C.; Desvard, A.; Martino, G. Process for regenerating used catalysts by means of hydrogen peroxide aqueous solution stabilized with an organic compound. U.S. Patent 4,830,997, 16 May 1989.
288. Sherwood, D.E. Process for the reactivation of spent alumina-supported hydrotreating catalysts. U.S. Patent 5,230,791, 27 July 1993.
289. Fung, S.C. Deactivation and regeneration/redispersion chemistry of Pt/KL-zeolite. In *Catalyst Deactivation 2001 (Studies in Surface Science and Catalysis)*; Spivey, J.J., Roberts, G.W., Davis, B.H., Eds.; Elsevier: Amsterdam, The Nethelands, 2001; Volume 139, pp. 399–406.
290. Didillon, B. Catalyst regeneration process and use of the catalyst in hydrocarbon conversion processes. U.S. Patent 5,672,801, 30 September 1997.
291. Tsao, Y.-Y.P.; von Ballmoos, R. Reactivating catalysts containing noble metals on molecular sieves containing oxides of aluminum and phosphorus. U.S. Patent 4,929,576, 29 May 1990.
292. Dufresne, P.; Brahma, N.; Girardier, F. Off-site regeneration of hydroprocessing catalysts. *Rev. Inst. Fr. Pet.* **1995**, *50*, 283–293.
293. Clark, F.T.; Hensley, A.L., Jr. Process for regenerating a spent resid hydroprocessing catalyst using a group IIA metal. U.S. Patent 5,275,990, 4 January 1994.

294. Brito, A.; Arvelo, R.; Gonzalez, A.R. Variation in structural characteristics of a hydrotreatment catalyst with deactivation/regeneration cycles. *Ind. Eng. Chem. Res.* **1998**, *37*, 374–379.
295. Teixeira-da-Silva, V.L.S.; Lima, F.P.; Dieguez, L.C. Regeneration of a deactivated hydrotreating catalyst. *Ind. Eng. Chem. Res.* **1998**, *37*, 882–886.
296. Snape, C.E.; Diaz, M.C.; Tyagi, Y.R.; Martin, S.C.; Hughes, R. Characterisation of coke on deactivated hydrodesulfurisation catalysts and a novel approach to catalyst regeneration. In *Catalyst Deactivation 2001 (Studies in Surface Science and Catalysis)*; Spivey, J.J., Roberts, G.W., Davis, B.H., Eds.; Elsevier: Amsterdam, The Nethelands, 2001; Volume 139, pp. 359–365.
297. Sherwood, D.E., Jr.; Hardee, J.R., Jr. Method for the reactivation of spent alumina-supported hydrotreating catalysts. U.S. Patent 5,445,728, 29 August 1995.
298. Maholland, M.K.; Fu, C.-M.; Lowery, R.E.; Kubicek, D.H.; Bertus, B.J. Demetallization and passivation of spent cracking catalysts. U.S. Patent 5,021,377, 4 June 1991.
299. Kubicek, D.H.; Fu, C.-M.; Lowery, R.E.; Maholland, K.M. Reactivation of spent cracking catalysts. U.S. Patent 5,141,904, 25 August 1992.
300. Fu, C.-M.; Maholland, M.; Lowery, R.E. Reactivation of spent, metal-containing cracking catalysts. U.S. Patent 5,151,391, 29 September 1992.
301. Hu, Y.; Luo, B.; Sun, K.; Yang, Q.; Gong, M.; Hu, J.; Fang, G.; Li, Y. Dry regeneration-demetalization technique for catalyst for residuum and/or heavy oil catalytic cracking. U.S. Patent 6,063,721, 16 May 2000.
302. Walker, P.L., Jr.; Rusinko, F., Jr.; Austin, L.G. Gas Reactions of Carbon. *Adv. Catal.* **1959**, *11*, 133–221.
303. Fulton, J.W. Regenerating Spent Catalyst. *Chem. Eng.* **1988**, *96*, 111–114.
304. Richardson, J.T. Experimental determination of catalyst fouling parameters. Carbon profiles. *Ind. Eng. Chem. Process Des. Dev.* **1972**, *11*, 8–11.
305. Weisz, P.B.; Goodwin, R.B. Combustion of carbonaceous deposits within porous catalyst particles: II. Intrinsic burning rate. *J. Catal.* **1966**, *6*, 227–236.
306. Rostrup-Nielsen, J.R. Some principles relating to the regeneration of sulfur-poisoned nickel catalyst. *J. Catal.* **1971**, *21*, 171–178.
307. Hartenstein, H. *Feasibility of SCR Technology for NO_x Control Technology for the Milton R. Young Station, Center, North Dakota*; Expert Report on behalf of the United States Department of Justice: Washington, DC, USA, July 2008.
308. Hartenstein, H.; Ehrnschwender, M.; Sibley, A.F. SCR Regeneration-10 Years of R&D and Commercial Application. In Proceedings of Power Plant Air Pollution Control Mega Symposium, Baltimore, MD, USA, 24–28 August 2008; Paper No. 104.
309. EPA; Office of Air and Radiation. Update on Cap and Trade Programs for SO_2 and NO_x. Presented at the Enviornmental Markets Association, 12 Annual Spring Conference, Miami, FL, USA, 29April–2 May 2008.
310. EPA. NO_x Budget Trading Program—Basic Information. Available online: http://www.epa.gov/airmarkt/progsregs/nox/docs/NBPbasicinfo.pdf (accessed on 31 October 2014).

311. McIlvaine Company. News Release: Coal to Play Bigger Role in Future Power Generation With World Capacity of 1450 GW by 2012. Available online: http://www.mcilvainecompany.com/brochures/Alerts_for_Internet/s9%20moni/1104coal%20to%20play%20bigger%20role%20in%20future%20power%20generation.htm (accessed on 31 October 2014).
312. Hjalmarsson, A.-K. *NO_x Control Technologies for Coal Combustion*; IEACR/24; IEA Coal Research: Lexington, KY, USA, 1990.
313. U.S. Department of Energy; Southern Company Services. Control of Nitrogen Oxide Emissions: Selective Catalytic Reduction. *Clean Coal Technology*; Topical Report 9; U.S. Department of Energy: Pittsburgh PA, USA; Southern Company Services: Birmingham AL, USA; 1997.
314. Janssen, F.; Meijer, R. Quality control of $DeNO_x$ catalysts: Performance testing, surface analysis and characterization of $DeNO_x$ catalysts. *Catal. Today* **1993**, *16*, 157–185.
315. Ashton, J.; Nackos, A.; Bartholomew, C.H.; Hecker, W.C.; Baxter, L. Poisoning/Deactivation of Vanadia/Titanium Dioxide SCR Catalysts in Coal Systems. Presented at the 19th Annual Western States Catalysis Club Symposium, Albuquerque, NM, USA, 25 February 2005.
316. Guo, X.; Nackos, A.; Ashton, J.; Bartholomew, C.H.; Hecker, W.C.; Baxter, L. Poisoning Study of V_2O_5-WO_3/TiO_2 Catalysts by Na, K, and Ca. Presented at 19th Annual Western States Catalysis Club Symposium, Albuquerque, NM, USA, 25 February 2005.
317. Forzatti, P.; Lietti, L.; Tronconi, E. Nitrogen Oxides Removal–Industrial. In *Encyclopedia of Catalysis*; Horváth, T.I., Ed.; Wiley, Hoboken, NJ, USA, 2003.
318. Rubin, E.S., Kalagnanam, J.R., Frey, C.H., Berkenpas, M.B. Integrated Environmental Control Modeling of Coal-Fired Power Systems. *Journal of the Air and Waste Management Association* **1997**, 47, 1180-1188.
319. Cochran, J.R.; Ferguson, A.W. Selective Catalytic Reduction for NO_x Emission Control. In Proceedings of the First International Conference on Air Pollution Zannetti, P., Brebbia, C.A., Garcia Gardea, J.E., Ayala Milian, G., Eds., Monterrey, Mexico, 16-18 Feb. 1993, Volume 1, pp. 703–718.
320. Bullock, P.E.; Hartenstein, H.U. O&M Cost Reduction of a Coal-Fired US Merchant Plant Through an Optimized SCR Management Strategy Involving Catalyst Regeneration. In Proceedings of the Conference on Selective Catalytic Reduction and Selective Non-Catalytic Reduction for NO_x Control, Pittsburgh, PA, USA, 15–17 May 2002.
321. Babcock Hitachi's Rejuvenation of Mehrum SCR Catalyst. *FGD and $DeNO_x$ Newsletter*; No. 315; The McIlvaine Company: Northfield, IL, USA; 2004.
322. McMahon, B. Catalyst regeneration: The business case. *Power* **2006**, *150*, 36-39.
323. Zheng, Y.; Jensen, A.; Johnsson, J. Laboratory investigation of selective catalytic reduction catalysts: Deactivation by potassium compounds and catalyst regeneration. *Ind. Eng. Chem. Res.* **2004**, *43*, 941–947.
324. Khodayari, R.; Odenbrand, C. Regeneration of commercial SCR catalysts by washing and sulphation: effect of sulphate groups on the activity. *Appl. Catal. B* **2001**, *33*, 277–291.
325. Khodayari, R.; Odenbrand, C. Regeneration of commercial TiO_2-V_2O_5-WO_3 SCR catalysts used in bio fuel plants. *Appl. Catal. B* **2001**, *30*, 87–89.
326. Dörr, H.-K.; Koch, G.; Bastuck, W. Method for renewed activation of honeycomb-shaped catalyst elements for denitrating flue gases. U.S. Patent, 6,387,836 (B1), 14 May 2002.

327. Schneider, P.; Bastuck, W. Method to re-enable honeycomb catalyst elements constructed for the denitrification of flue gases. DE Patent 10222915 (B4), 15 January 2004.
328. Budin, R.; Krotla, K.; Rabitsch, H. Process for regenerating used deNO_x or dedioxin catalytic converters. U.S. Patent, 6,484,733 (B2), 26 November 2002.
329. Cooper, M.; Harrison, K.; Lin, C. An Experimental Program to Optimize SCR Catalyst Regeneration for Lower Oxidation of SO_2 to SO_3. Proceedings of the 2006 Environmental Controls Conference, Pittsburgh, PA, USA, 16–18 May 2006.
330. Patel, N.; Hartenstein, H.-U.; Wenz, F. Process for decoating a washcoat catalyst substrate. U.S. Patent 7,559,993 (B1), 14 July 2009.
331. Patel, N.; Hartenstein, H.-U.; Wenz, F. Process for decoating a washcoat catalyst substrate. U.S. Patent 6,929,701, 16 August 2005.
332. Tate, A.; Skipper, J.; Wenz, F. Environmentally sound handling of deactivated SCR catalyst. *Coal Power*, 31 July 2008.
333. Hartenstein, H.U.; Hoffman, T. Method of regeneration of SCR catalyst. U.S. Patent 7,723,251, 25 May 2010.
334. Servatius, P.; Schluttig, A. Lifetime extension of SCR-DeNO_x catalysts using SCR-Tech's high efficiency ultrasonic regeneration process. In Proceedings of 2001 Conference of Selective Catalytic Reduction and Selective Non-Catalytic Reduction for NO_x Control, Pittsburgh, PA, USA, 16–18 May 2001.
335. Hartenstein, H.; Gutberlet, H. Catalyst Regeneration—An Integral Part of Proper Catalyst Management. Proceedings of the 2001 Workshop on Selective Catalytic Reduction, Baltimore, MD, USA, 13–15 November 2001.
336. Wenz, F.; Deneault, R.; Franklin, H.N. The Goals, Challenges and Successes of Regenerating Selective Catalytic Reduction Catalyst. In Proceedings of the Electric Power 2006 Conference–NO_x Control III–SCR Technologies, Atlanta, GA, USA, 2–4 May 2006.
337. CoaLogix. Available online: http://www.coalogix.com (accessed on 31 October 2014).
338. McCullen, S.B.; Wong, S.S.; Huang, T.J. Regeneration of noble metal-highly siliceous zeolite with sequential hydrogen halide and halogen or organic-halogen compound treatment. U.S. Patent 4,645,751, 24 February 1987.
339. Borghard, W.S.; Huang, T.J.; McCullen, S.B.; Schoennagel, H.J.; Tsao, Y.-P.; Wong, S.S. Redispersion of agglomerated noble metals on zeolite catalysts. U.S. Patent 4,657,874, 14 April 1987.
340. Fung, S.C.; Rice, R.W. Process using halogen/oxygen for reactivating iridium and selenium containing catalysts. U.S. Patent 4,491,636, 1 January 1985.
341. Fung, S.C. Redispersion of Ir catalysts by low temperature reduction step. U.S. Patent 4,467,045, 21 August 1984.
342. Landolt, G.R.; McHale, W.D.; Schoennagel, H.J. Catalyst regeneration procedure. U.S. Patent 4,359,400, 16 November 1982.
343. Fung, S.C.; Weissman, W.; Carter, J.L. Reactivation process for iridium-containing catalysts using low halogen flow rates. U.S. Patent 4,480,046, 30 October 1984.
344. Fung, S.C. Low temperature decoking process for reactivating iridium and selenium containing catalysts. U.S. Patent 4,492,767, 8 January 1985.

345. Fung, S.C.; Weissman, W.; Carter, J.L.; Kmak, W.S. Reactivating iridium and selenium containing catalysts with hydrogen halide and oxygen. U.S. Patent 4,491,635, 1 January 1985.
346. Mohr, D.H. Process for regenerating a monofunctional large-pore zeolite catalyst having high selectivity for paraffin dehydrocyclization. U.S. Patent 4,855,269, 8 August 1989.
347. Fung, S.C.; Tauster, S.J.; Koo, J.Y. Method of regenerating a deactivated catalyst. U.S. Patent 4,925,819, 15 May 1990.
348. Fung, S.C.; Kmak, W.S. Reactivation of iridium-containing catalysts by halide pretreat and oxygen redispersion. U.S. Patent 4,444,896, 24 April 1984.
349. Fung, S.C.; Weissman, W.; Carter, J.L. Reactivation process for iridium-containing catalysts using low halogen flow rates. U.S. Patent 4,444,895, 24 April 1984.
350. Boyle, J.P.; Gilbert, J.B. Reactivation of iridium-containing catalysts. U.S. Patent 4,517,076, 14 May 1985.
351. Buss, W.D.; Hughes, T.R. *In situ* hydrocarbon conversion catalyst regeneration and sulfur decontamination of vessels communicating with catalyst reactor. U.S. Patent 4,482,637, 13 November 1984.
352. Cheng, W.-H. Regeneration of methanol dissociation catalysts. U.S. Patent 4,855,267, 8 August 1989.
353. Huang, Y.-Y.; LaPierre, R.B.; McHale, W.D. Process for dispersing or redispersing a group VIII noble metal species on a porous inorganic support. European Patent 0,306,170 (B1), 8 March 1989.
354. Hucul, D.A. Redispersal of Ru, Os, Rh and Pd catalysts and processes therewith. U.S. Patent 4,891,346, 2 January, 1990.
355. Fung, S.C.; Rice, R.W. Process for reactivating iridium-containing catalysts. U.S. Patent 4,447,551, 8 May 1984.
356. Fung, S.C. Process for reactivating iridium-containing catalysts in series. U.S. Patent 4,472,514, 18 September 1984.
357. S.C. Fung; R.W. Rice Process for reactivating iridium-containing catalysts. U.S. Patent 4,473,656, 25 September 1984.
358. Huang, Y.-Y.; LaPierre, R.B.; McHale, W.D. Process for dispersing or redispersing a Group VIII noble metal species on a porous inorganic support. U.S. Patent 4,952,543, 28 August 1990.
359. Fung, S.C.; Weissman, W.; Carter, J.L.; Kmak, W.S. Reactivating iridium-containing catalysts with hydrogen halide and oxygen. U.S. Patent 4,444,897, 24 April 1984.
360. Fung, S.C. Low temperature decoking process for reactivating iridium containing catalysts. U.S. Patent 4,472,515 18 September 1984.
361. Dadyburjor, D.B. Regions of validity for models of regeneration of sintered supported metal catalysts. In *Catalyst Deactivation (Studies in Surface Science and Catalysis)*; Delmon, B., Froment, G.F., Eds.; Elsevier: Amsterdam, The Nethelands, 1980; Volume 6, pp. 341–351.
362. Jacobs, G.; Ma, W.; Gao, P.; Todic, B.; Bhatelia, T.; Bukur, D.B.; Davis, B.H. The application of synchrotron methods in characterizing iron and cobalt Fischer–Tropsch synthesis catalysts. *Catal. Today* **2013**, *214*, 100–139.

363. Van Steen, E.; Claeys, M.; Dry, M.E.; van de Loosdrecht, J.; Viljoen, E.L.; Visagie, J.L. Stability of nanocrystals: Thermodynamic analysis of oxidation and re-reduction of cobalt in water/hydrogen mixtures. *J. Phys. Chem. B* **2005**, *109*, 3575–3577.
364. Ma, W.; Jacobs, G.; Ji, Y.; Bhatelia, T.; Bukur, D.B.; Khalid, S.; Davis, B.H. Fischer–Tropsch synthesis: Influence of CO conversion on selectivities, H_2/CO usage ratios, and catalyst stability for a Ru promoted Co/Al_2O_3 catalyst using a slurry phase reactor. *Top. Catal.* **2011**, *54*, 757–767.
365. Jacobs, G.; Sarkar, A.; Ji, Y.; Patterson, P.M.; Das, T.K.; Luo, M.; Davis, B.H. Fischer-Tropsch synthesis: Characterization of interactions between reduction promoters and Co for Co/Al_2O_3–based GTL catalysts. In Proceedings of *AIChE Annual Meeting*, San Francisco, CA, USA, 12–17 November 2006.
366. Das, T.K.; Jacobs, G.; Patterson, P.M.; Conner, W.A.; Davis, B.H. Fischer–Tropsch synthesis: characterization and catalytic properties of rhenium promoted cobalt alumina catalysts. *Fuel* **2003**, *82*, 805–815.
367. Jacobs, G.; Das, T.K.; Patterson, P.M.; Luo, M.; Conner, W.A.; Davis, B.H. Fischer–Tropsch synthesis: Effect of water on Co/Al_2O_3 catalysts and XAFS characterization of reoxidation phenomena. *Appl. Catal. A* **2004**, *270*, 65–76.
368. Moodley, D.J.; Saib, A.M.; van de Loosdrecht, J.; Welker-Nieuwoudt, C.A.; Sigwebela, B.H.; Niemanstsverdriet, J.W. The impact of cobalt aluminate formation on the deactivation of cobalt-based Fischer–Tropsch synthesis catalysts. *Catal. Today* **2011**, *171*, 192–200.
369. Jermwongratanachai, T.; Jacobs, G.; Shafer, W.D.; Ma, W.; Pendyala, V.R.R.; Davis, B.H.; Kitiyanan, B.; Khalid, S.; Cronauer, D.C.; Kropf, A.J.; Marshall, C.L. Fischer–Tropsch synthesis: Oxidation of a fraction of cobalt crystallites in research catalysts at the onset of FT at partial pressures mimicking 50% CO conversion. *Top. Catal.* **2014**, *57*, 479–490.
370. Azzam, K.; Jacobs, G.; Ma, W.; Davis, B.H. Effect of cobalt particle size on the catalyst intrinsic activity for Fischer–Tropsch synthesis. *Catal. Lett.* **2014**, *144*, 389–394.
371. Saib, A.M.; Borgna, A.; van de Loosdrecht, J.; van Berge, P.J.; Niemanstsverdriet, J.W. XANES study of the susceptibility of nano-sized cobalt crystallites to oxidation during realistic Fischer–Tropsch synthesis. *Appl. Catal. A* **2006**, *312*, 12–19.
372. Dalai, A.K.; Davis, B.H. Fischer–Tropsch synthesis: A review of water effects on the performances of unsupported and supported Co catalysts. *Appl. Catal. A* **2008**, *348*, 1–15.
373. Sadeqzadeh, M.; Chambrey, S.; Piché, S.; Fongarland, P.; Luck, F.; Curulla-Ferré, D.; Schweich, D.; Bousquet, J.; Khodakov, A.Y. Deactivation of a Co/Al_2O_3 Fischer–Tropsch catalyst by water-induced sintering in slurry reactor: Modeling and experimental investigations. *Catal. Today* **2013**, *215*, 52–59.
374. Sadeqzadeh, M.; Hong, J.; Fongarland, P.; Curulla-Ferre, D.; Luck, F.; Bousquet, J.; Schweich, D.; Khodakov, A.Y. Mechanistic modeling of cobalt based catalyst sintering in a fixed bed reactor under different conditions of Fischer–Tropsch synthesis. *Ind. Eng. Chem. Res.* **2012**, *51*, 11955–11964.
375. Soled, S.L.; Kiss, G.; Kliewer, C.; Baumgartner, J.; El-Malki, E.-M. Learnings from Co Fischer-Tropsch catalyst studies. Present at 245th ACS National Meeting & Exposition, New Orleans, LA, USA, 7–11 April 2013.

376. Hauman, M.M.; Saib, A.M.; Moodley, D.J.; Plessis, E.D.; Claeys, M.; van Steen, E. Re-dispersion of cobalt on a model fischer–tropsch catalyst during reduction–oxidation–reduction cycles. *Chem. Catal. Chem.* **2012**, *4*, 1411–1419.
377. Weststrate, C.J.; Kizilkaya, A.C.; Rossen, E.T.R.; Verhoeven, M.W.G.M.; Ciobica, I.M.; Saib, A.M.; Niemanstsverdriet, J.W. Atomic and Polymeric Carbon on Co(0001): Surface Reconstruction, Graphene Formation, and Catalyst Poisoning. *J. Phys. Chem. C* **2012**, *116*, 11575–11583.
378. Weststrate, C.J.; Hauman, M.M.; Moodley, D.J.; Saib, A.M.; van Steen, E.; Niemanstsverdriet, J.W. Cobalt Fischer–Tropsch catalyst regeneration: The crucial role of the kirkendall effect for cobalt redispersion. *Top. Catal.* **2011**, *54*, 811–816.
379. Moodley, D.J.; van de Loosdrecht, J.; Saib, A.M.; Overett, M.J.; Datye, A.K.; Niemanstsverdriet, J.W. Carbon deposition as a deactivation mechanism of cobalt-based Fischer–Tropsch synthesis catalysts under realistic conditions. *Appl. Catal. A* **2009**, *354*, 102–110.
380. van de Loosdrecht, J.; Balzhinimaev, B.; Dalmon, J.-A.; Niemanstsverdriet, J.W.; Tsybulya, S.V.; Saib, A.M.; van Berge, P.J.; Visagie, J.L. Cobalt Fischer-Tropsch synthesis: Deactivation by oxidation?. *Catal. Today* **2007**, *123*, 293–302.
381. Saib, A.M.; Borgna, A.; van de Loosdrecht, J.; van Berge, P.J.; Niemanstsverdriet, J.W. In Situ surface oxidation study of a planar $Co/SiO_2/Si(100)$ model catalyst with nanosized cobalt crystallites under model Fischer−Tropsch synthesis conditions. *J. Phys. Chem. B* **2006**, *110*, 8657–8664.
382. Moodley, D.J.; van de Loosdrecht, J.; Saib, A.M.; Niemanstsverdriet, J.W. The formation and influence of carbon on cobalt-based Fischer-Tropsch synthesis catalysts: An integrated review. In *Advances in Fischer-Tropsch Synthesis*, *Catalysts*, *and Catalysis*; Davis, B.H., Occelli, M.L., Eds.; CRC Press Taylor & Francis Group: Boca Raton, FL, USA, 2010; pp. 49–81.
383. Bezemer, G.L.; Herman, J.H.; Kuipers, P.C.E.; Oosterbeek, H.; Holewign, J.E.; Xu, X.; Kapteijn, F.; van Dillen, A.J.; de Jong, K.P. Cobalt particle size effects in the Fischer−Tropsch reaction studied with carbon nanofiber supported catalysts. *J. Am. Chem. Soc.* **2006**, *128*, 3956–3964.
384. Jacobs, G.; Ribeiro, M.C.; Ma, W.; Ji, Y.; Khalid, S.; Sumodjo, P.T.A.; Davis, B.H. Group 11 (Cu, Ag, Au) promotion of $15\%Co/Al_2O_3$ Fischer–Tropsch synthesis catalysts. *Appl. Catal. A* **2009**, *361*, 137–151.